HYDROLOGICAL REGULATION ON DISSOLVED ORGANIC CARBON TRANSPORT FROM AGRICULTURAL AND FOREST SOILS TO STREAMS

By

Yi Mei

Dissertation

Submitted to the Faculty of the

Graduate School of Vanderbilt University

in partial fulfillment of the requirements

for the degree of

DOCTOR OF PHILOSOPHY

in

ENVIRONMENTAL ENGINEERING

August, 2013

Nashville, Tennessee

Approved:

George M. Hornberger

David Jon Furbish

Prodyot K Basu

David Kosson

To my Dad, Jixue Mei and Mom, Shuanggui Liang

ACKNOWLEDGEMENTS

During my five year Ph.D. study at Department of Civil and Environment Engineering at the Vanderbilt University, I've been fortunate to meet some of the finest people along the way.

Foremost, I would like to express my deepest and sincerest gratitude to my adviser Dr. George M. Hornberger for his insightful guidance, constant encouragement and endless support. George has shaped my research and life in a profound way by his patience, energy and inspiration. From basic English pronunciation to advanced scientific thinking and skills, George is always there to help no matter how slow I was. As his student, I feel extremely lucky to work with him and enjoy the light he has shown me for life and research. Every moments I spend with him will be cherished for my entire life.

I really appreciate the assistance of my research committee: Dr. Louis Kaplan, Dr. David Furbish, Dr. Prodyot K Basu and Dr. David S. Kosson. This dissertation could not have been done without their help. I would like to thank Lou for his guidance and help during my staying at Stroud Water Research Center for all those memorable summers. Lou's scientific preciseness and input to this research is greatly appreciated. Thanks also goes to Dr. Furbish, it's always a great fun to discuss with David about the research problems, his insights on the earth surface processes help me gain a better understanding of the physical aspect of hydrology and geomorphology. I am feeling lucky to sit in Dr. Basu's Finite-Element class and discuss modeling techniques with him, his class has greatly sharpen my modeling skills which benefits my research. Thank Dr. Kosson for serving on my dissertation committee, for contributing his

time and offering valuable comments on my research work.

The help from my advisers at Stroud Water Research Center: J Denis Newbold, Anthony K. Aufdenkampe and Dr.Chris Duffy at Penn State University is truly appreciated. I thank Denis for being a friend with a great critical mind which helps me shape my research ideas. I also thank Anthony and Chris for their help on research ideas and supports on the data and computation resources. My thanks also goes to all the folks at Stroud Water Research Center. Their help is the key of my successful experiments and field observations.

It's a great pleasure to work with the members in our research group: Debra Perrone, John Henry Jacobi, Leslie Lyons Duncan, Lanka Thabrew, John Crane, Janney Murphy, Thushara Gunda and Scott Worland. I appreciate their time to listen to my research presentations and review my posters and papers, their suggestions on all sorts of aspects about life in the U.S. made my life so much easier and enjoyable.

Thank CEE Grad students: You Ling, Tong Hui, Hao Yan, Bethany Smith for been such invaluable and tolerant friends during my five year study in the department.

Finally, most importantly, I would like to thank my family, my Dad, Mom, and my grandparents. Their endless love is the strength for me to move forward. No matter where I am, what my occupation is, no matter I succeed or fail, there will always be a spot called home for me to go back to stay, and they are there for me to love.

I acknowledge the financial support provide by the National Science Foundation project EAR 0450331"Hydrologic regulation of dissolved organic matter biogeochemistry from forests through river networks" the National Science Foundation project EAR-0724971 "Christina River Basin Critical Zone Observatory (CRB-CZO) and the National Science Foundation project DEB 1052716 "LTREB: Trajectory for the recovery of stream ecosystem structure and function during reforestation. I appreciate and experimental facilities provided by Stroud Water Research Center.

TABLE OF CONTENTS

LIST OF TABLES

LIST OF FIGURES

CHAPTER 1

INTRODUCTION

1 Perspective

Resolving the global CO_2 budget problem ("missing carbon") has assumed greater urgency as the global community of nations has begun serious negotiation of measures to mitigate greenhouse warming. Terrestrial plants and soils are a major sink of atmospheric CO_2 (Sundquist, 1993). Globally, forest vegetation and soils contain about 1146 petagrams of carbon, with two thirds of the carbon contained in soils and associated peat deposits (Dixon et al., 1994). The estimated capacity to sequester carbon in agricultural soils is about 20-30 petagrams over the next 50-100 years (Paustian et al., 1997). Each year about 0.25 petagrams of terrigenous dissolved organic carbon (DOC) enters the global ocean through riverine transport, the largest transfer of reduced C from the continents to the ocean (Hansell and Carlson, 2002)(Figure 1)[1].

DOC dynamics are central to the biogeochemistry of soil and aquatic ecosystems for they link energy flow and nutrient cycling (Qualls, 2000). DOC is an important constituent of soil solution that plays a role in many chemical and biological processes in soils (McDowell, 2003). The flux of DOC in soil facilitates transport of nutrients and contaminants in soils (Mertens et al., 2007). DOC supplies nutrients and energy for heterotrophic bacteria in surface waters and soils, affects the stream pH (Hruska et al., 2003), influences metal export and speciation in streams and rivers (Shafer et al., 1997), and affects attenuation of light in lakes (Morris et al., 1995).

[1]Reprint with permission from Nature Publishing Group

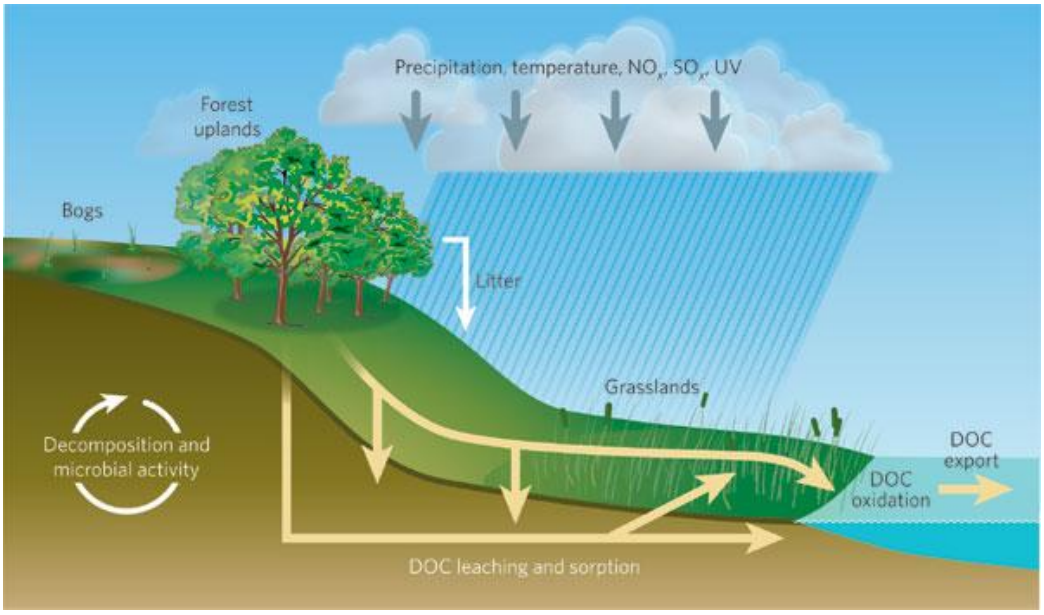

Figure 1: DOC deposition and delivery: The decomposition and subsequent leaching of organic litter in bogs, forests and wetlands are the principal sources of DOC in the terrestrial landscape (Roulet and Moore, 2006).

DOC is a very complex mix of organic compounds (Figure 2). A key to quantifying DOC dynamics is to establish useful approximations for behavior of this complex mixture. Neff and Asner (2001) point out that the distinction between biologically available and unavailable DOC is important to both conceptual and simulation models of DOC biogeochemistry. Biodegradable DOC (BDOC) is defined operationally as the fraction of the DOC that can be metabolized by bacteria within a period of a few days to a few months. Bioavailability of DOC changes temporally and spatially along a river (Leff and Meyer, 1991). The BDOC proportion of DOC ranges from $< 1\%$ to over 50%, and the bioavailability of DOC ranges over two orders of magnitude [Meyer, 1994]. Buffam et al. (2001) found that event DOC is more biodegradable, with a high aromatic component (Vidon et al., 2008), relative to stream DOC under baseflow conditions. This finding is consistent with work in White Clay Creek (WCC) in southeastern Pennsylvania, USA (Kaplan and Bott, 1983). Several studies there focused on stream BDOC measurements (Kaplan and Newbold, 1995), source

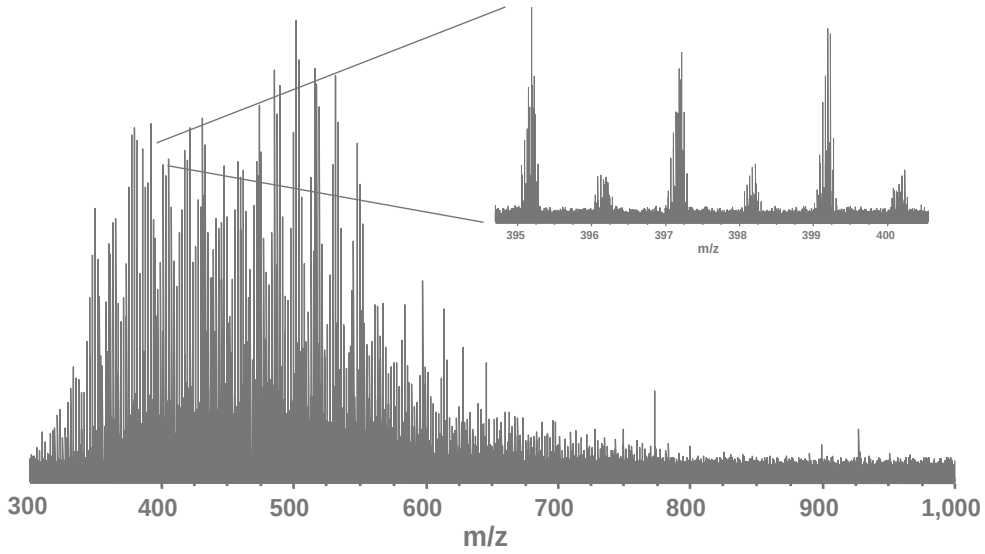

Figure 2: Ultra-high resolution mass spectra of DOM from White Clay Creek, the more than 3000 peaks provides a hint of the complexity of DOM

identification (Yano et al., 2000) and chemical composition (Volk et al., 1997).

Hydrology has a significant effect on the terrestrial portion of the carbon budget (Fraser et al., 2001). The formation of water-soluble organic materials can be increased through the positive effect of moisture on microbial activity (Falkengrengrerup and Tyler, 1993). DOC is leached downward across the soil horizons facilitated by precipitation events, and is flushed into the stream with groundwater. These impacts are significant especially during storms or snowmelt (Hinton et al., 1997), with as much as 86% of the annual DOC flux from small eastern United States forested watersheds exported during storms (Raymond and Saiers, 2010). Thus quantitatively understanding the processes that determine how hydrology and DOC interact across different spatial and temporal scales is of great importance.

2 Research questions

Significant progress has been made in the past several decades in identifying DOC sources influenced by catchment characteristics [McGlynn and McDonnell, 2003], exploring the role of hydrological pathways [Moore, 2003], and investigating the control

of soil moisture, temperature and snowmelt on DOC dynamic in soils (Kalbitz et al., 2000). Despite these significant advances, there is still only a very poor understanding of DOC transport mechanisms from soils to streams. Previous research has shown that the observed variation of DOC in streams over storm events may be due to "flushing" of DOC that builds up in unsaturated soils during dry periods (Boyer et al., 2000). As an alternative to the flushing hypothesis, McGlynn and McDonnell (2003) showed relative timing of riparian and hillslope source contributions and the connections and disconnections of dominant runoff contributing areas are the first-order catchment controls on stream DOC concentrations and mass export . Soil moisture, temperature, freeze/thaw cycles and snowmelt and amount of nitrate all exert some control on DOC in watersheds (Kalbitz et al., 2000). Understanding the DOC transport from forest and agricultural soils to streams should build on a correct understanding of the first order controls on the DOC dynamics in a catchment. A coherent, consistent theory and reliable robust modeling tools are needed to understand DOC delivery to streams.

Hence, the overarching questions of this research are: *How does DOC move from terrestrial sources to streams governed by hydrology and biogeochemistry at multiple spatial and temporal scales? What are the mechanisms related to the coupled processes?*.

Under this overarching question, a number of specific questions were addressed respectively in this dissertation. Question 0: how much DOC enters streams from terrestrial sources, and what are the major mechanisms controlling this process; Question 1: What fraction of DOC transport is from near-stream sources relative to upland parts of the hillslopes; Question 2: How is DOC transport affected by preferred flowpaths (macropores or "fractures"); Question 3: How is biologically available DOC (BDOC) transported in comparison with refractory DOC; Question 4: How do the hillslope hydrological properties affect the DOC concentration discharge relationship

in the stream; and, Question 5: How does DOC in the groundwater dynamically behave at the watershed scale.

3 Research hypothesis

To address the questions listed in the previous section, the major hypothesis for this dissertation are as follows.

A: Importance of riparian zone on DOC export

Previous works have shown that DOC concentrations decrease with soil depth (Dawson et al., 1981; Mertens et al., 2007; Guo et al., 2010) . Because of strong retention processes, it is reasonable to expect that the transport of DOC from hillslope soils to the water table and hence to streams will be inversely related to the length of the flowpath and residence time in the soils, that is, to the distance from the ground surface to the water table. Vertical flowpaths through the vadose zone to the water table typically are shorter near streams than at upslope locations. Thus we hypothesize that the riparian zone is a primary contributor to the transport of DOC from hillslope soils to streams across a watershed.

B. Hillslope DOC flushing

DOC dynamics in riparian hillslope soils and in adjoining streams are affected by a myriad of factors related to soils, vegetation, and watershed characteristics (Kalbitz et al., 2000). Determining the dominant mechanisms affecting DOC export is important as a process-level understanding can be used to inform generalizations across different watersheds. One general conceptual model of how DOC transport is enhanced during storms is that material accumulates during fair-weather periods and is subsequently leached by storm waters. Hornberger et al. (1994) used such a flushing hypothesis to explain a first-order mechanism of DOC entering a snowmelt dominated stream. This hypothesis suggests that solutes are leached from near-surface layers by a rising water table followed by a rapid lateral transport of these materials

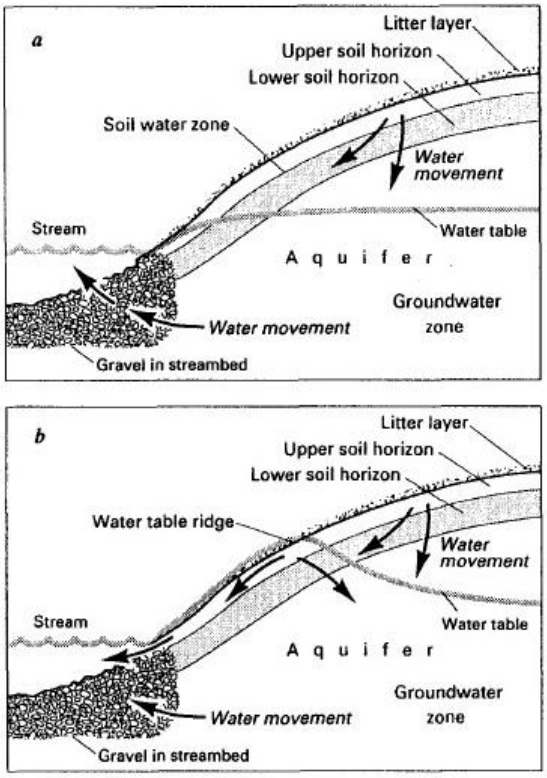

Figure 3: Schematic diagram of the mechanism of soil-water flushing: (a) under low baseflow conditions, subsurface flows are through lower soil horizons; (b) under high flow conditions, the water table is elevated and water flows toward the stream through upper as well as lower horizons (Hornberger et al., 1994)

to the stream via near-surface, saturation excess runoff in the riparian zone (Figure 3)[2]. Boyer et al. (1997) further explored this idea by quantifying characteristics of asynchronous snowmelt and its effect on DOC flushing using both an observational approach and a simple mixing model to understand DOC dynamics, including a peak in DOC concentration in the stream prior to the peak discharge. This hypothesis has not been tested at a mechanistic level using physically-based models.

4 Research objectives

This study seeks to increase the understanding of the role of hydrology in controlling DOC movement from watershed soils to streams. A field experiment, temporal

[2]Reprint with permission from Springer

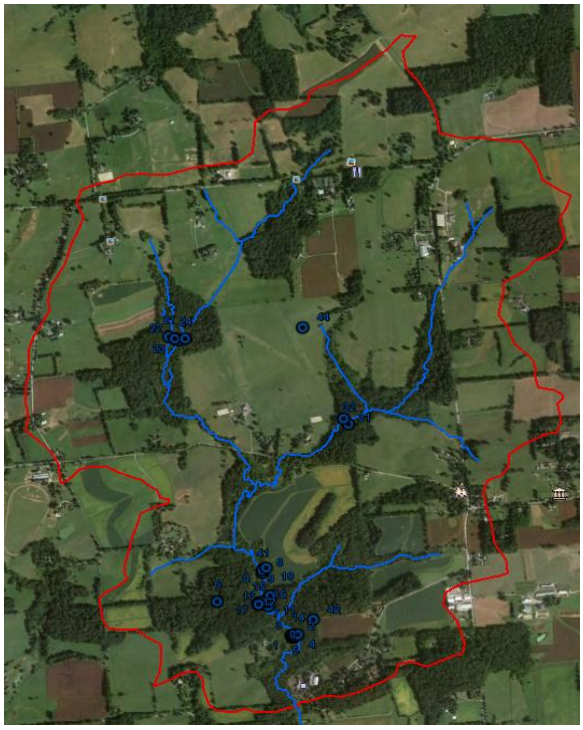

Figure 4: 3th order WCC watershed at the Stroud Water Research Center

monitoring, and mathematical modeling were used in a combined approach in this dissertation work to achieve the goal. The study site is the White Clay Creek (WCC) watershed located in southeastern Pennsylvania (Figure 4)[3]

The primary research objectives for my dissertation are as follows:

1. Conduct field soil core water infiltration experiment and develop a reliable numerical scheme to understand DOC leaching at a process level and scale up the model to the whole watershed.

2. Conduct hillslope field measurements and develop a stable two-dimensional variably saturated flow, heat transport and reactive transport model. Apply this model to the selected hillslope transect.

3. Using watershed hydrology and meteorology data develop a physically-based, distributed catchment scale DOC model and apply it to WCC watershed.

[3]from Google earth

By achieving the project objectives listed above, we will be able to provide some new understanding of the DOC contribution and delivery to streams as controlled by hydrology.

5 Dissertation organization

The first research objective was addressed in work reported in Chapter 2. A dual-permeability one dimensional (one dimensional Euclidean space, considering processes happening in one defined direction) soil core model was developed, calibrated, and verified against the in-situ soil core water leaching experimental data and then up-scaled to the entire watershed to address research questions 0,1,2 and 3. Hypothesis (A) was explored in this chapter. The second research objective was addressed in work reported in Chapter 3. A finite-element model for variably saturated subsurface flow, heat transfer, and DOC reactive transport was developed and calibrated against field hydrology and biogeochemistry data. Research questions 3 and 4 were addressed in this chapter. Hypothesis (B) was explored in this work. The final research objective was addressed in work reported in Chapter 4. A catchment-scale DOC transport model was developed and coupled with the Penn State Integrated Hydrological Model to simulate the hydrology and DOC transport in the White Clay Creek watershed. The model was calibrated using discharge and DOC data from WCC watershed. Research question 5 was addressed in this chapter.

Because each chapter covers topics that are related but in a way that addresses the questions and hypotheses as described above in different ways, an introduction to each chapter provides a review of the relevant literature, and associated detailed mathematical equations are provided for each chapter.

CHAPTER 2

ESTIMATION OF DISSOLVED ORGANIC CARBON CONTRIBUTION FROM HILLSLOPE SOILS TO A HEADWATER STREAM

1 Introduction

[1] Resolving carbon budgets from the small watershed scale to the global scale is requisite for better estimates of the amount of organic carbon exported from terrestrial sources to streams and rivers (Hope et al., 1997). Delivery of allochthonous inputs of organic carbon, including dissolved organic carbon (DOC), from carbon pools in headwater watersheds to stream ecosystems is widely accepted as an important process (Hynes, 1975; Mulholland, 1981; Hynes, 1983; Schiff et al., 1990; Hornberger et al., 1994). Hydrology strongly affects DOC export from terrestrial to aquatic ecosystems by impacting redox biogeochemistry and water flow paths through organic rich soil horizons which are typical DOC sources (Hinton et al., 1997; Schiff et al., 1998; Kawasaki et al., 2008).

It has been extensively reported that DOC concentrations decrease with soil depth including studies performed in forest soils in Washington State (Dawson et al., 1981); a boreal mire in Northeast China (Guo et al., 2010); and a flat agricultural field located near Merzenhausen, Germany (Mertens et al., 2007). All these studies suggest that DOC is removed during flow through a soil profile by biogeochemical processes such as adsorption and microbial activity.

Because of strong retention processes, it is reasonable to expect that the transport of DOC from hillslope soils to the water table and hence to stream will be inversely re-

[1] Reprint with permission from American Geophysical Union

lated to length of the flowpath and residence time in the soils, that is, to the distance from ground surface to the water table. Vertical flowpaths through the vadose zone to the water table typically are shorter near streams than at upslope locations. Thus it follows that the riparian zone is a primary contributor to the transport of DOC from hillslope soils to streams across a watershed. Transport mechanisms have been studied for stormflow responses in particular. For example, the dynamics of DOC transport to streams has been conceptualized as being facilitated by water-table incursions into shallow soil horizons (Hornberger et al., 1994) and by extensions of riparian areas as different parts of hillslopes become hydrologically connected over the course of a storm (McGlynn and McDonnell, 2003). The importance of riparian zone contributions to streamward DOC transport has been inferred from detailed measurements in many locations coupled with mass-balance calculations (e.g., (Dosskey and Bertsch, 1994; Hinton et al., 1998)) and also coupled with regression equations (e.g.,(Kohler et al., 2009)). This focus on stormflow dynamics is understandable given that a large fraction of the total export of organic carbon from forested watersheds occurs during storms (Raymond and Saiers, 2010).

Transport of DOC from hillslope soils to streams under baseflow conditions is also important, if not because of dominant significance to total export of carbon then to the supply of carbon to stream ecosystems during interstorm periods when most of the in-stream processing occurs. Because soil acts as a strong organic carbon "filter under baseflow even more than under stormflow conditions, the riparian zone is also expected to play a large role in regulating DOC transport during interstorm periods. Dosskey and Bertsch (1994) estimated from mass-balance considerations that the bulk of organic carbon in a mid-Atlantic stream originated from riparian wetlands. A quantitative, mechanistic description of DOC transport processes by subsurface flow is lacking at present, however.

We used a field experiment and mathematical model in a combined approach to

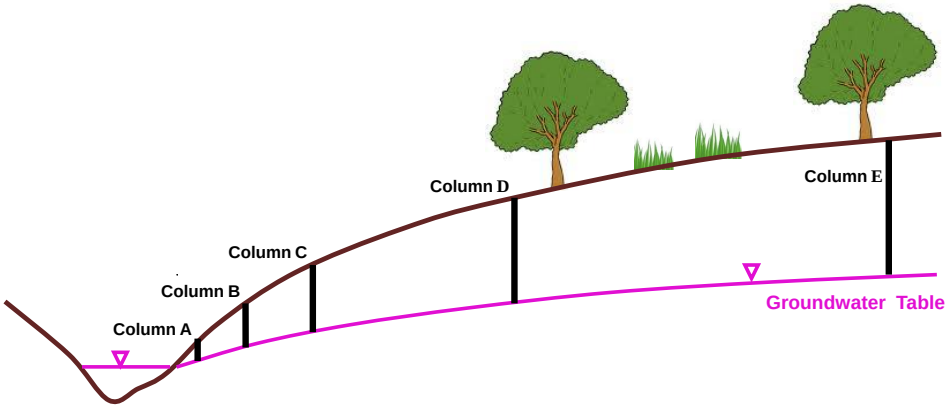

Figure 5: Conceptual diagram of vertical one-dimensional transport with a fixed water table. The DOC concentration at the bottom of each soil column is expected to be inversely related to the soil column length.

address questions related to the transport of DOC from the hillslope to the stream within White Clay Creek watershed, a watershed with a forested riparian zone. The main goal of this research is to examine our hypothesis that the DOC contributed from the land to the stream is primarily derived from the riparian zone, and to estimate the flux of DOC from terrestrial sources to the stream. Our conceptual model (Figure 5) is similar in spirit to that of Seibert et al. (2009), but rather than assume a fixed exponential concentration profile and a dynamic water table to examine stormflow response, we postulate a one-dimensional (vertical) transport through the vadose zone to a fixed water table to examine baseflow and stormflow transport. A flow unit "soil column is defined to represent the flow paths through the vadose zone soils and is assumed to be oriented vertically and extend from the soil surface to the water table. Thus, the entire vadose zone of the watershed can be decomposed into numerous vertical unit soil columns with different lengths. The model simulated DOC transport

through these soil columns with different lengths, and integrated the calculated DOC fluxes to the water table across the whole watershed. We assume that DOC vertically delivered to the water table along each soil column will be transported (laterally) by groundwater to the stream without further sorption or microbial uptake. We use our approach to estimate how DOC transport is affected by preferred flowpaths (macropores or "fractures), how labile biodegradable DOC (BDOC) is transported, and what fraction of DOC transport is from near-stream sources relative to upland parts of the hillslopes. Our results show that a dual permeability model for transport that accounts for preferential flow is required to describe data from experiments on a lysimeter and the model results suggest that a large fraction of DOC transported to the stream during baseflow and stormflow originates in the riparian zone.

2 Methods

2.1 Experiments

2.1.1 Site description and experimental setup

White Clay Creek (WCC) watershed is a 7.25 km^2, 3^{rd}-order watershed located in southeastern Pennsylvania. WCC drains agricultural and forested lands in the Piedmont province of southeastern Pennsylvania and northern Delaware (Newbold et al., 1997). Riparian areas have 30-300 m of mature forest buffer, except for a few meadow study reaches. Uplands are largely under pasture, hay or minimal-till row crops. WCC has a stream gradient of 8 m/km and a mean annual stream flow and precipitation of 0.115 m^3/s, and 1.05 m, respectively (Newbold et al., 1997). The soils are predominantly in the Glenelg-Manor-Chester association (Senior and Koerkle, 2003). Detailed data on the soils in the headwater catchment of this study can be obtained through the Christina River Basin Critical Zone Observatory (`http://www.udel.edu/czo/`). In the WCC, DOC concentrations under baseflow condition ranged from 0.8 to 2.0

ppm C, and increased up to 14 ppm in stream stormflow. Mean DOC concentrations were obtained from historical data for each of the 20 wells in the riparian zone. The mean over the 20 wells is 1.5 ppm, ranging from 0.4 ppm to 9.7 ppm. Statistical data from 3 deep wells located in the upland area show the mean DOC concentration in the upland area is about 0.51 ppm, ranging from 0.2 ppm to 0.9 ppm.

In 2006, soil lysimeters were installed within the WCC watershed on the property of Stroud Water Research Center (Figure 6). Intact soil cores were collected from the riparian zone and upland area of the watershed. Collection of the cores was done by pounding 0.11 m inside diameter PVC pipe into the soil to the prescribed depth, and then excavating the pipe with its intact core. Before reinstalling the cores under field conditions, they were wrapped in plastic and kept in a cool room while end caps to collect water draining from the cores were fabricated and attached. Twenty 0.46 m soil lysimeters, with ten from the riparian zone and ten from the upland area, were prepared in the same way. A field in-situ collection system was prepared by running a separate soil water drain and effluent tube from the end cap at the bottom of each lysimeter to a collection vessel. Drainage tubes were fed through a pipe chase into the collection box installed downslope in an excavated pit (Figure 6).

The field site for reburial of the soil lysimeters was selected under a mixed deciduous canopy on a hillslope along the east branch of WCC. A tree canopy covers the area and acts to provide organic matter to the lysimeters. The lysimeter group is designed to collect water leaching through the lysimeters under natural rainfall conditions over the long term. DOC Samples were collected from the effluent of those soil lysimeters for major storms starting from 2006. One of the lysimeters was made available for experimental additions of water for the research reported here.

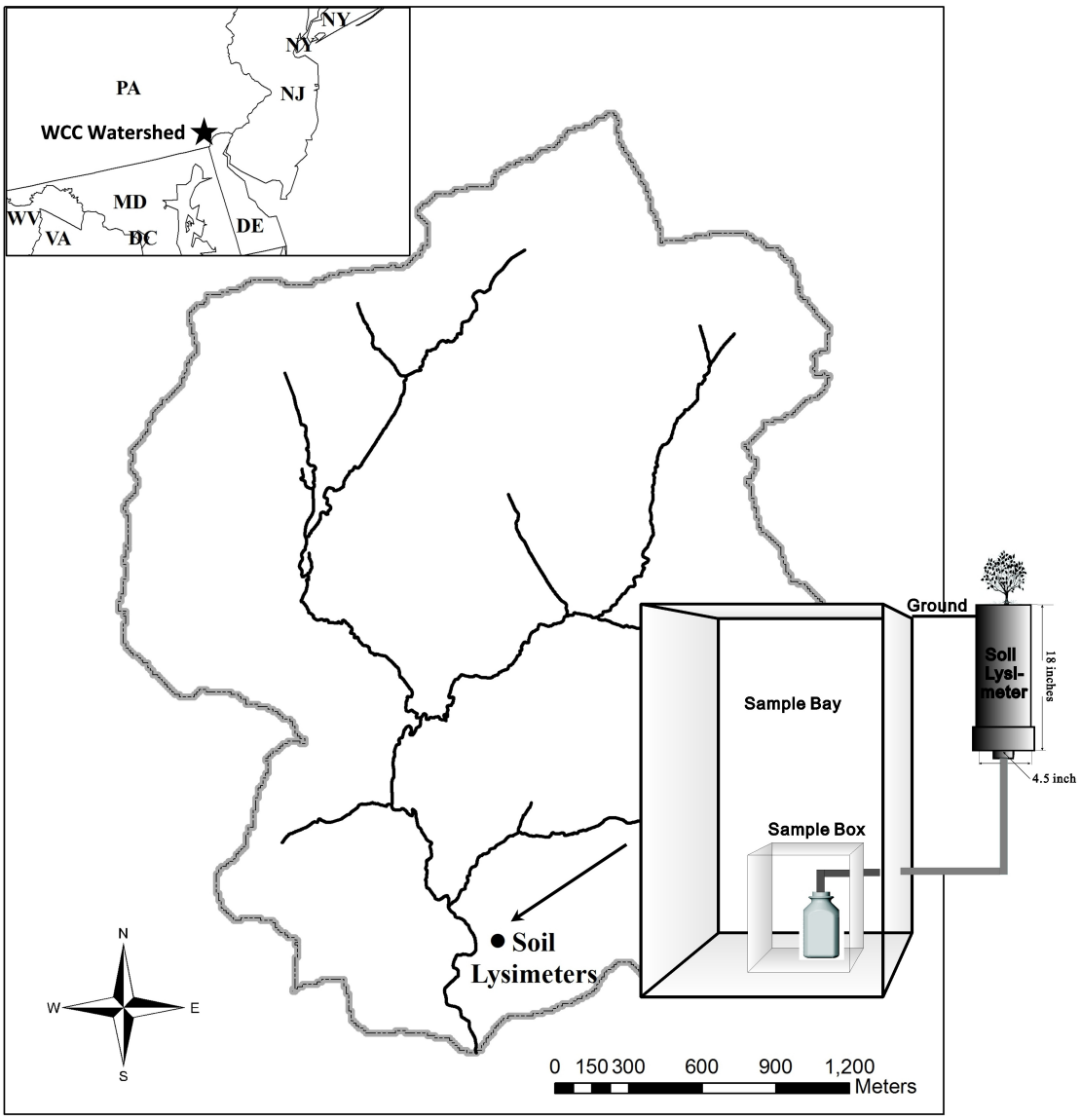

Figure 6: Soil lysimeter location and field setup. The soil core was extracted from the riparian zone and installed at the location marked (395142.85N, 754655.26W). The soil lysimeter has diameter: 4.5 inches and length 18 inches. The perennial forb growing on the lysimeter is *Aster cordifolius.*

2.1.2 Water addition experiments

A 0.46 m length lysimeter was selected for the transport experiment. This soil lysimeter was selected based on previous rainfall and effluent volume data from 2006-2009. The soil lysimeter with the highest correlation between the amount of rainfall and effluent volume was used. Two series of artificial rains were applied to the soil lysimeter on 22 July 2009. Deionized water amended with sodium bromide (1 ppm) was applied to the column.

The artificial rain was applied at a rate of 50 ml of solution every 10 min for 110 min, followed by a 30 min rest period. Subsequently an additional 550 ml of water were applied to the column at the rates described above. In this way, 1100ml of solution were added to the soil lysimeter in 240 min. The first two samples were collected every 20 min. These samples showed that the water came out very rapidly so subsequent sample collection was done every 10 min. Effluent from the soil lysimeter was collected in muffled (500 C for 6 hours) borosilicate bottles. Samples were kept in an ice box before returning them to the laboratory for analysis. A thermometer (Dual JTEK thermocouple thermometer) was used to track the temperature at the top of the soil lysimeter as well as the temperature 3 cm into the lysimeter during the experiments. Soil temperatures were recorded every 10 minutes as the experiments were performed. To avoid creating an artificial flow channel and disturbing the lysimeter, we did not place any soil moisture probes in the soil lysimeter.

After being taken back to the lab, samples were filtered through a pre-combusted 25-mm-diameter 0.7 um glass microfiber filter (Whatman GF/F) held in an acetyl resin syringe-type filter holder (Gelman Sci.). The total volumes for each sample were read through the graduated syringe. Ten ml from every filtered sample were collected and diluted 4X for DOC measurements, and a 5 ml sample was taken from each sample and filtered through a MillexGP 0.22 m filter for bromide analysis. The rest of the samples were Tyndallized (Tyndall, 1876) and kept in the refrigerator until

the initial analysis of DOC was obtained. The uv-persulfate oxidation method was used for DOC analysis (Kaplan, 1992) (Sievers 900 analyzer with inorganic carbon removal module).

2.1.3 Biofilm reactor

Natural DOC is a complex mix of organic compounds (Kim et al., 2006). A key to quantifying DOC dynamics is to establish useful approximations for behavior of this complex mixture. BDOC is defined operationally as the fraction of the DOC that can be metabolized by bacteria within a period of a few days to a few months (Servais et al., 1989) and total BDOC can be separated into labile and semi-labile categories (Kaplan et al., 2008). RDOC is defined to be the rest of the DOC. A number of methods have been proposed to estimate the amount of BDOC in water (Frias et al., 1992; Volk et al., 1994; Kaplan and Newbold, 1995; Yano et al., 2000; McDowell et al., 2006). In this research, a plug flow bioreactor with an empty bed contact time (EBCT) of 0.5 min, patterned after a design previously used for drinking water analysis (Ribas et al., 1991) was used to estimate the concentration of labile BDOC for all the samples. The RDOC and labile BDOC concentration was calculated using the DOC inflow and outflow concentrations from the bioreactors.

A series of bioreactors with different EBCT have been used to separate the labile and semi-labile constituents of BDOC, showing that the pool size of latter is approximately 3-fold larger than the former (Kaplan et al., 2008). The 0.5 min EBCT bioreactor was set up in a room with temperature at 18-20 $^{\circ}C$, covered in foil to eliminate light, and fed by water from WCC. The bioreactor was constructed of a borosilicate chromatography column with polyethylene bed supports (Chromaflex, Knotes) filled with borosilicate glass beads (Siran, Schott) (Kaplan and Newbold, 1995). A peristaltic pump perfuses WCC water through the bioreactor in an upflow direction at 4 ml/min, providing the bacterial inocula, C and energy sources for the

microbial community that colonizes the bioreactor. This bioreactor with a 0.5 min EBCT with a 2 ml bed volume estimates concentrations of the most labile part of BDOC and was used due to the limited sample volume collected.

To avoid significant adsorption reactions and eliminate break through if the microbial community is challenged by more C than it can process over the course of a measurement, the elevated DOC concentrations in the soil solution sample waters were diluted to match the concentrations in WCC water. Diluent was the Tyndallized effluent from a bioreactor with a 2.5 hr EBCT (bed volume 600 ml) that was biologically stable, or BDOC-free, while still providing the inorganic milieu and ionic strength of WCC water. This effluent was mixed with the samples to reduce the DOC concentration to approximately 1.5 ppm. The mixtures were sampled for DOC before applying them to the bioreactor used to estimate labile BDOC. Three bed volumes (6ml) of the sample were sent to waste before starting to collect the effluent. After the desired volume was collected for each sample, the collected effluent was analyzed for DOC concentration. The inflow line of the bioreactor was transferred to a reservoir with WCC water, and a minimum of 3 bed volumes were passed through the bioreactor to waste before starting with the next sample. The original labile BDOC (C_B) and RDOC (C_R) concentration before dilution can be calculated using the following formula:

$$C_R = \frac{C_{lys} - C_{in}}{C_{in} - C_e} \times (C_{out} - C_e) + C_{out} \tag{1}$$

$$C_B = C_{lys} - C_R \tag{2}$$

where, C_{lys} is the original DOC concentration from the soil lysimeter; C_e the DOC concentration of the BDOC-free diluent; C_{in} the inflow and C_{out} the outflow DOC concentration from the bioreactor.

2.2 Model Development

2.2.1 Overview

Our model couples soil water flow with a heat transport model and reactive-transport models for bromide, RDOC and labile BDOC in soil. Dual permeability concepts were used in the model. The soil column was assumed to have two distinct pore systems: fractures (macropores) and soil matrix. Water and solute exchange between the two systems in response to pressure head and concentration gradients (Gerke and van Genuchten, 1993a,b; Simunek et al., 2003). The flow model generates soil moisture distributions and the Darcy velocity field along the soil column at each time step. The calculated flow was used as an input to the transport models. A transient temperature profile of the soil lysimeter was generated by the heat model and was used as input to the BDOC model, which considers the kinetics of the biogeochemical uptake of BDOC.

Our model took soil organic matter (SOM) content as a reasonable simplification of the carbon source pool in the soil lysimeter. The SOM source is modeled to account for leaching from the organic carbon rich layer of soil by soil water. Once converted from SOM to DOC, the biodegradable part is available to be consumed by microbial activity. The SOM values in the model were estimated from previous work in the WCC watershed. SOM values declined from about 25 mg/g at the ground surface to about 0.9 mg/g at one half meter below the ground surface (CM Chen and LA Kaplan, unpublished data), and was divided into two parts, the most biologically-labile part and the refractory part. The most biologically-labile part was assumed to be 10% of total SOM based on the previous results from the bioreactor with EBCT 0.5 min and calibrated.

2.2.2 Mathematical formulation

One-dimensional vertical water flow h-based Richards equations with a root uptake sink term are used to describe the soil water dynamics in the soil column. The soil column was assumed to be homogeneous for macropores and matrix respectively.

$$C_f \frac{\partial h_f}{\partial t} = \frac{\partial}{\partial z}\left(K_f \frac{\partial h_f}{\partial z}\right) + \frac{\partial h_f}{\partial z} - \frac{\Gamma_w}{w_f} - S \tag{3}$$

$$C_m \frac{\partial h_m}{\partial t} = \frac{\partial}{\partial z}\left(K_m \frac{\partial h_m}{\partial z}\right) + \frac{\partial h_m}{\partial z} + \frac{\Gamma_w}{1 - w_f} - S \tag{4}$$

where, subscripts f , m denote the variables in fracture (macropores) and matrix domain respectively; C is specific moisture capacity[L^{-1}]; $h$is the capillary pressure head [L]; K is the hydraulic conductivity [LT^{-1}]; t is time [T]; S is the root uptake sink term [T^{-1}] (Section 5.1);w_f is the fraction of the fractures [-]; and Γ_w is water transfer rate between fracture and matrix [T^{-1}] (Section 5.3).

Convection-dispersion equations were used to describe bromide transport in macropores and soil matrix:

$$\frac{\partial}{\partial t}\left(\theta_f C_f\right) = \frac{\partial}{\partial z}\left(\theta_f D_f \frac{\partial C_f}{\partial z}\right) - \frac{\partial\left(q_f C_f\right)}{\partial z} - \frac{\Gamma_s}{w_f} \tag{5}$$

$$\frac{\partial}{\partial t}\left(\theta_m C_m\right) = \frac{\partial}{\partial z}\left(\theta_m D_m \frac{\partial C_m}{\partial z}\right) - \frac{\partial\left(q_m C_m\right)}{\partial z} + \frac{\Gamma_s}{1 - w_f} \tag{6}$$

where, subscripts f , m denote the variables in fracture (macropores) and matrix domains respectively; D is a hydrodynamic dispersion coefficient [L^2T^{-1}] (Section 5.2.1); C is resident concentration [ML^{-3}], θ is the volumetric soil moisture content[L^3L^{-3}]; q is specific discharge [LT^{-1}]; Γ_s is the solute transfer rate between fracture and matrix pore regions [$MT^{-1}L^{-3}$] (Section 5.3);

We use a single domain model for the heat transport:

$$\frac{\partial}{\partial t}\left(C_p T\right) = \frac{\partial}{\partial z}\left[\lambda\left(\theta\right)\frac{\partial T}{\partial z}\right] - C_w \frac{\partial qT}{\partial z} \tag{7}$$

where, T denotes temperature [K], $\lambda\left(\theta\right)$ is coefficient of the apparent thermal conductivity of the soil [$\mathrm{MLT^{-3}K^{-1}}$]; C_p and C_w are volumetric heat capacities [$\mathrm{ML^{-1}T^{-2}K^{-1}}$] of the porous medium and the liquid phase respectively (Section 5.2.1);

We accounted for both adsorption and microbial uptake in our model for RDOC and BDOC. Adsorption is likely responsible for maintaining low DOC substrate concentrations in the mineral soil and preventing its loss into stream water (Qualls and Haines, 1992). We used a one-site non-equilibrum, first-order rate kinetics model for DOC adsorption, and a first order decay term to represent the biodegradation (Yurova et al., 2008). Sorption was treated as a reversible processes. A first order rate coefficient (τ) and a constant sorption equilibrium distribution coefficient (K_d) were applied to model DOC transfer between sorbed and dissolved phases. Microbial uptake was considered only in the BDOC model. A modified van Hoff equation (Section 5.2.2) was used for the first order rate coefficient to represent temperature effects on microbial uptake in the BDOC model. Soil moisture control on the biodegradation rate was also considered by multiplying the rate coefficient in the first order decay term within the BDOC model by the soil moisture.

The model for RDOC is described by the following equations:

$$\frac{\partial}{\partial t}\left(\theta_f C_{R,f}\right) = \frac{\partial}{\partial z}\left(\theta_f D_f \frac{\partial C_{R,f}}{\partial z}\right) - \frac{\partial\left(q_f C_{R,f}\right)}{\partial z} + \tau_f \rho_f \left(s_{R,f} - K_{d,f} C_{R,f}\right) - \frac{\Gamma_{R,s}}{w_{R,f}} \tag{8}$$

$$\rho_f \frac{\partial s_{R,f}}{\partial t} = -\tau_f \rho_f \left(s_{R,f} - K_{d,f} C_{R,f}\right) \tag{9}$$

$$\frac{\partial}{\partial t}\left(\theta_m C_{R,m}\right) = \frac{\partial}{\partial z}\left(\theta_m D_m \frac{\partial C_{R,m}}{\partial z}\right) - \frac{\partial\left(q_m C_{R,m}\right)}{\partial z} + \tau_m \rho_m \left(s_{R,m} - K_{d,m} C_{R,m}\right) + \frac{\Gamma_{R,s}}{1 - w_{R,f}} \quad (10)$$

$$\rho_m \frac{\partial s_{R,m}}{\partial t} = -\tau_m \rho_m \left(s_{R,m} - K_{d,m} C_{R,m}\right) \quad (11)$$

while the model for BDOC is described by the following equations:

$$\frac{\partial}{\partial t}\left(\theta_f C_{B,f}\right) = \frac{\partial}{\partial z}\left(\theta_f D_f \frac{\partial C_{B,f}}{\partial z}\right) - \frac{\partial\left(q_f C_{B,f}\right)}{\partial z} + \tau_f \rho_f \left(s_{B,f} - K_{d,f} C_{B,f}\right) - \mu_f \theta_f C_{B,f} - \frac{\Gamma_{B,s}}{w_{B,f}} \quad (12)$$

$$\rho_f \frac{\partial s_{B,f}}{\partial t} = -\tau_f \rho_f \left(s_{B,f} - K_{d,f} C_{B,f}\right) \quad (13)$$

$$\frac{\partial}{\partial t}\left(\theta_m C_{B,m}\right) = \frac{\partial}{\partial z}\left(\theta_m D_m \frac{\partial C_{B,m}}{\partial z}\right) - \frac{\partial\left(q_m C_{B,m}\right)}{\partial z} + \tau_m \rho_m \left(s_{B,m} - K_{d,m} C_{B,m}\right) - \mu_m \theta_m C_{B,m} + \frac{\Gamma_{B,s}}{1 - w_{B,f}} \quad (14)$$

$$\rho_m \frac{\partial s_{B,m}}{\partial t} = -\tau_m \rho_m \left(s_{B,m} - K_{d,m} C_{B,m}\right) \quad (15)$$

where, subscripts f,m denote the variables in fracture (macropores) and matrix domain respectively; subscripts R and B denote the RDOC and labile BDOC respectively; s is the soil organic carbon content [MM^{-1}]; $D$is a hydrodynamic dispersion coefficient [L^2T^{-1}]; C is resident concentration [ML^{-3}]; q is specific discharge [LT^{-1}]; K_d is the sorption equilibrium distribution constant [L^3M^{-1}]; τ is the first order mass transfer coefficient [T^{-1}]; ρ is the bulk density of the soil [ML^{-3}]; Γ_s is the solute mass transfer term between fracture and matrix [$ML^{-3}T^{-1}$] (Section 5.3); μ is the first-order microbial DOC mineralization coefficient [T^{-1}].

2.2.3 Numerical implementation

Due to the highly nonlinear nature of Richards equation, some numerical solutions can generate unacceptable mass balance errors (Celia et al., 1990). A fully implicit finite volume scheme proposed by Berg [1999], was adopted to solve the Richards equation in our work to ensure mass balance. This scheme uses a gradually increasing underrelaxation technique to obtain fast convergence and uses a standard chord slope approximation for the storage term C (Rathfelder and Abriola, 1994). Numerical instability issues often occur in solving convection dispersion type equations when the Peclet number is high (Pinder and Gray, 1977; Hornberger and Wiberg, 2005). An upstream scheme was adopted for the convective term to avoid numerical oscillation and overshot for all the transport models in our work (Zheng and Wang, 1999).

The same temporal and spatial discretization was used for all the models. A spatial grid size of 2 cm was used and 1 minute was selected as the time step. A 2m model was used for model calibration. The model length was set to be 1m, 2m, 4m, 8m, 14m, and 22m to simulate the DOC flux to groundwater table at different hillslope positions (Figure 5). The time step was changed to 5 minutes when the model was driven to calculate annual DOC flux to groundwater.

2.2.4 Initial and boundary conditions

For the field experiments, the initial condition of the flow model was adjusted in calibration (Table 1). Initial bromide concentrations were set to zero along the lysimeter. The initial temperature profile was interpolated from the field data. The initial condition for annual simulation of flow model was taken to be a pressure head distribution for zero vertical flow. The final temperature profile from a one-year simulation was used as the initial condition for annual simulation in heat model. An equilibrium initial condition was used for RDOC and BDOC for both macropore and matrix domains for both experimental and annual simulation.

Table 1: Initial and Boundary conditions†

Model	Upper boundaries	Lower boundaries	Initial conditions
Flow model	$K\left(\frac{\partial h}{\partial z}+1\right)\Big\vert_{z=L^-}=Q_0$	Annual: $h\vert_{z=0}=0$ Experiment: $\frac{\partial h}{\partial z}\Big\vert_{z=0^+}=0$	Annual:$h_0(z)=-z$ Experiment: Calibrated
Bromide model	$\left(-\theta D\frac{\partial C}{\partial z}+qC\right)\Big\vert_{L^-}=qC_0$	$(\partial C/\partial z)\vert_{z=0^+}=0$	$C=0$
Heat model	$T\vert_{z=L^-}=T_0(L,t)$	$(\partial T/\partial z)\vert_{z=0^+}=0$	Annual:Results from one year simulation Experiment:Interpolation of data
RDOC model	$(\partial C_R/\partial z)\vert_{z=L^-}=0$	$(\partial C_R/\partial z)\vert_{z=0^+}=0$	$C_{R,0}(z)=s(z)/K_D$
BDOC model	$(\partial C_B/\partial z)\vert_{z=L^-}=0$	$(\partial C_B/\partial z)\vert_{z=0^+}=0$	$C_{B,0}(z)=\frac{\tau\rho s(z)}{K_D\tau\rho+\mu\theta(z)}$

† where h is the soil water capillary pressure head [L]; Q_0 is the prescribed artificial rainfall rate or rainfall data from NOAA station [LT^{-1}]; K is the hydraulic conductivity [LT^{-1}]; C_0 is the pulse-type injection concentration [ML^{-3}], q is the specific discharge [LT^{-1}], C is the residence bromide concentration [ML^{-3}]. T is the temperature [K]; C_R is RDOC concentration [ML^{-3}], C_B is labile BDOC concentration [ML^{-3}].

In flow model, a free drainage boundary was applied at the bottom of the soil lysimeter when the model was used to simulate the field experiments (Table 1). The lower boundary was set to a specific head boundary ($h = 0$) to represent the water table at the bottom of the soil column for annual simulations. A flux boundary condition was applied on the top of the flow model for all the simulations, representing the amount of rainfall (Section 5.1).

To preserve mass balance, a third type boundary condition was used on the top for bromide model as suggested by van Genuchten and Parker (1984). A zero concentration gradient was applied as the lower boundary condition. A Dirichlet boundary condition was applied on the top of the heat transport model and a zero temperature gradient boundary was used at the bottom of the model. For both RDOC and BDOC, a zero concentration gradient boundary was applied at both the top and bottom of the model.

2.3 Model calibration and parameter selection

A priori ranges for van Genuchten model (Section 5.1) parameter values were obtained by running Rosetta, a model developed by USDA (Schaap et al., 2001), using soil

texture information as inputs. The other parameter values for the flow model were obtained from the literature (Vrugt et al., 2001; Simunek et al., 2005; Guber et al., 2006). The ranges of the parameter values for the transport models were also obtained from the literature (Chung and Horton, 1987; Beven et al., 1993; Hopmans et al., 2002; Gu et al., 2007; Yurova et al., 2008) (Table 2).

The models were calibrated in sequence. A trial and adjustment method was used to calibrate all the models initially and subsequently UCODE (Poeter and Hill, 1999), developed by USGS, was used for parameter optimization for selected parameters. Initial conditions and flow model parameters have a significant effect on the calculated bromide breakthrough curve, so the flow model and bromide model (dispersivity) were calibrated together. After parameters of the flow model and the dispersivity value of the bromide model were selected, they were used in the RDOC and BDOC model. Trial values of the equilibrium distribution coefficient K_d, and the first order rate coefficient τ in the RDOC model and K_d, τ, and basal microbial DOC mineralization rate μ_{basal} in the BDOC model were obtained from the literature and calibrated using the experimental data.

Table 2: Input parameters for the model

Parameters	fracture/matrix	Source
van Genuchten soil characteristic parameter,α, 1/cm	0.0059/0.004	Calibrated, Rosetta and range from Guber et al. [2006]
van Genuchten soil characteristic parameter, n, -	1.7/1.4	Calibrated, Rosetta and range from Guber et al. [2006]
Saturated soil moisture, θ_s, -/-	0.4/0.4	Calibrated, Rosetta and range from Guber et al. [2006]
Residual soil moisture, θ_r, -/-	0.005/0.054	Calibrated, Rosetta and range from Guber et al. [2006]
Saturated hydraulic conductivity, K_s, cm/min	32/0.9	Calibrated
Empirical constant for root water uptake distribution, a^*, cm-1	1.0/1.0	J. Simunek et al. [2005]
Osmotic head when water extraction rate is reduced by 50%, h50	-53.3/-53.3	Vrugt et al. [2001]
Experimental constants in root water uptake stress response function, p, -	3.0/3.0	J. Simunek et al., [2005]
RDOC sorption distribution constant, K_d, L/g	0.29/5.7	Calibrated, Range from Yin et al.[2002]
BDOC sorption distribution constant, K_d, L/g	0.359/4.9	Calibrated, Range from Yin et al.[2002]
RDOC first order mass transfer coefficient , τ, min^{-1}	1.3e-7/1.3e-7	Calibrated, range from Gu [2007]
BDOC first order mass transfer coefficient, τ, min^{-1}	1e-7/1e-7	Calibrated, range from Gu [2007]
Longitude dispersivity of bromide, RDOC and labile BDOC, α_L, cm	37.4/2.18	Calibrated, range from Beven [1993]
Empirical constant for hydrodynamic dispersion coefficient, n, -	1.0/1.0	Beven [1993]
Soil Bulk density, ρ, g/L	1200.0/1200.0	Unreported data in WCC watershed
Reference temperature, basal rates of microbial DOC degradation rates, T_{basal}, °C	20/20	Yurova et al [2008]
Relative rate of increase in metabolic rates per 10 °C, Q_{10},	1.7/1.7	Yurova et al [2008]
DOC biodegradation rate at temperature T_{basal}, μ_{basal}, 1/min	5e-7/9e-7	Calibrated range from Yurova et al [2008]
Volumetric fraction of solid phase, θ_n, -/-	0.6	$1 - \theta_s$,
Volumetric fraction of organic phase, θ_o, -/-	0.001	J. Simunek et al [2005]
Volumetric water heat capacity, C_w, Jm^{-3}K^{-1}	4.18e+6	J. Simunek et al [2005]
Empirical parameter for thermal conductivity , b_0	0.234	Chung and Horton [1987]
Empirical parameter for thermal conductivity, b_1	0.392	Chung and Horton [1987]
Empirical parameter for thermal conductivity, b_2	1.53	Chung and Horton [1987]
Thermal dispersivity, β, m	1.8	Calibrated using UCODE
First-order transfer coefficient for water between matrix and fracture, a_w, (cm*min)$^{-1}$	2.0e-8	Calibrated, range from Gerke and van Genutchen [1993]
Solute transfer coefficient, a_s, min^{-1}	0.0001	Calibrated, range from Gerke and van Genutchen [1993]
Volumetric weighting factor, w_f	0.4	Calibrated from Experimental Data

2.4 Annual DOC recharge to groundwater

Meteorological data for 1997 were used to drive the calibrated model for an annual simulation. Due to the lack of an annual soil temperature record at our research site, we used data from Ellicott, Howard County, MD as an upper boundary for the heat model. This site is about 70 miles southwest of our research site. Good correlation was found between the recent soil temperature data there and the contemporaneous

soil surface temperature measured in the WCC watershed.

The regional water table is considered a subdued replica of the land surface under certain conditions (Haitjema and Mitchell-Bruker, 2005). This concept was used to generate the groundwater level distribution for the WCC watershed. The elevation of the water table measured in wells relative to the elevation of the nearest stream channel was regressed against horizontal distance of the well from the stream. The resulting regression equation was applied to the watershed to estimate the distribution of depth to water table below ground surface (Tsang et al., 2013). After the groundwater depth distribution was generated, the watershed was divided into 6 groundwater depth regions (Figure 7). The model was run for these six regions using a representative length of soil column above water table for each region. RDOC and labile BDOC annual fluxes to groundwater for 1997 were obtained for each region and summed to get the total DOC recharge to groundwater estimated for 1997.

2.5 Uncertainty analysis

The experimental condition in the field is imperfect. The data obtained from the experiment are inadequate to calibrate rigorously the dual permeability model. We implemented an uncertainty analysis to assess the effect of the lack of a rigorous calibration. Our goal for the uncertainty analysis is to show how the variation of parameters that describe soil properties affects the model output regarding the annual DOC subsurface transport to the stream.

The sensitivities of all the parameters for the system were evaluated using UCODE. Composite Scaled Sensitivity (CSS) was used as a measure for the sensitivities of parameters in the RDOC and BDOC model (Hill, 1998). The rank of the CSS value were calculated (Figure 8). The five parameters with the highest CSS values were selected for uncertainty analysis. Monte Carlo simulations were conducted by selecting parameter values from within designated ranges (Table 3) using a Latin Hypercube

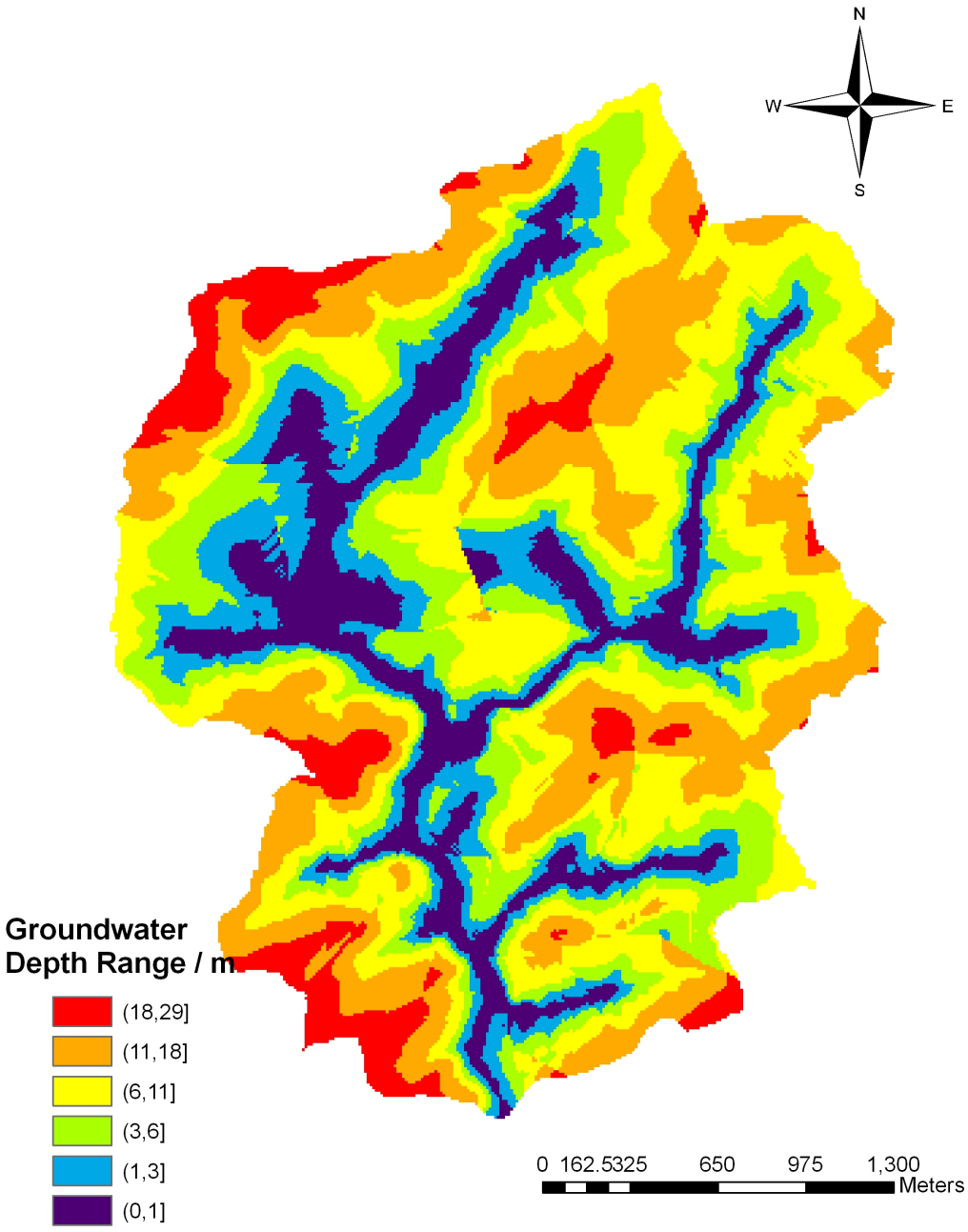

Figure 7: Groundwater depth distribution. The watershed was divided into 6 groundwater depth regions. The representative lengths for groundwater depth used in simulations are 1m, 2m, 4m, 8m, 14m, and 22m for the six regions.

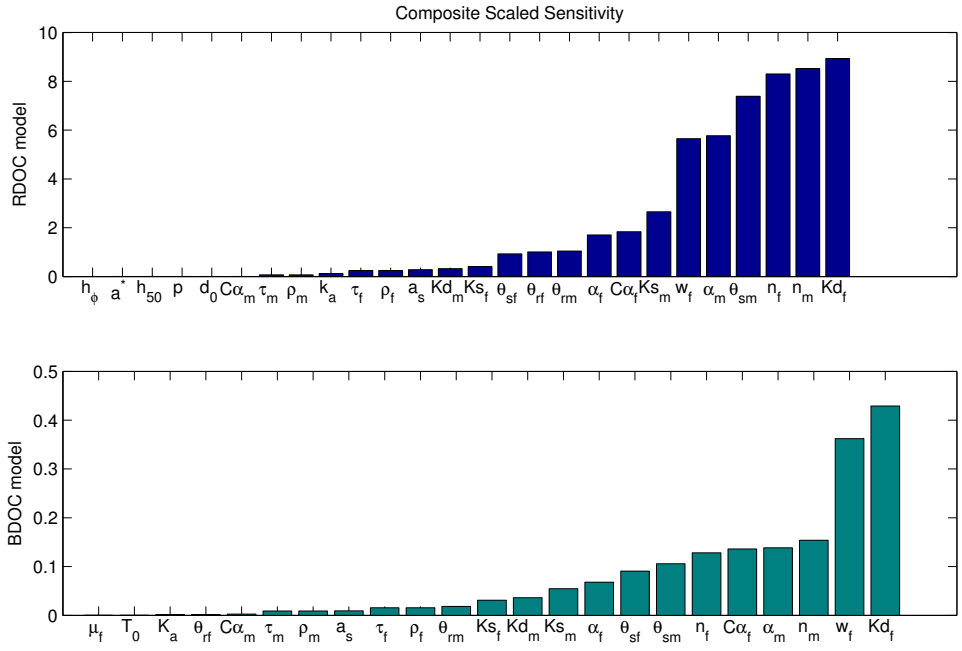

Figure 8: Rank of the Composite Scaled Sensitivity values for all the parameters.

Sampler (LHS) (McKay et al., 1979). Those selected parameters are van Genuchten parameters as well as the longitudinal dispersivity of DOC in the soil. These parameters represent the variation of the soil properties (van Genuchten parameters) as well as variation of a transport property (dispersivity) of the soil of the watershed. Fifty Monte Carlo realizations were performed for each soil column and for both RDOC and BDOC models, ten times the number of selected parameters as suggested by Sieber and Uhlenbrook (2005). The integration of DOC flux from the whole watershed for both the RDOC model and the BDOC model were treated as one realization during the LHS sampling. The distribution of the total DOC export was obtained by calculating the statistics of all the 50 Monte Carlo realizations results.

Table 3: Range of parameters and composite scaled sensitivity (CSS)

RDOC model[b]	Rank	CSS	Calibrated value	Min[a]	Max	BDOC model	Rank	CSS	Calibrated value	Min	Max
Kd_f	1	8.93	0.29	0.23	0.34	Kd_f	1	0.43	0.36	0.28	0.43
n_m	2	8.53	1.40	1.26	1.54	w_f	2	0.36	0.4	0.36	0.44
n_f	3	8.3	1.70	1.53	1.87	n_m	3	0.15	1.4	1.26	1.54
θ_m	4	7.39	0.40	0.36	0.44	α_m	4	0.14	0.004	0.0036	0.0044
α_m	5	5.77	0.004	0.0036	0.0044	αL_f	5	0.14	37.4	31.79	43.01

[a] Min and Max mean the minimum and maximum value of the parameter sampling range. Our calibrated value of Kd_f is within the range provided by Yin et al. (2002). We used minus and plus 20% of the calibrated value as the uncertainty, which is in accordance with data shown by You et al. (1999). The sampling range of van Genutchen model parameters n for the fracture and matrix domain, θ_s_m and α_m were set as minus and plus 10% of the calibrated value, as suggested by Rosetta output.

[b] The top five parameters in Composite Scaled Sensitivity ranking are listed. f and m denote the parameters in fracture and matrix respectively.

3 Results

3.1 Experimental results

Bromide concentrations rose at the beginning of the breakthrough curve and then decreased 70 min after the beginning of the first application of water (Figure 9). Concentrations continued to decrease until we applied the second artificial rain. Bromide concentration started increasing again when the second water application was initiated and decreased again after water application ceased.

The highest DOC concentration of 20 mg C/L was obtained from the first sample in the effluent, and then concentrations dropped rapidly and reached a relatively constant value of 6-8 ppm (Figure 9). The DOC concentration held steady at approximately the same level until the second application of water. DOC concentration increased slightly at the beginning of the second artificial rain and then declined until water outflow ceased. Only low concentrations of labile BDOC were detected, and these in only 9 of 17 samples (8 samples with zero labile BDOC concentration). The pattern of our experimental results is consistent with the pedon results from Jardine et al. (1990).

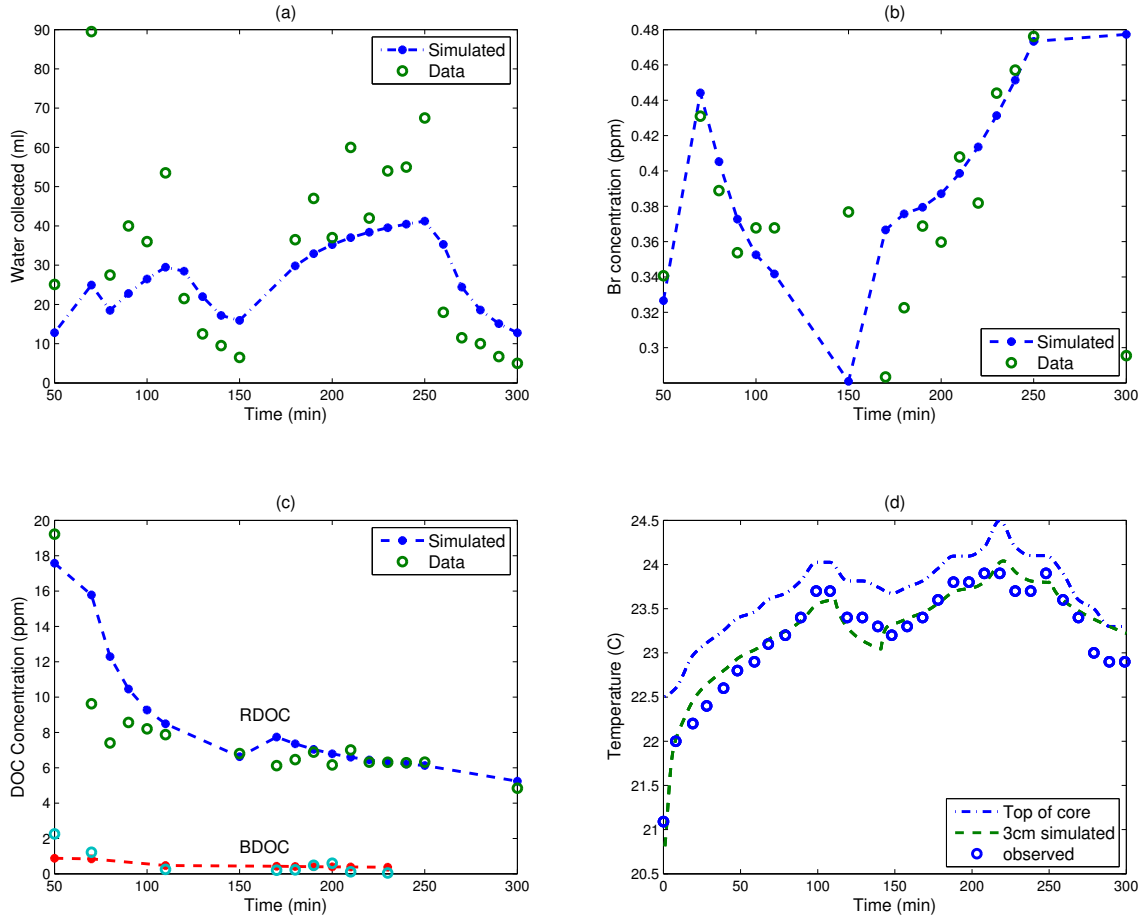

Figure 9: Calibration results for all the models: (a) water flow; (b) bromide; (c) RDOC and labile BDOC; (d) temperature. Open circles represent the experimental data, and the lines represent model simulation results.

3.2 Simulation results

The observed water flux, bromide, RDOC, temperature, and labile BDOC data were used to fit the model. The output from the calibrated model matched the observed data reasonably well (Figure 9).

As expected, the model shows that water flow is faster in fractures than in the matrix. Bromide in the fracture domain breaks through first due to higher dispersivity and faster flux of water in this region (Figure 10); water in the matrix starts to break

through and mix with the solution from the fracture domain after a short time period, which decreases the total effluent bromide concentration because the matrix water is more dilute. The concentration of bromide keeps decreasing once breakthrough occurs from the matrix due to a larger portion of total flow low concentration bromide coming from the low-bromide soil matrix region. When the second flush of water reaches the bottom of the column at about 150 minutes, the effluent concentration builds up because the growing bromide concentration from the first water application is pushed from the matrix to mix with the high bromide water from the macropores. This upward trend in concentration persists until the end of the simulation because the slowly increasing concentrations from the matrix outweigh decreases in concentration in the macropores. RDOC and labile BDOC in the column at the start of the simulation were flushed initially from both the fracture and matrix regions, followed by dilution by the applied artificial rain.

The mass transfer pattern between two domains behaved as expected (Figure 12). The pressure head of the fracture region builds up faster than for the matrix due to the higher permeability of this domain. The pressure difference between the fracture domain and the matrix domain initially drives water transfer from fractures to the matrix. As the water moves along the column, the pressure peak in the fractures moves down the column, so the water transfer rate peak also moves downward with time. After the water application is stopped, the water pressure drops faster in the fracture domain than in the matrix, and water is transferred from the matrix to fracture along the soil column at the end of the experiment. The simulation results show that RDOC and labile BDOC are always transferred from the fracture domain to the matrix domain.

The simulation results for DOC recharge to groundwater across the WCC watershed showed that the riparian zone (groundwater depth less than or equal to 1m) contributes the largest fraction of DOC to groundwater, accounting for about 91% of

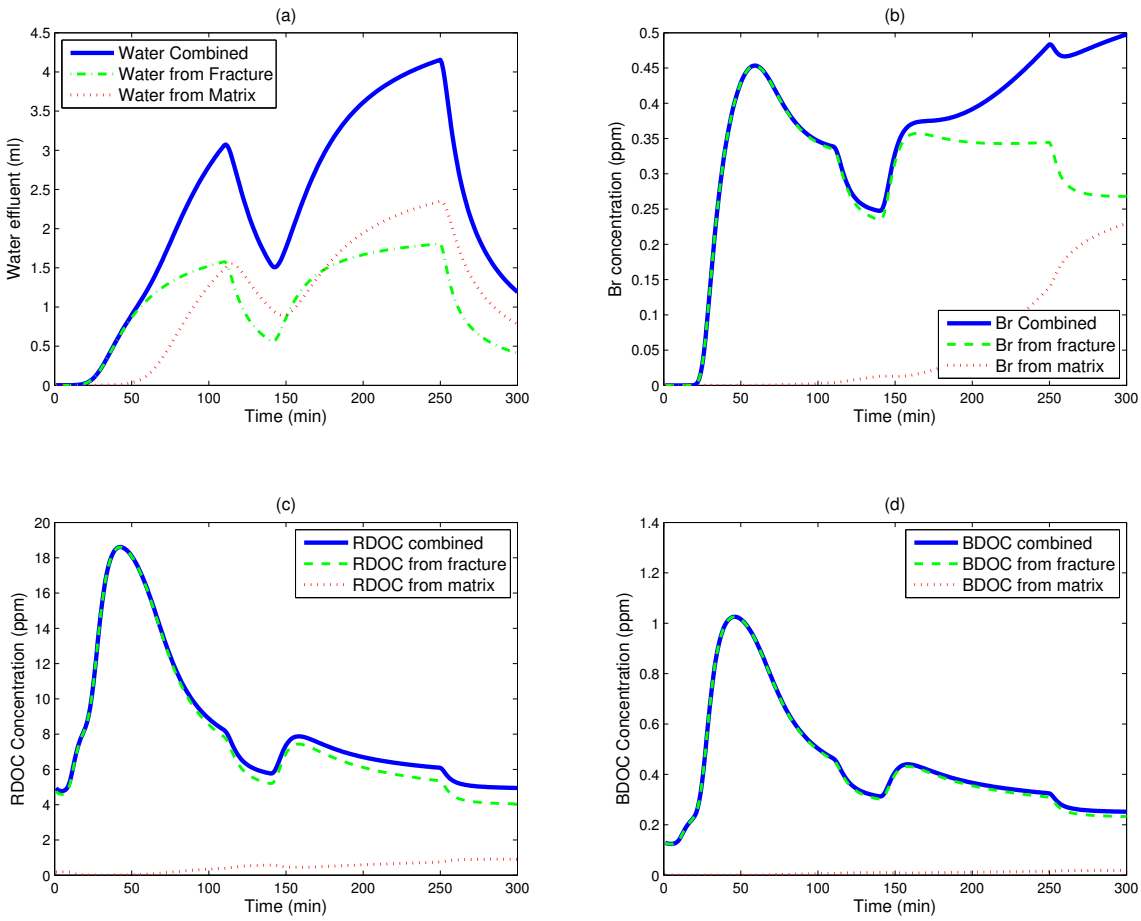

Figure 10: Dual permeability mixing of water, bromide, RDOC and labile BDOC from macropores and matrix domains: (a) simulated amount of water flow; (b) simulated bromide concentration; (c) simulated RDOC concentration; (d) simulated labile BDOC concentration.

the DOC flux (Table 4). The area of groundwater depth from 1 to 3m contributes the second largest portion of DOC, about 8.8%. The rest of the area contributes less than 1% in total. The total amount of labile BDOC is about 6% of the total amount of RDOC, which based on our experimental design would include the semi-labile fraction of BDOC. With the assumption that all DOC delivered to the water table is exported from the watershed, the estimate for the total amount of DOC export from subsurface flow in 1997 is about 6600 kg C/year using the calibrated parameters.

Table 4: Annual DOC recharges groundwater for each of the subareas [a]

GW Depth range (m)	Depth of the Column used (m)	Area(m^2)	RDOC flux(kgC year-1m-2)	Labile BDOC flux(kgC $year^{-1}m^{-2}$)	RDOC flux for each area(KgC $year^{-1}$)	Labile BDOC flux for each area (KgC $year^{-1}$)	DOC from fast flow region (Kg C $year^{-1}$)	Total DOC Recharge Percentage(%)[b]	Percent of DOC from fast flow region(%)
(0,1]	1	9.1E+5	6.1E-3	3.9E-4	5.6E+3	3.6E+2	5.5E+3	91.1	92
(1,3]	2	1.0E+6	5.3E-4	3.5E-05	5.4E+2	3.5E+1	5.5E+2	8.8	95
(3,6]	4	1.3E+6	3.5E-06	0.0	4.5	2.9E-1	4.5	0.07	95
(6,11]	8	1.9E+6	0.0	0.0	9.6E-3	8.2E-4	0.0	0.0	-
(11,18]	14	1.6E+6	0.0	0.0	7.4E-5	0.0	0.0	0.0	-
(18,29]	22	5.1E+5	0.0	0.0	0.0	0.0	0.0	0.0	-
Total		7.2E+6			6.2E+3	3.9E+2	6.1E+3	100	92.6[c]

[a] All the calculated values less than 1.0E-6 were taken as zero in the table.
[b] Total DOC flux from each area / Total DOC recharge of the whole watershed.
[c] Total DOC flux from macropores / Total DOC flux

The uncertainty analysis results show that for the given parameter space for selected parameters, the output distribution of estimated annual DOC subsurface export follows a normal distribution at the 5% significance level using a one-sample Kolmogorov-Smirnov test, with a mean 6600 kg/y, standard deviation: 520 kg/y (Figure 11). The sensitivity results (Table 3) can be interpreted in light of this computation. As reported by (Hill and Tiedeman, 2007), the CSS value can be interpreted as the average amount that the simulated values of DOC export would change given a one percent change in the parameter value. This sensitivity is expressed as a percent of the standard deviation of the observation error. The calculated values of the CSS indicate that the most sensitive parameter in the RDOC model is Kd in the fracture domain with a CSS value 8.93. A one percent change of the Kd value would produce

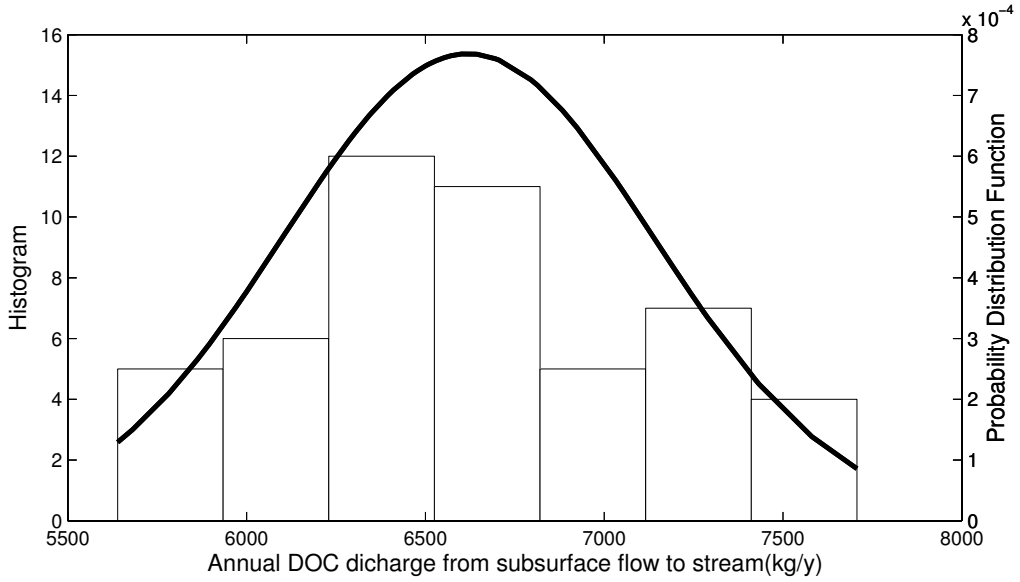

Figure 11: Distribution of the Latin Hypercube Sampling results. The mean of the annual DOC subsurface flux to stream is about 6600 kg/y in 1997; the standard deviation is 520 kg/y.

a change in the simulated DOC result equivalent to 8.93% of the standard deviation 520 kg/year, which is 46 kg/year. The van Genuchten parameter n in the matrix domain ranked second with a CSS value 8.53; a one percent change of n would result in a 44 kg/year change in the calculated DOC export; The most sensitive parameter in the BDOC model is also Kd in the fracture domain with a CSS value 0.43; a one percent change of this parameter would result in about a 2 kg/year change in the calculated total DOC export.

4 Discussion

Mathematical models play an important role in understanding and predicting DOC flux in soil and its delivery to streams. Early attempts to model DOC dynamics used a lumped hydrological model together with a simple DOC model. Grieve used the Birkenes model together with a DOC submodel to test soil water DOC flux (Grieve, 1991); Boyer et al. (2000) used TOPMODEL combined with a simple mixing model to quantify characteristics of the asynchronous snow melt and its effect on DOC flushing.

Further, several process-based models of DOC in soils have been developed (Neff and Asner, 2001; Michalzik et al., 2003). A model of DOC flux in mire water based on a simple model coupled with convection-dispersion equations was put forward by Yurova et al. (2008). These authors pointed out that a more appropriate hydrological scheme than they used was needed to describe water flow. Xu and Saiers (2010) applied a modified version of a two-domain, mobile-immobile model to describe the mobilization and transport of DOC through a forest soil during simulated rainfall events.

Our experimental results from a single field lysimeter indicate that a dual permeability hydrological model is necessary to describe DOC transport in WCC. A traditional convection dispersion model (single domain model) was used to test the data prior to the dual permeability approach described here. It failed to explain the bromide concentration dropping at 70 min after the start of our experiment, with concentration increasing until 110 min, which contradicts the experimental data (Figure 9). Our dual permeability approach does explain the observed pattern. Although dual permeability models are routinely used to represent the effects of macropores on transport of organic contaminants (e.g., pesticides) (Gardenas et al., 2006; Kodesova et al., 2009), they are not routinely used for modeling transport of natural organic matter in forested watersheds. As pointed out by Kalbitz et al. (2000): The high adsorption capacity of soil clay minerals and oxides for DOM shown in laboratory studies may not control the transport of DOM in soils in the field if macropore fluxes dominate under field conditions.

Our work represents an attempt to evaluate macropore effects on DOC transport in the field. For our soil lysimeter experiments, the transfer rates of RDOC and labile BDOC for the calibrated model are positive, indicating that DOC is always transferred from macropores to matrix during the experiment (Figure 12). These model results indicate that part of the DOC in macropores is transferred to the matrix,

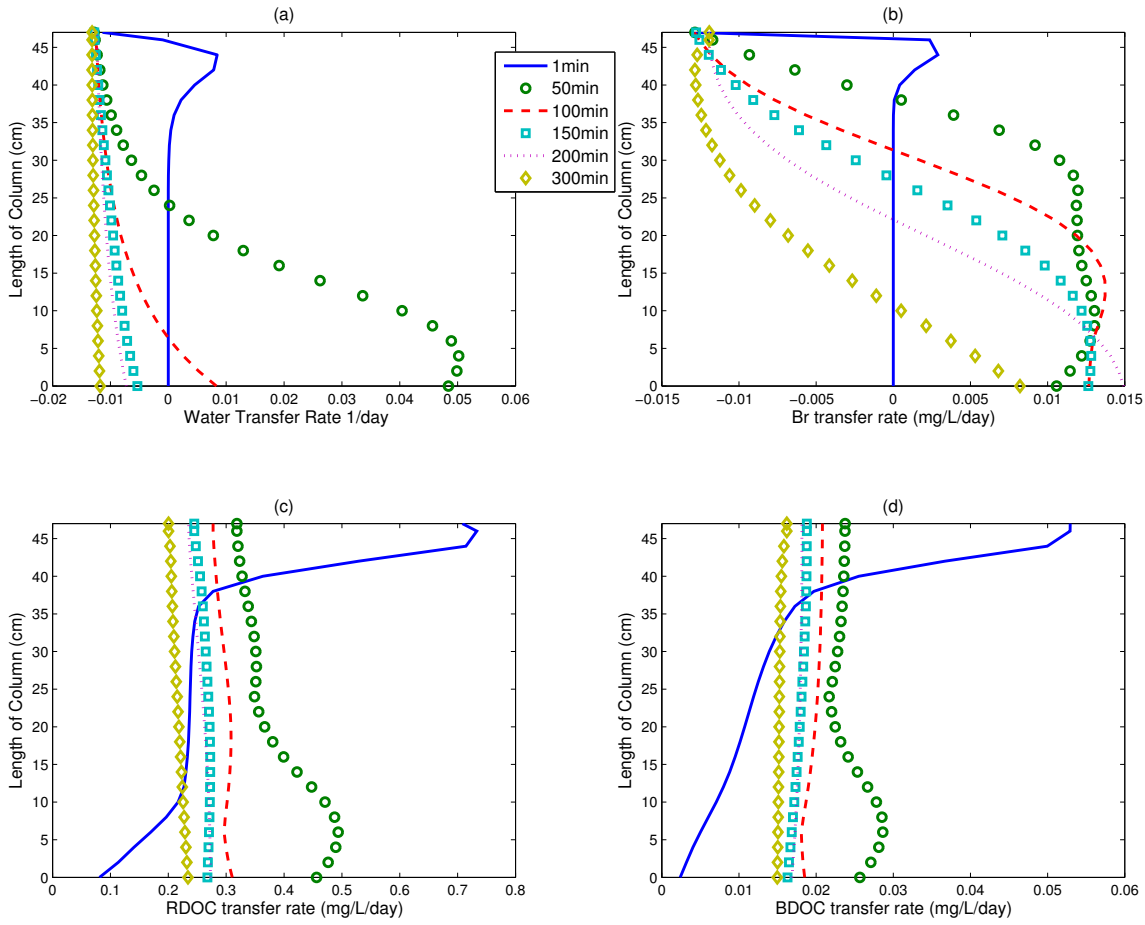

Figure 12: Simulated mass transfer rate between macropores and matrix along the soil lysimeter (0 to 46 cm is from bottom of the soil lysimeter to the top). Positive values indicate mass transfer from macropores to the matrix, negative values indicate mass transfer from matrix to macropores: (a) mass transfer rate for water; (b) mass transfer rate for bromide; (c) mass transfer rate for RDOC; (d) mass transfer rate for labile BDOC.

where the vertical DOC migration rate is slower, and a part is either transported to the water table or sorbed to soil within the macropore domain. The calculated annual DOC recharge from macropores to groundwater in 1997 accounts for about 92% of the total amount of vertical DOC flux through soils to the water table, suggesting that macropores have a significant control on DOC transport in the WCC watershed (Table 4). This estimate for the fraction of total transport due to macropore flow seems rather high. (Vidon and Cuadra, 2010) observed a prominent role for macropore transport and point out that the contribution of macropore flow to total flow significantly increased with precipitation amount. In our research, in order to obtain enough water for labile BDOC analysis, we applied rainfall at rates which exceed those of most storms in a given year, but are similar to a five-year storm in Chester County, PA (Cahill, 1994). This might affect the model calibration. Nevertheless, the important point is that our estimate suggests a dominant role for macropore transport. This observation is consistent with other reports indicating that, at least under certain conditions, macropore flow can be important for transport of dissolved and suspended constituents, including DOC (Jarvis, 2007). Kumar et al. (1998) indicate that atrazine transport in an agricultural soil is essentially completely dependent on macropore flow. The model used by Michalzik et al. (2003) to explain observations at several temperate watersheds assumes 100% transport in macropores.

We used our model to calculate the annual DOC flux to groundwater for 1997. Although this calculation represents a bold extrapolation that assumes that the conditions embodied in the conceptual and mathematical models hold for the entire catchment, we think that it is still interesting to look at the implications of such a calculation. A fairly complete stream DOC sampling at the outlet of WCC was done in that year (Kaplan and Newbold, 2002) and thus we can compare our estimate of total DOC transport by groundwater with the total annual export of DOC from WCC as measured at the watershed outlet. The annual export of DOC from WCC

in 1997 was about 9200 kg C (Kaplan and Newbold, 2002). The estimated annual DOC recharge to the groundwater from the model was about 6600 kg C, which, with the assumption that this represents DOC transported to the stream, can be taken as an estimate of subsurface export of DOC from the watershed. Although this assumption cannot be literally true, given the observed steep declines in DOC along vertical flow paths (e.g., (Kawasaki et al., 2005)) it is a reasonable first approximation. The estimated portion of DOC exported through subsurface flow using our model incorporates the assumption that the only impact of transient flows in the vadose zone due to precipitation events is to deliver DOC from soils to the groundwater table. Although there is no explicit treatment of lateral flows through the riparian zone during storms, the computation can be taken to include implicitly the subsurface flow that would be counted as stormflow. The computation indicates that subsurface export from the riparian zone may account for 72% of the total DOC export in WCC. Newbold et al. (1997) estimate that about 30% of the total input of dissolved organic matter to WCC is from groundwater inflow under baseflow conditions, so we can infer that the remaining 42% is due to subsurface stormflow. Based on the uncertainty analysis using plus or minus two standard deviations, the DOC flux to the stream from subsurface flow ranges from 5600 kg to 7600 kg. This indicates that the subsurface export fraction of total DOC from WCC ranges from 61% to 83%, with the contribution from subsurface storm flow ranging from 31% to 53%. This estimate is broadly consistent with an estimate for the WCC watershed that between 1996 and 1998 75% of the annual DOC flux occurred during storms (Kaplan and Newbold, unpublished data) and results reported by others. Raymond and Saiers (2010) estimate that 86% of DOC export from forested watersheds in the Eastern U.S. occurs during storm events but do not distinguish whether the stormflow is from a subsurface path. Dosskey and Bertsch (1994) estimate that 90% of the carbon transported from a watershed in South Carolina is from riparian wetlands and that 50% is exported under baseflow.

McGlynn and McDonnell (2003) and Sanderman et al. (2009) show that subsurface stormflow is a major influx of DOC to streams, with stream DOC highest on the rising limb of the hydrograph because a large source of labile DOC is made available for lateral subsurface transport to the stream from riparian soils early during storm events.

It has been suggested that the DOC contribution from the landscape to the stream is mostly from the riparian zone (Hornberger et al., 1994). DOC produced in the upland areas of the watershed will be strongly sorbed, and consumed by biogeochemical process along flow pathways in the soil, so DOC from upland areas of hillslopes is not likely to affect the stream DOC concentration (Wallis, 1979). Our model is consistent with this expectation, showing that 91% of the total DOC and the labile BDOC that reaches groundwater is from the region (12% of the watershed area) where the depth to the water table is less than or equal than one meter. The majority of the watershed area where the depth to the water table is greater than 3 meters (73% of the watershed area) contributes less than 1% of the DOC to the groundwater. This indicates that most of the labile BDOC and the RDOC in the subsurface contribution to the stream is from the riparian zone of the watershed.

Our research scales up the one-dimensional model by horizontally integrating the vertical soil column across the watershed assuming a uniform soil type, land use, and land cover. Nelson et al. (1993) point out that different soil types can affect DOC dynamics in soils by virtue of their different adsorption capacity. In this research, DOC sampling results from all the 20 lysimeters (0.46 m) from 2006 to 2010 during different rainfall events were used to provide background information for the effects of spatial variability of soil properties on DOC flux. Monte Carlo simulations were implemented for 20 single rainfall events in 1997, by sampling the selected parameters within our designated ranges. The simulated range of the total DOC eluted is from 2.2 mg to 6.2 mg, and the distribution of values is consistent with observations (Figure

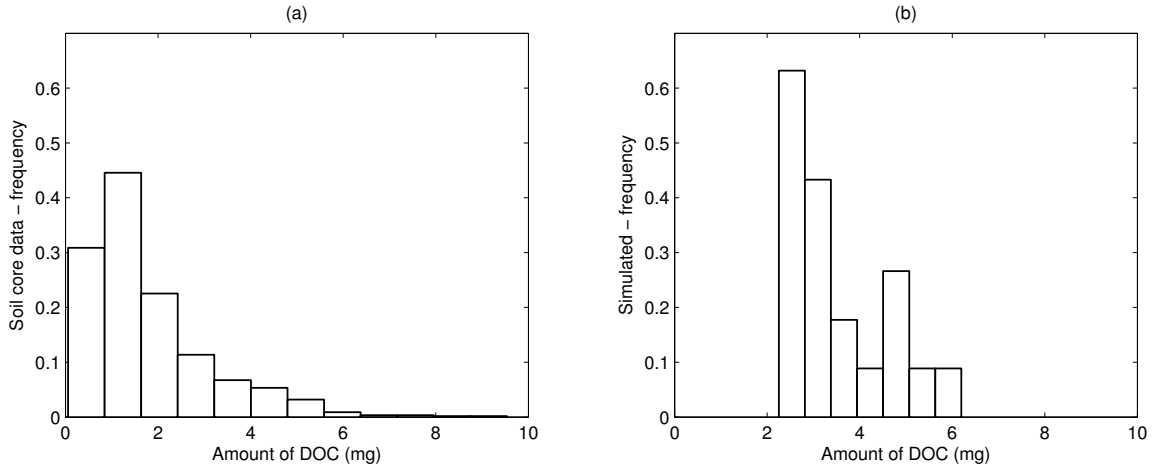

Figure 13: DOC flux from soil cores (0.46 m length) for single events. (a) Field data from 20 lysimeters from 2006 to 2010, 713 DOC samples were used in total. (b) Monte Carlo simulation results of the selected 20 rainfall events in 1997.

13). This result is comparable to the field data, which shows a DOC flux for single events ranging from 0.05 mg to 9.5 mg. We infer from this that our sensitivity analyses appropriately bound the soil variability in the watershed with respect to DOC elution.

Water table fluctuations and lateral flow to streams were not considered in our modeling approach. The groundwater level in the riparian zone rises when the stream stage rises rapidly during the rain. DOC flux to the groundwater will increase when the water table reaches major DOC sources in the upper soil layers. DOC flux removal along the lateral groundwater flow path is not considered in this work. Nevertheless, our main goal in this work was to explore the idea that the most influential area within the watershed for delivering DOC to the stream is the riparian zone, and the assumptions we adopted allow the assessment. A more sophisticated model taking into account DOC removal along groundwater lateral flow paths, the effects of variability in soils and land cover, and the dynamic conversion of near-stream potions of the vadose zone into saturated zones that contribute DOC to the stream through lateral flow would be needed to refine the estimates we present.

5 Detailed mathematical formulations for chapter 2

5.1 Formulations in the one dimensional flow model

The unsaturated soil hydraulic properties of the soil columns were described by a set of closed-form equations (van Genuchten, 1980). The soil water retention function is given by:

$$S_e = \frac{\theta - \theta_r}{\theta_s - \theta_r} = \left(\frac{1}{1 + |\alpha h|^n} \right)^m \tag{16}$$

The hydraulic conductivity function is:

$$K = K_s {S_e}^{1/2} \left[1 - \left(1 - {S_e}^{1/m} \right)^m \right]^2 \tag{17}$$

where θ is soil moisture content $[L^3 L^{-3}]$; θ_r is residual soil moisture content $[L^3 L^{-3}]$; θ_s denotes saturated moisture content $[L^3 L^{-3}]$; α is an empirical parameter $[L^{-1}]$; n and m are related empirical parameters, $m = 1 - 1/n$; Ks is the saturated hydraulic conductivity$[LT^{-1}]$.

A root water uptake distribution function together with a water stress response function was applied in the sink term in Richards equation:

$$S = \alpha(h)\, b(z)\, T_p \tag{18}$$

where $\alpha(h)$ is root-water uptake water stress response function (van Genuchten, 1987); $b(z)$ is the normalized water uptake distribution function, an exponential expression with a maximum at the soil surface (Raats, 1974):

$$\alpha(h) = \left[1 + (h/h_{50})^p \right]^{-1} \tag{19}$$

$$b(z) = a^* \exp\left[-a^* (L_r - z) \right] \tag{20}$$

where h_{50} is the pressure head at which the water extraction rate is reduced by 50%; p is the experimental constants, L_r is the z-coordinate of soil surface $[L]$, a^* is a empirical constant $[L^{-1}]$. (Hamon, 1963), equation was used to calculate daily potential evaportranpiration:

$$PET = \frac{29.8 \times DL \times ea^*\left(T_a\right)}{T_a + 273.2} \tag{21}$$

$$ea^*\left(T_a\right) = 0.6108 \exp\left(\frac{17.27 T_a}{237 + T_a}\right) \tag{22}$$

where PET is daily average potential evaportranspiration $[L]$; D_L is the number of daylight hours, Ta is mean daily temperature $[K]$; $e_a^*\left(T_a\right)$ is saturation vapor pressure $[ML^{-1}T^{-2}]$ evaluated at the atmospheric temperature T_a.

In this work, PET is assumed to be zero before sunrise and after sunset. A sinusoidal function was used to account for the diurnal fluctuations of the PET:

$$T_p\left(t\right) = \frac{\pi}{2DL} \sin\left(\frac{t\pi}{DL}\right) \times PET \tag{23}$$

where $Tp(t)$ is the PET at time t; t is number of hours since sunrise. The integration of the function above over the total day light hours gives the total PET in the day (Liu et al., 2005).

5.2 Formulations in the transport models

5.2.1 Heat transport model

The volumetric heat capacity of the porous media $C_p(theta)$ can be expressed as:

$$C_p\left(\theta\right) = C_n\theta_n + C_o\theta_o + C_w\theta + C_a a_v \tag{24}$$

where C_n ,C_o ,C_w ,C_a stand for soil volumetric heat capacity of solid phase, organic matter, liquid phase, and gas phase $[ML^{-1}T^{-2}K^{-1}]$; θ_n, θ_o, θ are the volume metric content of soil, organic matter and water $[L^3L^{-3}]$; a_v stands for the air content $[L^3L^{-3}]$ (de Vries, 1963); the air term was ignored in this research.

The effective thermal conductivity in the one dimensional case can be parameterized as:

$$\lambda(\theta) = \lambda_0(\theta) + \beta_L C_w |q| \tag{25}$$

where $\lambda_0(\theta)$ is bulk soil thermal conductivity which is a function of mineral type, geometrical arrangement of various phases and water content $[MLT^{-3}K^{-1}]$. An empirical expression for bulk soil thermal conductivity as suggested by Chung and Horton (1987) was used here:

$$\lambda_0 = b_0 + b_1\theta + b_2\theta^{0.5} \tag{26}$$

where b_0 ,b_1 ,b_2 are empirical constants; β_L is the longitudinal heat dispersivity $[L]$;

5.2.2 Reactive transport model

The hydrodynamic dispersion coefficient for bromide tracer, RDOC and BDOC can be expressed as:

$$D = D^* + \alpha_L |v|^n, v = q/\theta \tag{27}$$

where D^* is the molecular diffusion coefficient $[L^2T^{-1}]$; α_L is the longitudinal dispersivity $[L]$; v is pore velocity $[LT^{-1}]$ and q is specific discharge $[LT^{-1}]$.

A modified van Hoff equation was applied in the BDOC model to account for the effects of biodegradation (Yurova et al., 2008).

$$\mu = \mu_{basal} Q_{10}{}^{(T-T_{basal})/10} \tag{28}$$

where Q_{10} is the relative rate of increasing in metabolic rates per 10 $^\circ C$ increase in

temperature; T_{basal} is a reference temperature at which basal rates of microbial DOC degradation rate are estimated; μ is the first-order microbial DOC mineralization coefficient $[T^{-1}]$; $_{basal}$ is the basal microbial DOC mineralization rate $[T^{-1}]$.

5.3 Formulations of the water and solute mass exchange term between two pore systems

According to Gerke and van Genuchten (1993a), the exchange term of water and solutes can be as follows:

$$\Gamma_w = a_w \left(h_f - h_m\right) \tag{29}$$

$$\Gamma_s = (1-d)\,\Gamma_w \phi_f c_f + d\Gamma_w \phi_m c_m + a_s \left(1 - w_f\right) \theta_m \left(c_f - c_m\right) \tag{30}$$

$$d = 0.5\left(1 - \frac{\Gamma_w}{|\Gamma_w|}\right), \quad \Gamma_w \neq 0 \tag{31}$$

$$\phi_f = w_f \frac{\theta_f}{\theta}, \quad \phi_m = \left(1 - w_f\right) \frac{\theta_m}{\theta} \tag{32}$$

where aw is a first-order transfer coefficient for water between soil matrix and fracture [$L^{-1}T^{-1}$]; as is the solute transfer coefficient between soil matrix and fracture[T^{-1}]; Γ_w is water transfer rate between fracture and matrix [T^{-1}], if $\Gamma_w > 0$, water will be transferred from macropores to matrix; if $\Gamma_w < 0$, water will be transferred from matrix to macropores; Γ_s is the solute transfer rate between fracture and matrix pore regions [$MT^{-1}L^{-3}$]; h_f, h_m, θ_f, θ_m represent the pressure head and volumetric soil moisture in macropores and soil matrix respectively.

CHAPTER 3

THE DELIVERY OF DISSOLVED ORGANIC CARBON FROM A FORESTED RIPARIAN HILLSLOPE TO A HEADWATER STREAM

1 Introduction

Dissolved organic carbon (DOC) is an important constituent of soil solutions that impacts many chemical and biological processes in soils (McDowell, 2003). DOC dynamics are central to the biogeochemistry of soil and aquatic ecosystems because they link energy flow and cycling of nutrients (Qualls, 2000). In forested upland watersheds, soil biota and terrestrial plants are the primary DOC sources to a stream (Thurman, 1985). Hydrology regulates the delivery of DOC from those sources to the stream by impacting redox biogeochemistry and water flow paths (Schiff et al., 1998; Kawasaki et al., 2008). These impacts are significant especially during storms or snowmelt (Hinton et al., 1997), with as much as 86% of the annual DOC flux from small eastern United States forested watersheds exported during storms (Raymond and Saiers, 2010).

DOC dynamics in riparian hillslope soils and in adjoining streams are affected by a myriad of factors related to soils, vegetation, and watershed characteristics (Kalbitz et al., 2000). Determining the dominant mechanisms affecting DOC export is important as a process-level understanding can be used to inform generalizations across different watersheds. One general conceptual model of how DOC transport is enhanced during storms is that material accumulates during fair-weather periods and is subsequently leached by storm waters. Hornberger et al. (1994) used such a flushing hypothesis to explain a first-order mechanism of DOC entering a snowmelt dominated

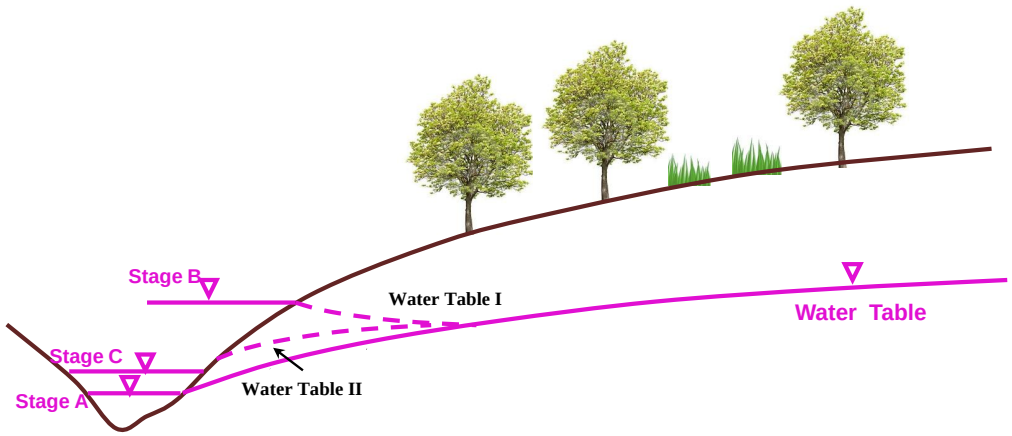

Figure 14: Schematic diagram of flushing hypothesis, rising stream stage results in rising water table in riparian zone, and thus "flushing" down high concentration DOC from organic rich soil layers (Stage B represents peak of the storm hydrograph when there is no DOC flux contribute to the stream and stage C is on the falling limb of the hydrograph when the DOC concentration in the stream peaks)

stream. This hypothesis suggests that solutes are leached from near-surface layers by a rising water table followed by a rapid lateral transport of these materials to the stream via near-surface, saturation excess runoff in the riparian zone (Figure 14). Boyer et al. (1997, 2000) further explored this idea by quantifying characteristics of asynchronous snowmelt and its effect on DOC flushing using both an observational approach and a simple mixing model to understand DOC dynamics, including a peak in DOC concentration in the stream prior to the peak discharge.

Solute flushing has been invoked as an explanation for variations in stream water chemical composition observed in numerous watersheds under various hydrologic conditions (McDowell and Likens, 1988; Moore, 1989). Creed et al. (1996) tested the hypothesis of nitrogen flushing in a watershed in a sugar maple forest by applying the Regional Hydro-Ecological Simulation System model. They concluded that nitrate accumulates during low soil moisture saturation periods and is released during high soil moisture saturation periods. Other approaches have been adopted to examine

solute mobilization, including a virtual experiment approach (Weiler and McDonnell, 2006) and using end-member mixing analysis with naturally occurring tracers (van Verseveld et al., 2008).

Conceptually the flushing hypothesis for DOC in forested catchments envisions a rising water table during storms or snowmelt that intersects DOC-rich soil horizons and leaches material to the stream. It is reasonable to expect that factors controlling the dynamics of the riparian zone water table will affect the delivery of DOC to the stream. The groundwater level at a hillslope-stream connection is affected by local riparian-zone recharge, movement of groundwater from upslope, and interactions with the stream itself. In particular, groundwater levels will respond to changes in stream stage caused by stormflow processes throughout the catchment. At the riparian zone of a specific hillslope, the riparian water table will respond to increases in stream stage on the rising limb of the hydrograph, and DOC delivery to the stream may be interrupted by a hydraulic gradient associated with bank infiltration. DOC flushing from the hillslope will recommence on the falling limb of the hydrograph. During this time the riparian water table rises and, if the conditions are right, the hillslope groundwater discharge on the falling limb of the hydrograph will have high DOC concentrations derived from the upper soil layers. This process would generate a peak DOC outflow concentration from the hillslope to the stream after the peak of stream stage. Thus it follows that the factors controlling the dynamics of the riparian water table will affect the DOC concentration-discharge hysteresis of the watershed with a peak concentration on the falling limb of the hydrograph; these factors include the hydraulic properties of the riparian soil (e.g. hydraulic conductivity) (Whiting and Pomeranets, 1997), the hydraulic characteristics of the watershed (e.g. shape and slope of the hillslope (Kasahara and Wondzell, 2003)), and the stream stage fluctuation (Li et al., 2008).

The overall goal of this research was to examine mechanistically a DOC flush-

ing hypothesis. We hypothesize that the DOC discharge-concentration relationship in the watershed with a peak concentration on the failing limb is partly controlled by the hydraulic properties of the riparian soil, the hydraulic characteristics of the hillslope, and by the storm-induced variation in stream stage. We report a combined modeling and field monitoring study of hydrologic interactions between stream water and groundwater on a watershed hillslope to address the questions related to DOC delivery from hillslope to streams. We used a physically based model to examine the role of lateral groundwater flow and groundwater and surface water interaction on the DOC export from the hillslope and how the vertical and horizontal movement of subsurface flow contributes DOC to the stream. Our model simulation results are consistent with field observations and with a previous study showing that the majority of the DOC contribution to the stream is derived from the riparian zone (Mei et al., 2012). We used the model to explore the major factors controlling the DOC concentration-discharge relationships for a hillslope.

2 Methods

2.1 Field observations

2.1.1 Site description

This study was conducted within a 3rd-order section of White Clay Creek (WCC) with a watershed area of 7.25 km^2 (Figure 15). The WCC watershed is predominantly composed of agricultural (74%) and forested lands (23%) in the Piedmont Province of southeastern Pennsylvania [Newbold et al., 1997]. DOC concentrations in 20 shallow wells in the riparian zone were, on average, 1.5 ppm, ranging from 0.4 ppm to 9.7 ppm. Three deep wells located in the upland area had a mean DOC concentration of 0.51 ppm, ranging from 0.2 ppm to 0.9 ppm. In the stream, DOC concentrations under baseflow conditions ranged from 0.8 to < 2.0 ppm, and increased up to 14 ppm

during stormflow conditions (Mei et al., 2012).

An instrumented transect from the stream to the uplands was selected for the model and included wells on the flood plain (well 3, well 4), mid-hillslope (well 14), and the top of the hill (well 42) (Figure 15). The transect line is nearly perpendicular to the stream and parallel to the presumed flow direction of shallow phreatic groundwater. Wells 3 and 4 in the riparian zone are within 1 m of each other and parallel to the stream channel. We used hydraulic head measurements from well 3 and water chemistry measurements from well 4 to develop the model. Two soil types present along this transect include the Codorus series soils in the riparian zone and Edgemont series soils in the uplands. The bedrock below the soils is predominantly Setters Quartzite (Berg et al., 1980).

2.1.2 Field sampling and data collection

In July 2010, two instrument nests consisting of a pressure transducer and probes for soil temperature and soil moisture were established in the research transect, one in the riparian zone and the other in the uplands. Two soil moisture and temperature probes (Decagon device 5TM) were installed 10 cm below the ground surface in the instrument nests and pressure transducers were installed in wells 3 and 42. Nine piezometers had previously been installed in the stream bed at the bottom of the transect, 3 each at depths of 10cm, 30cm and 50cm (Battin et al., 2003). Stream water temperatures and well and streambed piezometer DOC concentrations have been measured for this transect over the past 2 decades. Soil texture analyses were conducted in 2003.

Pressure transducers were installed in a PVC pipe secured to the stream bed at the transect to collect stream stage data from July 2010. Data for peak flows proved reliable, but base flow data were not because of a temperature compensation issue with the transducer. The stream stage data from 2011 with a new pressure

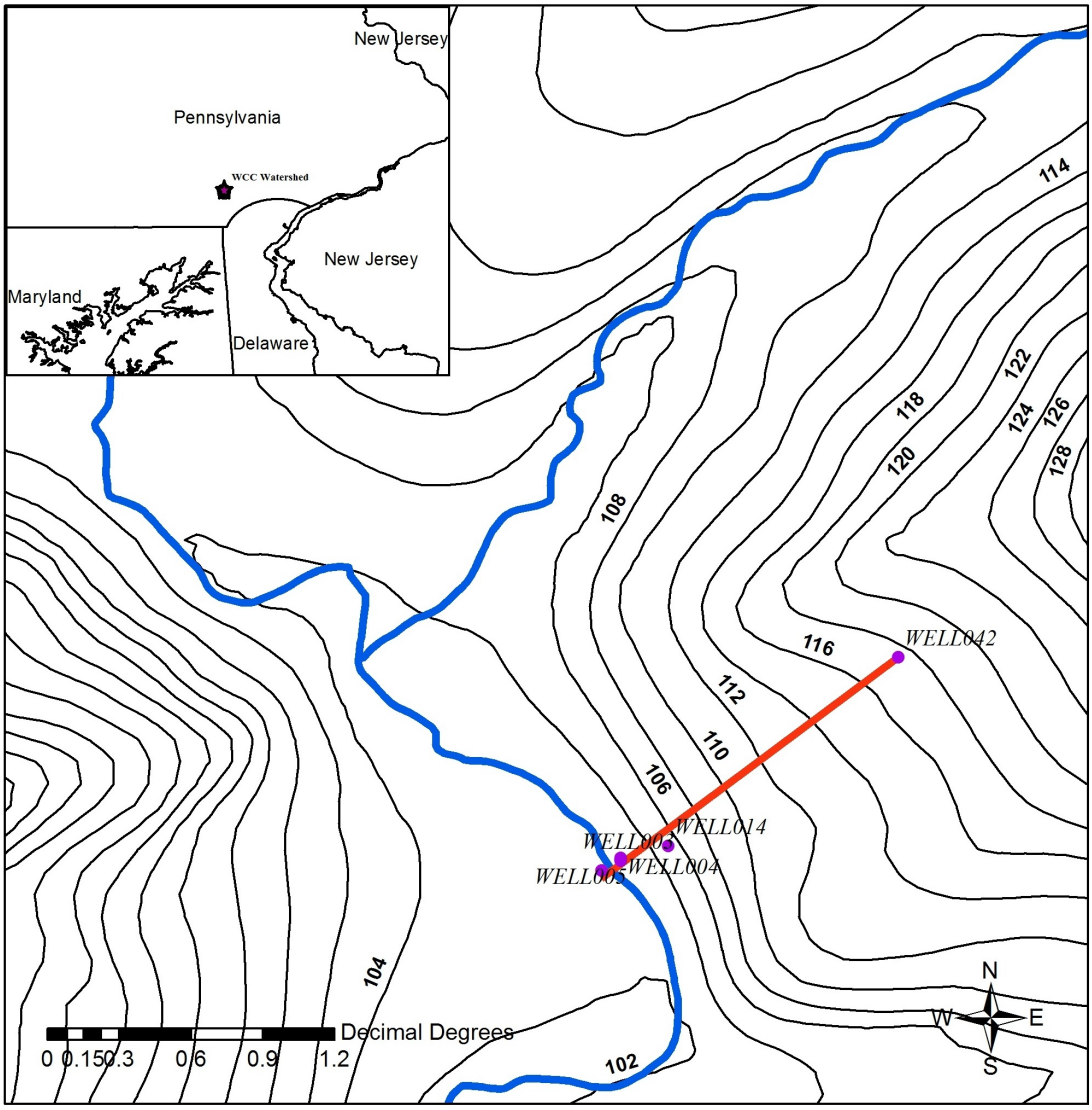

Figure 15: Contour map of area around the research transect at White Clay Creek watershed, and the location of the wells. The red line represents our research transect with length about 140 m long. The blue line represents the White Clay Creek stream channel. The transect is located around the geographic coordination 395142.85N, 754655.26W.

transducer at base flow were compared to data from the outlet of the watershed (about 0.5 km downstream) for the same time period. A linear regression model was established using these two data sets and was used to estimate the base flow stage at the transect. Stream stage and groundwater level data were collected at 15 minute intervals, starting from July 8, 2010.

Stream water was collected during storms with an ISCO sampler (Teledyne Isco, Inc, Lincoln, Nebraska) in 2010. The sampler was programmed to take samples at a two hour time interval. Sampling was conducted during storms on July 12-13 (Event A), July 14 (Event B) and on July 19 (Event C). DOC samples from one storm (Event C) were taken from the sampler installed about 180m downstream of research transect and the rest of the DOC samples from storms were taken from the sampler at the transect. These two series of samples were considered to be consistent given the proximity of the two stream locations.

Samples on the hillslope were collected from well 4. The well was purged and sampled twice during the interval between storms (between Event A and Event B and 2 days after Event B before Event C).

2.1.3 Laboratory measurements

Water samples were filtered through pre-combusted (400C for 4 h) glass fiber filters (Whatman GF/F) using a peristaltic pump. Ten mL of filtrate were diluted 4X with deionized water. Additional volumes of filtrate were Tyndallized and kept in the refrigerator for biodegradable DOC (BDOC) analyses using plug-flow bioreactors with a bed volume of 600 mL (Kaplan and Newbold, 1995). BDOC was defined as the difference in DOC concentrations between the bioreactor influent and effluent waters. Refractory DOC (RDOC) was defined as the concentration of DOC in the bioreactor effluent. The Tyndallized stream water was diluted with biologically stable bioreactor effluent to a concentration of approximately 1.5 mg C/L prior to loading

onto the bioreactors (McLaughlin and Kaplan 2013, Biological lability of dissolved organic carbon in stream water and contributing terrestrial sources, submitted to Journal of Freshwater Science). A minimum of 3 bed volumes from each sample was discarded before samples of bioreactor effluent were collected for analysis. A total of two liters was needed for each bioreactor sample including the amount of water sent to waste, two inflow samples and two analyzed for DOC concentrations with a Sievers 900 analyzer equipped with an inorganic carbon removal module. The pump speed was set to 4mL/min. In total about 15 hours were needed for each run. A minimum of three bed volumes of baseflow stream water was run through the bioreactors between analyses of storm-water or well-water samples. The original RDOC and BDOC concentrations before dilution were calculated using the method given by Mei et al. (2012).

The BDOC analysis assumes that C is limiting (Kaplan and Newbold, 1995). To verify this, additional well samples were collected from well 4 on Aug 10, 2011, the samples were split into two groups, one amended with nutrients and the other unamended. KH_2PO_4, $Ca(NO_3)_2$-$4H_2O$ and NH_4Cl solutions were added to the nutrient amended treatment using the Redfield ratio (Redfield, 1958) as the composition. Both samples were diluted and run though the bioreactor following the standard procedure.

2.2 Model development

2.2.1 Model overview

Numerous models have been put forward to simulate DOC concentration dynamics in soils and streams. They include lumped models (Grieve, 1991; Hornberger et al., 1994; Boyer et al., 2000; Jutras et al., 2011; Xu et al., 2012), process-based models (Neff and Asner, 2001; Michalzik et al., 2003; Futter et al., 2007) and regression models (Worrall and Burt, 2005; Kohler et al., 2009). Relatively few models have adopted the physically-based, distributed modeling approach (Yurova et al., 2008; Fan et al., 2010;

Mei et al., 2012), partially due to the complexity of model parameter selection and large data requirements. The physically-based models have an advantage, however, of providing much more detailed information about processes. Finite element models (FEM) have been applied in simulating variably saturated flow and reactive transport of solutes on hillslopes (Neuman and Withersp, 1971; Neuman, 1973; Pinder and Gray, 1977). Recently, Gu et al. (2008) and Gu et al. (2012) successfully applied a FEM to test the nutrient (nitrate) reduction hypothesis when groundwater flows through a riparian buffer zone near streams.

A vertical two-dimensional FEM for variably saturated and unsaturated flow, heat transport and reactive transport of DOC in the subsurface porous media on hillslopes was developed for this study and applied on our research transect. DOC, RDOC, and BDOC were considered in the model. Soil organic matter (SOM) was used as a pool for DOC to account for leaching from the organic carbon rich layer of the soil by groundwater. Once converted from SOM to DOC, the biodegradable part is available to be consumed by microbial activity. The SOM values in the model were estimated from previous work in the WCC watershed. Spatial heterogeneity of hydraulic properties was considered by dividing the hillslope into different parameter zones.

2.2.2 Mathematical governing formulations

According to the geological and soil conditions described in the previous section, a two-dimensional slice for our selected transect was described using a heterogeneous, isotropic, saturated-unsaturated model. The model is Pinder and Gray (1977):

$$\frac{\partial}{\partial x_i}\left[K_{si}k_r\left(\frac{\partial h}{\partial x_i}+e\right)\right]-R=\left(C+\frac{\theta}{n}S_s\right)\frac{\partial h}{\partial t} \tag{33}$$

where, K_{si} is the second-order saturated hydraulic conductivity tensor [LT^{-1}]; k_r is the relative hydraulic conductivity [-] (Section 5.1); xi are coordinates in the Cartesian system; e is the unit vector in the vertical direction; R is the root uptake sink term; C is the specific moisture capacity [L^{-1}]; h is the pressure head [L]; θ is the volumetric soil moisture content [L^3L^{-3}]; n is the porosity [-]; t is time [T]; and S_s is the specific storage [L^{-1}].

Temperature was considered as an important control on DOC biodegradation (Winterdahl et al., 2011). A two-dimensional heat transport model was used to simulate the soil temperature along the transect following Sophocleous (1979):

$$\frac{\partial}{\partial t}\left(C_p T\right) = \frac{\partial}{\partial x_i}\left(\lambda_{ij}\frac{\partial T}{\partial x_j}\right) - C_w q_i \frac{\partial T}{\partial x_i} \tag{34}$$

where, T denotes temperature [K], λ_{ij} is the second-order tensor of the coefficient of apparent thermal conductivity in the soil [$MLT^{-3}K^{-1}$] (Section 5.2); Cp and Cw are volumetric heat capacities [$ML^{-1}T^{-2}K^{-1}$] of the porous medium and the liquid phase respectively; and q is the specific discharge [LT^{-1}].

Adsorption was taken into account in the RDOC model. Both adsorption and microbial uptake were included in the BDOC model. Sorption was treated as a reversible processes. Organic carbon can transfer between the sorbed phase and aqueous phase. The two-dimensional reactive transport model for RDOC is:

$$\frac{\partial}{\partial t}\left(\theta c_R + \rho s_R\right) = \frac{\partial}{\partial x_i}\left(\theta D_{ii}\frac{\partial c_R}{\partial x_i} + \theta D_{ij}\frac{\partial c_R}{\partial x_j}\right) - q_i\frac{\partial c_R}{\partial x_i} \tag{35}$$

$$\frac{\partial s_R}{\partial t} = -\tau\left(s_R - K_D c_R\right) \tag{36}$$

and the two-dimensional reactive transport model for BDOC is:

$$\frac{\partial}{\partial t}\left(\theta c_B + \rho s_B\right) = \frac{\partial}{\partial x_i}\left(\theta D_{ii}\frac{\partial c_B}{\partial x_i} + \theta D_{ij}\frac{\partial c_B}{\partial x_j}\right) - q_i\frac{\partial c_B}{\partial x_i} - \mu\theta c_B \tag{37}$$

$$\frac{\partial s_B}{\partial t} = -\tau \left(s_B - K_D c_B \right) \tag{38}$$

where, subscripts R and B denote RDOC and BDOC respectively; s is the soil organic carbon content [MM^{-1}]; D_{ij} is a second-order tensor for the hydrodynamic dispersion coefficient [L^2T^{-1}] (Section 5.2); c is resident concentration [ML^{-3}]; q is specific discharge [LT^{-1}]; K_d is the sorption equilibrium distribution constant [L^3M^{-1}]; τ is the first order mass transfer coefficient [T^{-1}]; ρ is the bulk density of the soil [ML^{-3}]; μ is the first-order microbial DOC mineralization coefficient [T^{-1}]; and θ is the soil moisture content [-].

2.2.3 Model Implementation

In total 5,248 nodes and 9,980 linear triangular FEM elements were generated for our research transect. The mesh near the stream was refined to obtain high accuracy. In our model, the stream bed length is 2m, half of the total stream bed width, the model horizontal length is 139m, and the highest place of the terrain is 116.4 m above sea level. The bottom of the model was assumed to be located 10 m below the stream bed. Three parameter zones were incorporated in the model to represent the spatial heterogeneity including the zones for Codorous soil, Edgemont soil and bedrock. The Codorous zone was set near the stream, and the Edgemont soil zone was set on the hillslope area; both were assumed to be about 1m thick above the bedrock zone (Figure 16). The root uptake term was applied only to the unsaturated nodes in the model.

Five vertical sections were set up in the model along the transect (3m, 7m, 13m, 21.25m and 43 m from the origin in the x direction) (Figure 16). The sum of the product of the nodal flux of water and the DOC concentrations of all the saturated nodes was used to represent the DOC flux variation along the groundwater flow path (Section 5.3.1). The DOC concentration delivered from the hillslope to the stream

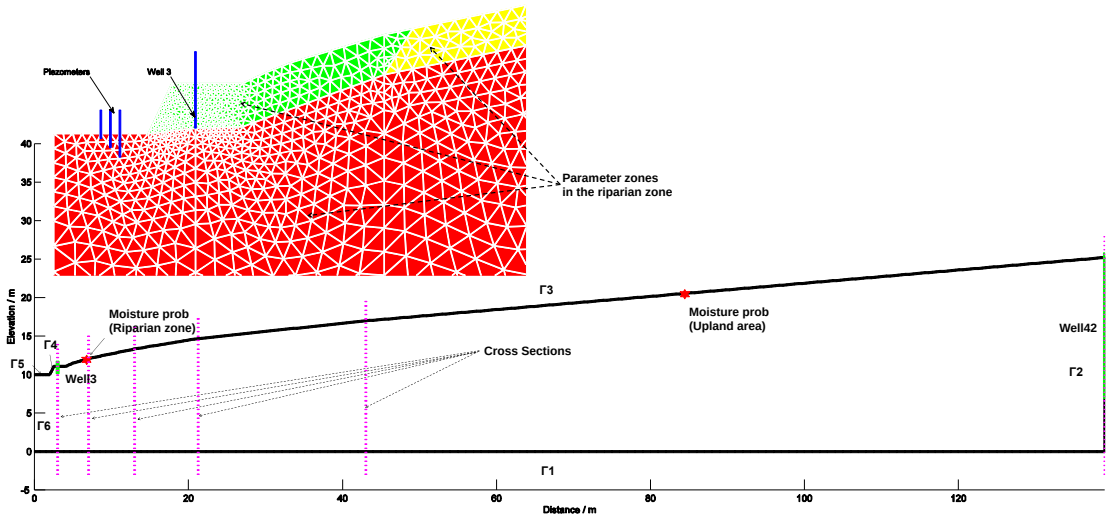

Figure 16: The generated FEM mesh, the parameter zones and the field installation on our research transect. Each boundary segment was marked with signs from bottom boundary segment 1 to left side boundary segment 6 counterclockwise.

was calculated by weighting the DOC concentration across all the saturated nodes with the nodal water flux at the stream boundary (Section 5.3.2).

2.2.4 Initial and boundary conditions

The flow model was initialized by solving a steady state flow problem, with a Dirichlet boundary condition at the right boundary of the hillslope (Γ_2) at the beginning of the simulation period.

$$\frac{\partial}{\partial x_i}\left[K_{si}k_r\left(\frac{\partial h}{\partial x_i}+e\right)\right]-R=0 \tag{39}$$

After the steady state solution was obtained, the solution was used to initialize the dynamic model. The model was driven starting from a rain event before our three events, to avoid initial artifacts.

The heat model was initialized by running the heat model for several days. The RDOC and BDOC models were initialized using an equilibrium condition between the sorbed and aqueous phases of organic carbon.

A no flow boundary condition was applied to the boundaries (Γ_1,Γ_2, Γ_6) (Figure 16), and a Neumann boundary condition was applied to the top of the domain (Table 5). The boundary condition at the boundary Γ_4 contains a saturated part below the stream stage, a seepage face (saturated segment above the stage), and an unsaturated part (above the seepage face). The seepage face location was adjusted continually using an iterative process following Neuman (1973). This guaranteed that the calculated water flow was out from the saturated part of the boundary. All the nodes below the stream stage were specified as a Dirichlet boundary with a prescribed pressure value equal to the difference between the stage value and the elevation of the nodes. All the nodes at the seepage face were treated as a prescribed pressure head boundary with $h = 0$, and all the nodes on the unsaturated segment were prescribed as a zero flux boundary. The nodes on the stream bed (segment Γ_5) were specified as a Dirichlet boundary using the stream stage time series data.

Table 5: Boundary conditions [a]

Segment	Flow model[b]	Heat model	DOC model
$\lambda_1 \cup \lambda_2 \cup \lambda_6$	$-K_{ij}k_r\left(\frac{\partial h}{\partial x_j}+e\right)n_i = 0$	$-\lambda_{ij}\frac{\partial T}{\partial x_j}n_i = 0$	$\left(-\theta D_{ij}\frac{\partial c}{\partial x_j}+q_i c\right)n_i = q_i n_i c_0$
λ_3	$-K_{ij}k_r\left(\frac{\partial h}{\partial x_j}+e\right)n_i = Q_0$ $h(x,z,t) = h_0(x,z,t)$	$T(x,z,t) = T_0(t)$	$-\theta D_{ij}\frac{\partial c}{\partial x_j}n_i = 0$
λ_4	$h(x,z,t) = 0$ $-K_{ij}k_r\left(\frac{\partial h}{\partial x_j}+e\right)n_i = 0$	$T(x,z,t) = T_0(t)$	$-\theta D_{ij}\frac{\partial c}{\partial x_j}n_i = 0$
λ_5	$h(x,z,t) = h_0(x,z,t)$	$T(x,z,t) = T_0(t)$	$-\theta D_{ij}\frac{\partial c}{\partial x_j}n_i = 0$ During bank storage:$C = C_0$

[a] where, h is the pressure head [L]; K_{ij} is the second-order tensor of saturated hydraulic conductivity [LT^{-1}]; k_r is the relative hydraulic conductivity [LT^{-1}]; e is the unit vector in the vertical direction; n_i is the outward unit normal vector; Q_0 is the prescribed rainfall rate [LT^{-1}]; h_0 is the prescribed pressure head at the channel [L]. T is the temperature [K]; T_0 is the prescribed temperature boundary value at the top of the domain [K]; λ_{ij} is the second-order tensor of coefficient of the apparent thermal conductivity in the soil [$MLT^{-3}K^{-1}$]; θ is the soil moisture [-]; qi is the specific discharge [LT^{-1}]; c is the residence concentration of DOC [ML^{-3}]; D_{ij} is the second-order tensor of hydrodynamic dispersion coefficient [L^2T^{-1}]; c_0 is the concentration of the inflow fluid from outside the boundary [LT^{-1}].

[b] In the flow model, three different boundary conditions were applied at boundary Λ_4 depending on the conditions. All the nodes below and on the stream surface are given a prescribed pressure value computed from the stream stage and elevation of the nodes; The nodes at the seepage face were prescribed a pressure equals zero; The nodes above the seepage face were set to be no flux condition.

In the heat model, a Neumann type boundary was applied to the boundary segment Γ_1, Γ_2, Γ_6 (Table 5). Dirchlet boundary conditions were applied to the segments

Γ_3, Γ_4 and Γ_5. Prescribed stream water temperature was applied on segment Γ_5 and prescribed soil temperature was specified on the nodes on segment Γ_3 except for a 1-meter zone near the stream. A 1 meter transition zone was used with linearly interpolated temperature values on the top boundary from the stream temperature to the hillslope temperature to provide a smooth temperature variation at the soil surface.

The RDOC and BDOC models share the same boundary conditions (Table 5). A Neumann type boundary was applied to the boundaries (Γ_1, Γ_2, Γ_6). whereas a third-type boundary condition was used on the segment Γ_3 (van Genuchten and Parker, 1984), with an inflow RDOC concentration of 9.4 ppm and a BDOC concentration of 5.8 ppm from the throughfall. Because we do not have measured RDOC and BDOC values from throughfall at our research site, we used values measured from a bulked throughfall sample collected beneath a northern red oak stand at the Harvard Forest Long-Term Ecological Research (LTER) site (McDowell et al., 2006). The total DOC (RDOC+BDOC) value is within the range given by Levia et al. (2012) with the sampling mostly done in the eastern USA close to our site. The results do not depend on the throughfall concentrations strongly because the soil leaching, sorption, and biodegradation processes control modeled concentrations.

2.3 Model calibration and parameter selection

Preliminary parameter values in the van Genuchten model (Section 5.1) for all three parameter zones were obtained by running Rosetta, a model developed by USDA (Schaap et al., 2001), using soil texture information as inputs. Final values of these parameters were obtained by calibration using a trial and error method within the range given by Guber et al. (2006) (Table 6).

Table 6: Input parameters for the model

Parameters	Bd/Co/Ed †	Source
van Genuchten soil characteristic parameter, α, 1/m	3.27/1.32/1.02	Calibrated, Rosetta and range from Guber et al. [2006]
van Genuchten soil characteristic parameter, n, -	1.3/1.7/1.45	Calibrated, Rosetta and range from Guber et al. [2006]
Saturated soil moisture, θ_s, -/-	0.2/0.43/0.43	Calibrated, Rosetta and range from Guber et al. [2006]
Residual soil moisture, θ_r, -/-	0.05/0.05/0.05	Calibrated, Rosetta and range from Guber et al. [2006]
Saturated hydraulic conductivity, Ks_x, m/min	5.7E-05/0.01/0.02	Calibrated
Saturated hydraulic conductivity, Ks_z, m/min	5.7E-05/0.001/0.002	Calibrated
Specific storage, Ss, 1/m	0.0001	Gu [2008]
Porosity, n, -/-	0.4	Gu [2008]
RDOC sorption distribution constant, K_d, L/g	0.5	Calibrated, Range from Yin et al.[2002]
RDOC first order mass transfer coefficient , τ, min-1	8.3E-05	Calibrated, Range from Jadine et al.[1992]
BDOC sorption distribution constant, K_d, L/g	0.3	Calibrated, Range from Yin et al.[2002]
BDOC first order mass transfer coefficient , K_d, min-1	8.3E-05	Calibrated, Range from Jadine et al.[1992]
Molecular diffusion coefficient for RDOC and BDOC	7.2E-05	Gu [2008]
Longitude dispersivity for RDOC and BDOC, m	0.1	Calibrated
Transverse dispersivity for RDOC and BDOC, m	0.01	Calibrated
Soil Bulk density, ρ, g/L	1200	Unreported data in WCC watershed
Reference temperature, basal rates of microbial DOC degradation rates, $Tbasal$, $^\circ C$	20	Yurova et al [2008]
Relative rate of increase in metabolic rates per 10C, Q_{10},	1.7	Yurova et al [2008]
DOC biodegradation rate at temperature $Tbasal$, μ_{basal}, 1/min	6e-7	Calibrated range from Yurova et al [2008]
Thermal dispersivity, β, m	1.8	Mei et al [2012]
Volumetric water heat capacity, C_w, $Jm^{-3}K^{-1}$	4.18e+6	J. Simunek et al [2005]

† where Co represents Codorus soil; Ed represents Edgemont soil; Bd represents bedrock

The models were calibrated in sequence, the flow model first followed by the chemical reactive transport model. Three parameter zones were calibrated in sequence from the upslope area towards the stream. In the bed rock zone, hydraulic conductivity was calibrated against the pressure transducer data from well 42. Then the van Genuchten model parameters in the Edgemont soil zone were calibrated using the soil moisture data from the upslope location. After the parameters in these two zones were calibrated, the van Genuchten model parameters in the Codorous soil zone were calibrated using the pressure transducer data from well 3 and the soil moisture data from the riparian zone (Table 6).

Due to the limited data available, only one set of parameters was used for all three zones for the heat model and DOC reactive transport models. The thermal

dispersivity from the heat model was obtained from Mei et al. (2012). DOC model parameters (e.g. K_d, τ, D_0) were calibrated within the range given in the literature (Jardine et al., 1992; Gu et al., 2008; Yurova et al., 2008; Mei et al., 2012).

2.4 Lag between stream stage peak and DOC concentration peak

As noted previously, we postulate that several factors affect the nature of stream-groundwater interactions with respect to flushing of DOC from a hillslope. In particular, we propose that the peak in DOC efflux from a hillslope will lag behind the peak in stream stage and that the lag time will be related to the properties of the stream hydrograph (e.g., the rapidity of ascent of the rising limb) and to the hydraulic properties of the riparian soils. Some factors (e.g. the existence of bogs in the watershed) might lead to a peak in DOC concentration prior to a peak in stream discharge, but such factors are not considered in our two-dimensional hillslope model. We examined dependency of the lag time of stream stage and DOC concentration peak from the hillslope on the riparian hydraulic parameters and the stream stage hydrograph properties by performing a Monte Carlo simulation varying parameters as described below, followed by a multivariate linear regression on the simulation results. We used

$$H(t) = h_0 e^{\pi/2} e^{-\omega t} (1 - \cos \omega t) \tag{40}$$

to represent the shape of the stream wave (Cooper and Rorabaugh, 1963; Gu et al., 2008), where h_0 is the maximum rise of the stream stage; $\omega = 2\pi/\tau$; τ is the duration of the wave.

The hydraulic properties of the riparian zone are represented by the van Genuchten model parameters. Three parameters (α, n and k_x) from the FEM combined with the two parameters (h_0, τ) respectively from the stream stage equation were used to perform Monte Carlo simulations. Vertical hydraulic conductivity k_z was varied

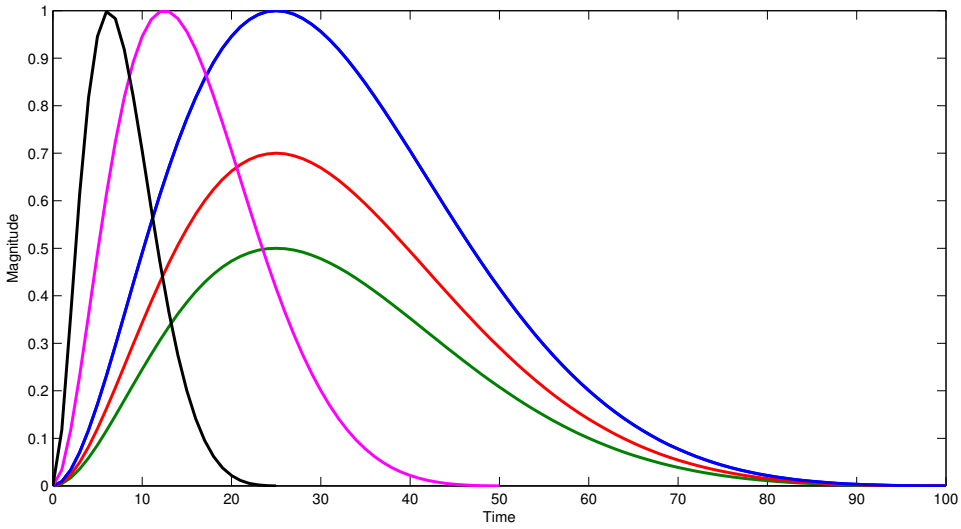

Figure 17: The floodwave shape controled by the parameter τ and h_0

according to k_x by maintaining the same anisotropy ratio. These parameters were assumed to be uniformly distributed within designated ranges. We used +/-20% of the calibrated value for and n as the upper and lower bounds. The range for was set from 3 hours to 36 hours. The range of the stream stage rise was taken as 0.3m to 0.8m. The hydraulic conductivities were varied by 2 orders of magnitude. Monte Carlo simulations were conducted by selecting parameters from the designated ranges using a Latin Hypercube Sampler (LHS) (McKay et al., 1979). Fifty realizations were generated by Monte Carlo simulation, ten times the number of the varied parameters as is suggested by Sieber and Uhlenbrook (2005).

The lag times from the Monte Carlo simulation results were regressed against the sampled values of selected model parameters. Coefficients in a multivariate regression model were estimated using a least squares approach.

$$\widehat{\mathbf{y}} = \mathbf{X}\beta \tag{41}$$

$$\beta = \left(\mathbf{X}^T\mathbf{X}\right)^{-1}\left(\mathbf{X}^T\mathbf{y}\right) \tag{42}$$

where $\hat{\mathbf{y}}$ is a vector of the predicted lag times from the regression model; $\mathbf{X}$ is the matrix containing the value of the sampled parameters [1 $\mathbf{x_1}$ $\mathbf{x_2}$...]; β is vector of the regression coefficients. $\mathbf{y}$ is a vector of lag time from the output of the LHS results.

To identify the relative importance of the selected parameter on the lag time, the standard partial regression coefficients B_k were calculated (Davis and Sampson, 1986).

$$B_k = \beta_k \frac{s_k}{s_y} \tag{43}$$

where B_k stands for standard partial regression coefficients; s_k is the standard deviation of each of the variables x_k (the parameters in LHS); s_y is the standard deviation of the vector y; β_k is the regression coefficient corresponding to each of the variables.

3 Results

3.1 Field results

Well sampling results for July 2010 show that the DOC concentration ranged from 1.9 ppm to 2.3 ppm with a median value of 2.0 ppm for well 4 (Table 7). These values can be compared with results from intermittent sampling carried out since 1998 (Figure 18). DOC sampling conducted from 1998 until now showed a median value 2.7 ppm from the riparian zone wells, with a range from 0.7 ppm to 6.7 ppm. The comparison shows consistency for wells in the riparian zone. The concentration values are generally lower in summer and higher for autumn. Piezometer DOC data collected from the stream bed had a median DOC value 0.7 ppm, ranging from 0.2 ppm to 2.7 ppm. Historical data from streambed piezometers show that the DOC concentrations in the stream bed are lower than the riparian well DOC concentrations (Figure 18).

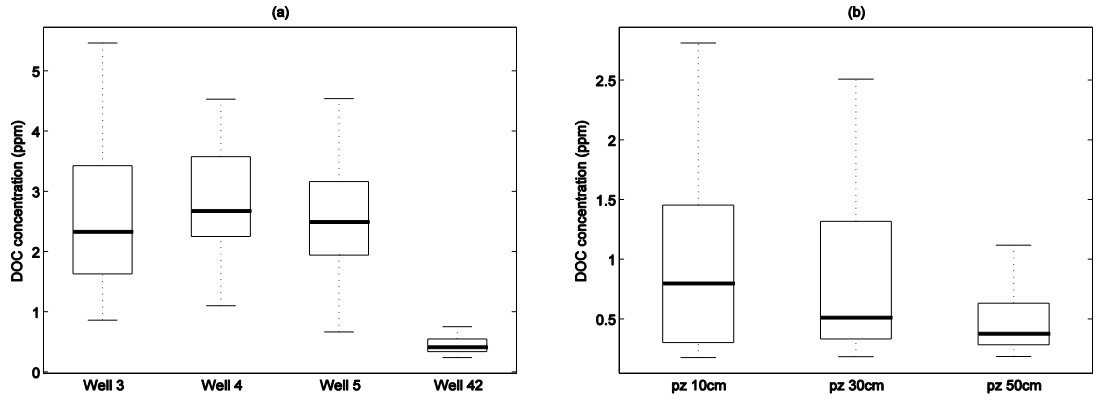

Figure 18: (a): DOC concentration measurement in the five wells on our research transect well3,well4 and well5 are in the riparion zone, the median values are 2.3 ppm, 2.7 ppm and 2.5 ppm respectively and well 42 on the top of the hillslope with a median 0.4 ppm. (b) Piezometer DOC data from the last decades in the stream bed, with median value 0.8 ppm, 0.5 ppm and 0.4 ppm for depth 10cm, 30 cm and 50 cm respectively.

Table 7: The DOC sampling results from well 4

Date	Time	DOC(ppm)	RDOC(ppm)	BDOC(ppm)	BDOC %
14-Jul-10	16:45	2.25	1.95	0.3	13.33
16-Jul-10	18:44	1.94	1.93	0.01	0.52
20-Jul-10	18:21	2.03	2.03	0	0

The measured BDOC concentration in well 4 ranged from 0.0 ppm to 0.3 ppm, and the RDOC concentration was about 1.9 ppm (Table 7). Measurements of BDOC on samples from the riparian wells were not biased by nutrient limitation. The BDOC values in samples with added nutrient solution were equal to those in the samples without nutrient added, confirming the initial low BDOC concentration measurement from well 4.

Stream RDOC and BDOC increased as stream stage rose during the three storms and then decreased back to baseflow values, although this occurred more slowly than the return of discharge to baseflow values. BDOC concentrations increased and decreased faster than RDOC concentrations. The peak value was approximately 10 ppm for DOC and 4.5 ppm and 5.5 ppm for RDOC and BDOC respectively. The baseflow

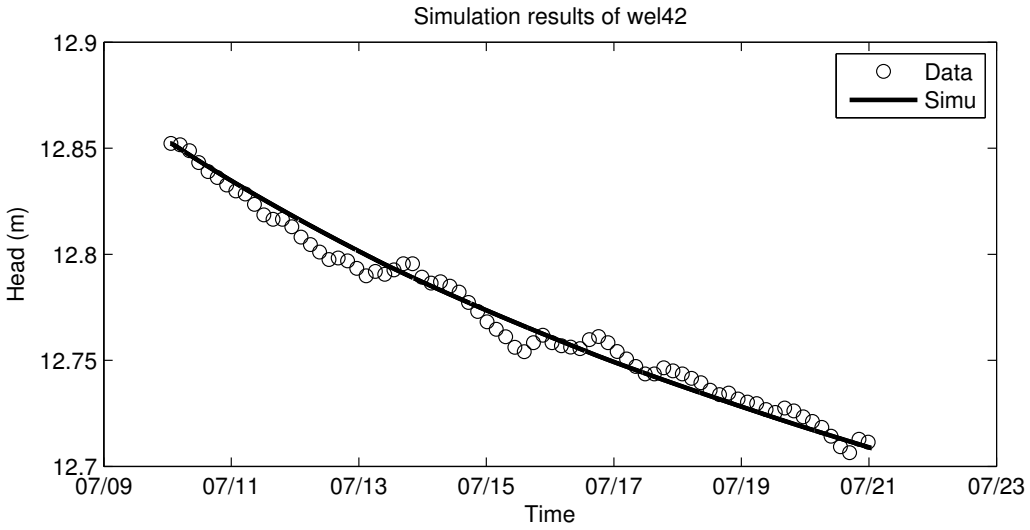

Figure 19: Comparison of observed hydraulic heads at well 42 for July 2010 to predictions from the two-dimensional finite element model. The solid red line denotes model prediction, and the dotted line denotes the field observations.

concentrations for RDOC and BDOC were 1.5 ppm and 0.5 ppm respectively. The peak value of the DOC happened after the peak value of the stream stage.

3.2 Simulation results

The simulation results show a good fit of data for the groundwater hydraulic head at well 3 and well 42 and the soil moisture in the riparian zone, and a reasonably good fit for the soil moisture in the upland area (Figure 21, 19, 20). As expected, on the top of the hillslope, the deep water table experienced continuous slow relaxation during our simulation period due to steady drainage (Figure 19). On the other hand, the water table in the riparian zone responded to the stream stage dynamic signal relatively rapidly due to proximity to the stream and to the relatively high hydraulic conductivity of the riparian zone soils. Bank storage (i.e., flow from the stream into the bank) occurred during the high flow periods of Event A and Event C when the stream stage was higher than the riparian zone groundwater level (Figure 21).

Simulations show that the water flow in the saturated zone was essentially horizontal towards the stream until it approached the riparian zone, where the flow direction

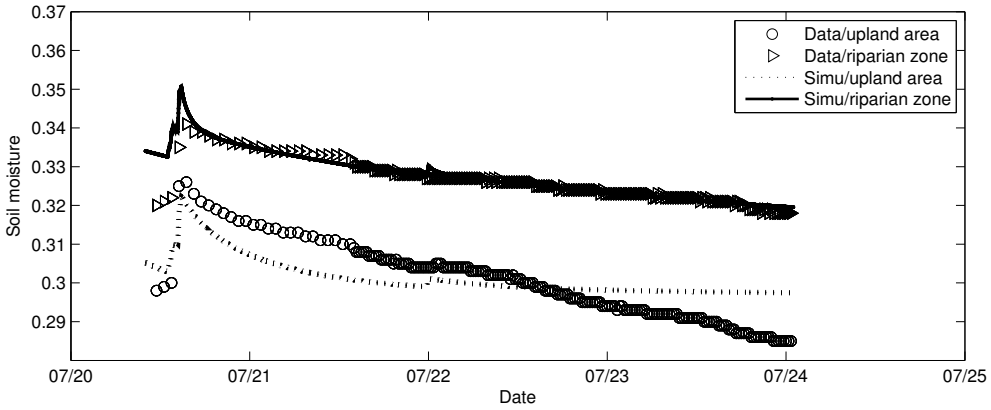

Figure 20: Comparison of observed soil moisture in the riparian zone and upland area to predictions from the two-dimensional finite element model.

gradually began to bend upward. Due to the relatively high hydraulic conductivity of the Codorus soil, deep groundwater ("old water" in the bedrock) tends to flow and mix with the shallow water ("new water") at the interface between the bed rock and Codorus soil in the riparian zone (Figure 22).

The simulated RDOC concentration in the stream bed was about 0.7 ppm and the simulated BDOC concentration in the stream bed was approximately 0.0 ppm resulting in a total DOC concentration of 0.7 ppm. This value is consistent with historic data from the piezometers in the stream bed with a median value 0.7 ppm (Figure 18). The simulated results in well 4 show RDOC concentrations of about 1.3 ppm and BDOC concentrations of about 0.3 ppm. Both values are broadly consistent with the sampling data and historic data. The simulated DOC concentrations in the deep well (well 42) on the top of the hillslope were lower than the median value of the historical observation, with RDOC of 0.1 ppm and BDOC of 0.0 ppm, but they were broadly consistent with the historic data for that well.

The simulated pattern of RDOC and BDOC concentration in outflow to the stream was similar to the observed pattern in the stream: the RDOC concentration rose and fell more slowly than the BDOC concentration. The baseflow and peak value of the RDOC and BDOC concentrations were broadly consistent with the stream

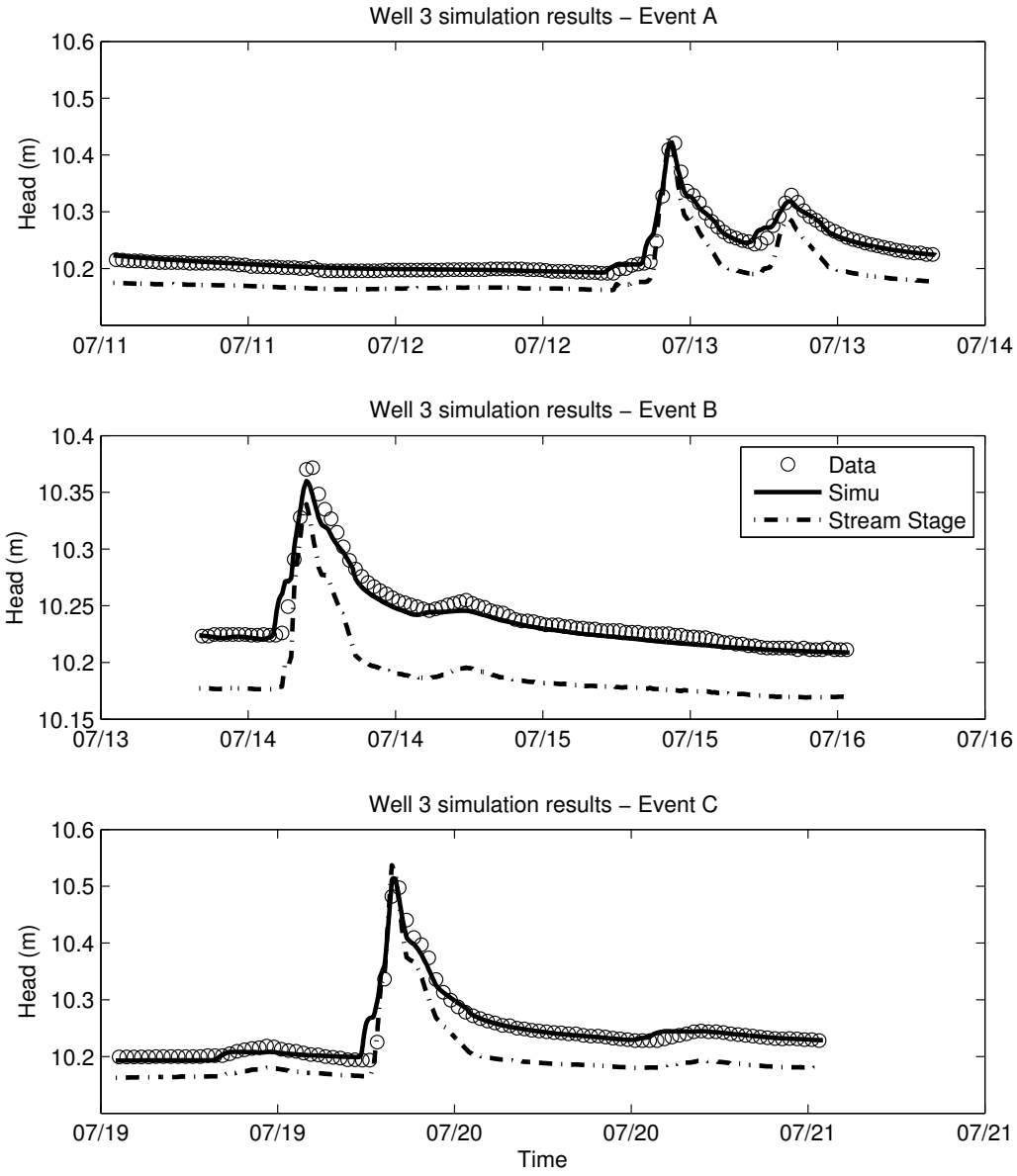

Figure 21: Comparison of observed hydraulic heads at well 3 during events A, B, and C to predictions from the two-dimensional finite element model. The green line is stream stage. The solid blank line denotes model prediction, and the dotted line denotes the field observations.

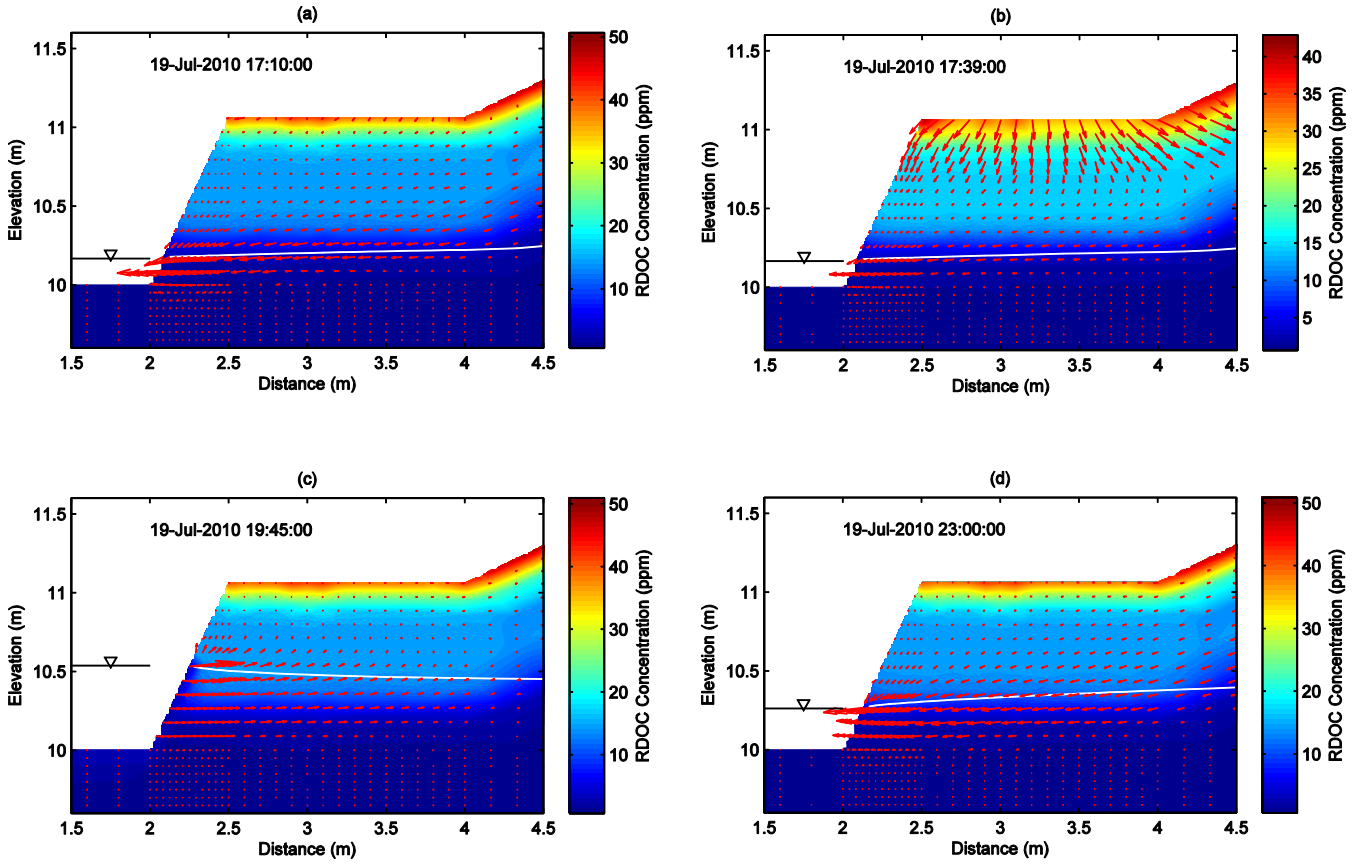

Figure 22: Simulation results for the DOC flushing during rainfall (Event C). White line represent groundwater table; Red arrows represent specific discharge. (a) Before the rain, baseflow condition; (b) During the rain, as the rain water was infiltrating down to the water table, the stream stage was rising; (c) Stream stage raised to its peak and bank storage happened, the riparian water table raised to organic carbon rich layer; (d) As the stream stage was dropping, the groundwater contacted high organic carbon layer was delivered to the stream by the strong outward hydraulic gradient.

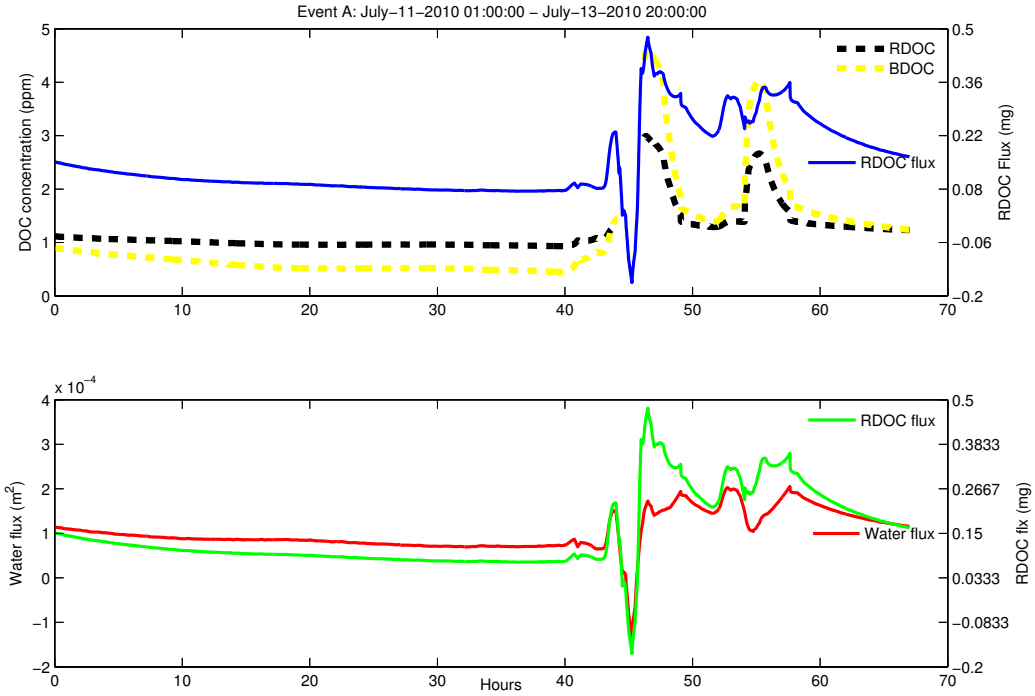

Figure 23: Simulated stream DOC concentration, event A.

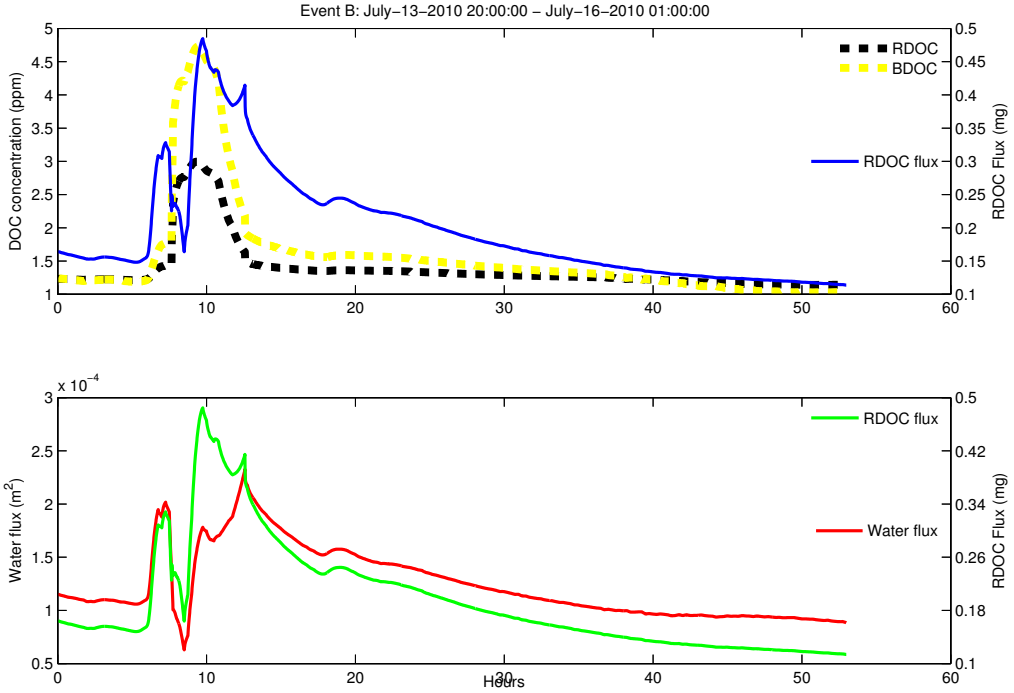

Figure 24: Simulated stream DOC concentration, event B.

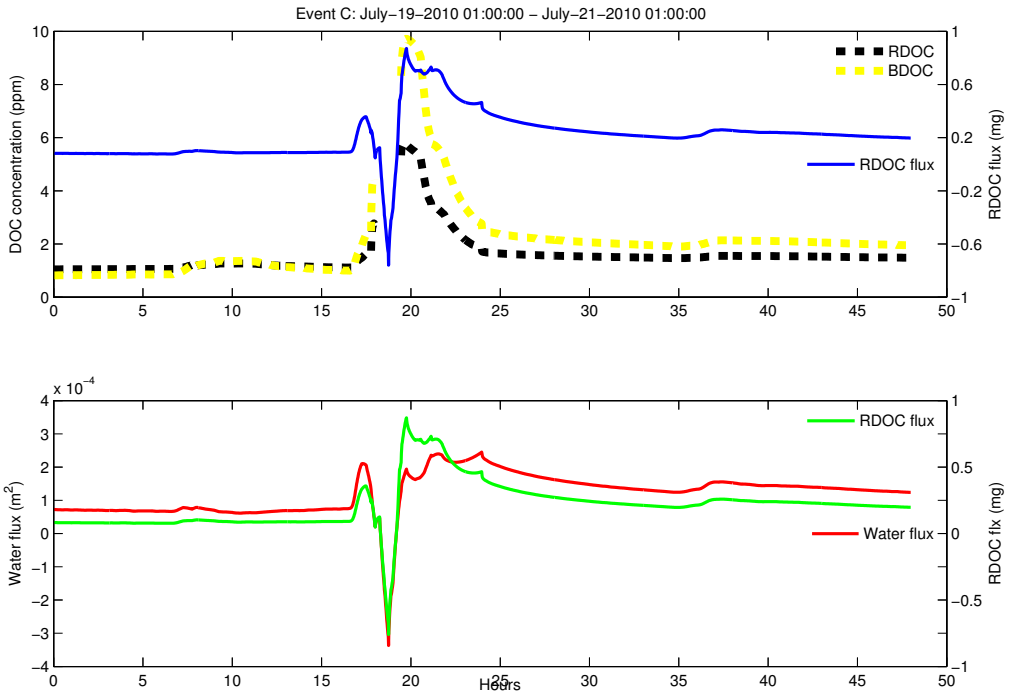

Figure 25: Simulated stream DOC concentration, event C.

observations (Figure 23,24, 25). The simulated concentrations of RDOC and BDOC from the hillslope lagged behind the peak of the stream stage. The peak of RDOC and BDOC concentrations was slightly later than the peak of stream stage if the event was relatively small (Event B) with a much greater lag during larger events when bank storage occurred (Event A and Event C) (Figure 23,25). The calculated DOC mass fluxes during the three precipitation events were high near the stream and declined rapidly towards the upland area (Figure 27).

Table 8: The regression coefficients and the standard partial regression coefficients

-	α (1/m)	n (-)	k_x (m/min)	τ (hour)	h_0 (m)
Sampling range [Minimum, Maximum]	[1.056, 1.584]	[1.36, 2.04]	[0.0012, 0.12]	[3, 36]	[0.3, 0.8]
β_k	0.131	0.221	-5.273	0.048	0.957
B_k	0.035	0.077	-0.321	0.815	0.244

The multiple linear regression results showed the relationship of lag time on the

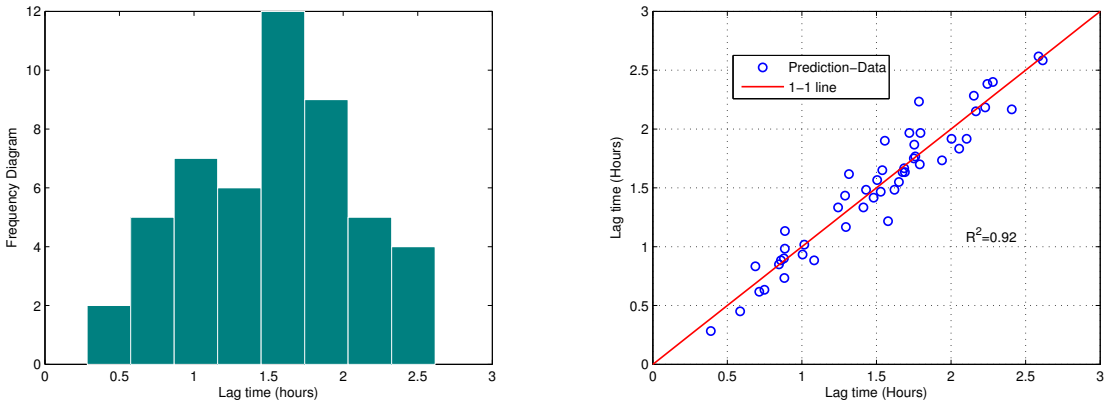

Figure 26: a: Monte Carlo simulation results; b: Multiple linear regression analysis of the Monte Carlo simulation results for the lag time between peak stream stage and peak DOC concentration ($R_2 = 0.92$). x axis represents the calculation results of the lag time from the regression model: $\widehat{\mathbf{y}} = \mathbf{X}\beta$; and y axis represents the Monte Carlo simulation results of the lag time

hydrograph characteristics and the riparian zone hydraulic parameters (Figure 26). The wave duration time (τ) has the highest standard partial regression coefficients 0.815 and the van Genutchen parameter (α) has the smallest standard partial regression coefficients 0.035 (Table 8).

4 Discussion

Samples from riparian wells and from streambed piezometers (Table 7 and Figure 18) compared favorably with measured stream water concentrations suggesting that the stream composition results from a mixing of high DOC from the riparian soil and low DOC from deep groundwater. Our model results are consistent with this interpretation. Because the riparian soil has a much higher hydraulic conductivity compared to the underlying bed rock, the flow lines point upward even at interface of the bed rock and riparian soils (Figure 22). This indicates that the mixing of the deep groundwater and shallow soil water actually happens both at the bottom of the floodplain soils and in the stream. This observation is consistent with those of Chanat and Hornberger (2003) and Jencso et al. (2010)

The approximate 0.7 ppm DOC concentration in the stream bed, consisting of only RDOC, indicates that the DOC in the stream bed was mostly from deep groundwater. The BDOC was mostly removed before water reached the stream bed through the deep groundwater flow path. This indicates that the measured BDOC in the stream water was derived from the shallow terrestrial sources (e.g., riparian zone). This inference is consistent with Mei et al. (2012). Our simulation results show that during the rising stream stage, the outward hydraulic gradients were generally reduced at the stream bed, and the outward hydraulic gradients at the bank generally increased on the falling limb of the stream stage (Figure 22). This result helps explain how the BDOC concentration rises from a baseflow value of about 0.5 ppm to 5.5 ppm during storms as more water is contributed from the shallow soil and storm water than from the deep groundwater during the passage of a hydrograph wave. Previous research has shown similar results, including a study the biological lability of DOC in WCC that showed that both the concentration of BDOC and the percentage of DOC that is BDOC increased during the storms suggesting a preferential transport of BDOC to the stream during storms (McLaughlin and Kaplan 2013, Biological lability of dissolved organic carbon in stream water and contributing terrestrial sources, submitted to Journal of Freshwater Science).

Our simulation results follow a similar pattern as the data during the three events showing the peak of the DOC concentration occurring later than the peak of stream stage regardless of whether bank storage occurred (Figure 23). The lag times between the peak DOC concentration and the peak stream stage are different for the three events – shorter for a small event (Event B) and longer for larger events (Event A, C). This lag time between the peak stream stage and peak DOC concentration can affect the shape of the concentration-discharge (C-Q) hysteresis curve. DOC C-Q relationships have been extensively discussed in the literature (Evans and Davies, 1998; Chanat et al., 2002; Butturini et al., 2006). Our simulation result is consistent

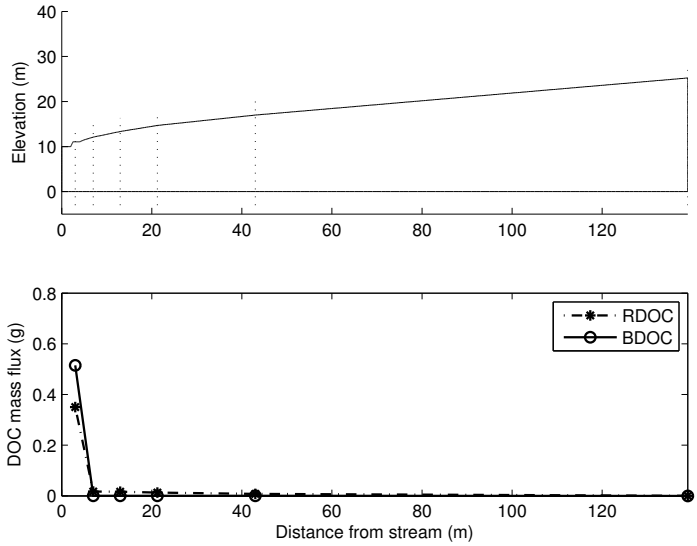

Figure 27: Simulated RDOC and BDOC fluxes along the hillslope transect during Event C. DOC flux is high in the riparian zone and decline rapidly towards the uplands.

with Inamdar and Mitchell (2006) and Hagedorn et al. (2000) that the peak of DOC occurs later than peak stream stage. This phenomenon is different from the type of DOC flushing reported by Boyer et al. (2000) showing that the peak DOC happens before the peak discharge in a snowmelt dominated watershed. This different concentration discharge relationship can be attributed to different dominant runoff mechanisms between rainfall events and snow melt events and to different time scales associated with these two types of hydrological phenomena (Inamdar and Mitchell, 2006). Furthermore, in watersheds with a very large snowmelt event, there is enough water flowing through the shallow soils to overwhelm the production rate of DOC and dilute the outflow from the hillslope.

The rise of the stream stage and the increase in rain water infiltration are the major factors that cause the rise of the water table in the riparian zone. The water table in the riparian zone can rise to the upper soil layer as indicated schematically in Figure 14 (stage B). The DOC concentration in groundwater then increases due to the contact with the shallow soils. As indicated previously, the outward hydraulic

gradients at the bank are greatly increased on the falling limb of the stream stage, after a short period of decrease during the rise of the stream stage (Figure 23). For example, during Event C, the calculated peak out flow water flux on the falling limb of the stream stage is about 3 times the baseflow groundwater outflow flux. The high DOC concentration in water contacting shallow soils will be released during the falling limb of the stream stage hydrograph forced by this high outward hydraulic gradient. This causes the peak DOC to occur on the falling limb of the stream stage. During the bank storage period (which occurred during Events A and C), the outward groundwater and DOC flux is interrupted by an inward hydraulic gradient; hence there is no contribution of DOC to the stream from this hilllslope during the period with an adverse hydraulic gradient. Our model results indicate that the hydraulic properties of the riparian soils also will affect the responses of the water table to the stream stage (e.g., higher hydraulic conductivity in the riparian zone will lead to a faster rise of the riparian groundwater table, and a much larger zone of influence in the riparian zone), which is consistent with results of Whiting and Pomeranets (1997).

In watersheds where the riparian zone is relatively flat, stage fluctuations in the stream can have a significant influence on the water table in the riparian zone (Gu et al., 2008), with impacts on the biogeochemistry of stream-groundwater interaction in the riparian zone (Gu et al., 2012). Our Monte-Carlo simulation and subsequent multiple regression analysis is consistent with this suggestion, showing that the duration of the flood wave in the channel and the hydraulic conductivity (k_x) of the riparian zone are the major controls on the lag time of the C-Q peaks from the hillslope. The van Genuchten parameters and n have a relatively smaller effect on the lag time. Although our work is for a unit width of hillslope, this finding has implications for the watershed given that the watershed can be considered as an assemblage of multiple hillslopes.

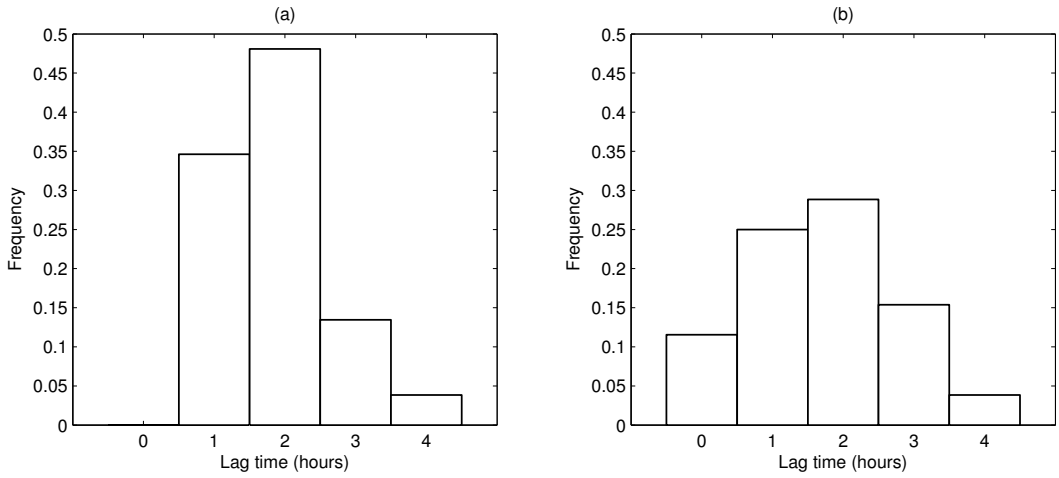

Figure 28: Comparison of the peak stage and peak DOC concentration lag time distribution for 50 storms from 1997 to 1998. (a) Simulated lag time distribution from the 50 storms. (b) Sampled lag time distribtuion from the 50 storms.

The lag time between peaks in concentration and in discharge in WCC was further examined by running our calibrated model for 50 storms during 1997 and 1998 when we have the a fairly complete storm DOC records. The results show that even though our model simulates only the DOC delivery from a specific hillslope, the simulated lag time distribution is similar to the observed lag time between the measured DOC peak and stream stage (Figure 28). There are a small number of storms where the peak of DOC happened before the peak of discharge, a result that is not approachable with our hillslope model. (The peak of the DOC concentration happening prior to the discharge peak could be caused by spatial heterogeneity within the watershed, (e.g. the existence of a riparian wetland.)) Nevertheless, our model gave a comparable distribution to the data showing that a lag time of 2 hours ranks first among all the lag times for the 50 storms in the watershed. The riparian zone is likely to provide a first order control on DOC export to the stream in watersheds (Hornberger et al., 1994; McClain et al., 1997). The groundwater table typically is shallow in the riparian zone, so DOC produced in the riparian areas of the watershed can be easily delivered to the groundwater and to the adjacent stream (Mei et al., 2012). Conversely, DOC produced in the upland area is less likely to affect the stream DOC

concentration due to the strong sorption and biodegradation biogeochemical processes along flow pathways in the soil (Wallis, 1979). Our two-dimensional model simulation results demonstrate the joint effects of coupled processes: DOC fluxes are high near the stream and decline rapidly towards the upland area (Figure 27). The simulation results show that BDOC concentration in outflow to the stream rises and falls faster than RDOC, indicating that BDOC is concentrated in the upper soil. This is consistent with observations made in other studies (McDowell et al., 2006).

Our research focused on one hillslope, looked at the DOC concentration in the stream and riparian zone and DOC fluxes along lateral groundwater flow paths, and examined how peak DOC efflux from the hillslope is affected by the stream hydrograph and by riparian zone hydraulic properties. Although our two dimensional model can capture only the dynamic pattern of the DOC variation generated from a specific hillslope in WCC, the results indicate plausible mechanisms that produce results that are consistent with our field measurements and with observations made on other watersheds. In particular, a riparian zone flushing mechanism is consistent with observed patterns of DOC C-Q relationships in rainstorms.

5 Detailed mathematical formulations for chapter 3

5.1 Flow model details

The van Genuchten soil characteristic curve is used in our flow model [van Genuchten, 1980]:

$$S_e = (\theta - \theta_r) \,/\, (\theta_s - \theta_r) = (1 + |\alpha h|^n)^{-m} \tag{44}$$

$$K = K_s {S_e}^{1/2} \left[1 - \left(1 - {S_e}^{1/m} \right)^m \right]^2 \tag{45}$$

where θ is soil moisture content [L^3L^{-3}]; r is residual soil moisture content [L^3L^{-3}]; θ_s denotes saturated moisture content [L^3L^{-3}]; α is an empirical parameter [L^{-1}]; n and m are related empirical parameters, $m = 1 - 1/n$; K_s is the saturated hydraulic

conductivity tensor [LT^{-1}]. The porous media was assumed to be anisotropic in this study. Root uptake term is a combination of stress response function and normalized water uptake distribution function (Raats, 1974; van Genuchten, 1987). Full details of those formulations are given by Mei et al. (2012). The root uptake term was only applied to the unsaturated zone in this work.

5.2 Transport model details

We assume that the porous medium is isotropic with respect to hydrodynamic dispersion. In the two-dimensional problem, the tensor of the dispersion coefficient can be expressed as follows (Bear, 1988) and (Zheng and Wang, 1999):

$$\begin{aligned} \widetilde{D}_{xx} &= \theta D_{xx} = \alpha_L q_x^2/|q| + \alpha_T q_y^2/|q| + \theta D_0 \\ \widetilde{D}_{yy} &= \theta D_{yy} = \alpha_L q_y^2/|q| + \alpha_T q_x^2/|q| + \theta D_0 \\ \widetilde{D}_{xy} &= \widetilde{D}_{yx} = (\alpha_L - \alpha_T)\, q_x q_y/|q| \end{aligned} \tag{46}$$

where θ is volumetric water content [-]; q,q_x ,q_y stands for Darcy velocity [LT^{-1}] and its component at x and y directions in the Cartesian system and D_0 is the molecular diffusion coefficient [L^2T^{-1}]; α_L is the longitudinal dispersivity of the porous medium [L] and α_T is the transversal dispersivity of the porous medium [L], the ratio of transverse dispersivity to longitudinal dispersivity is assumed to be 0.1 in this research; an apparent dispersivity tensor [L^2T^{-1}] instead of a hydrodynamic dispersion coefficient D was used for the programming convenience.

Identically, the apparent thermal conductivity λ_{ij} is given by Simunek and Sejna (1999):

$$\lambda_{xx} = \lambda_L C_w {q_x}^2/|q| + \lambda_T C_w {q_x}^2/|q| + \lambda_0$$
$$\lambda_{zz} = \lambda_L C_w {q_z}^2/|q| + \lambda_T C_w {q_x}^2/|q| + \lambda_0 \quad (47)$$
$$\lambda_{xz} = \lambda_{zx} = (\lambda_L - \lambda_T) C_w q_x q_z/|q|$$

where λ_L and λ_T are the longitudinal and transverse thermal dispersivity respectively [L]; C_w is the volumetric heat capacities of water [$ML^{-1}T^{-2}K^{-1}$]; λ_0 is thermal conductivity [$MLT^{-3}K^{-1}$] following Chung and Horton (1987):

$$\lambda_0 = b_0 + b_1\theta + b_2\theta^{0.5} \quad (48)$$

where b_0, b_1, b_2 are empirical constants [-]; θ is volumetric water content [-].

The first-order microbial DOC mineralization coefficient was calculated using a modified van Hoff equation to account for the effects of biodegradation, full details are given by Yurova et al. (2008).

5.3 Numerical Solution

5.3.1 Finite element model details

The Galerkin finite element method is used to determine approximate solutions to equations under appropriate initial and boundary conditions (Neuman, 1973). For our problem, a triangular mesh and linear shape functions were used. The terms C, K_r, θ and S within each element can be approximated using the linear shape function N_l with their values on the corners of triangles:

$$K_r = K_{rl}N_l, \quad C = C_l N_l, \quad \theta = \theta_l N_l, \; S = S_l N_l \quad (49)$$

where, l stands for the corners of the triangle; the Einstein summation convention is applied.

The resulting linear system can be written in the following form:

$$\mathbf{A}\mathbf{h} + \mathbf{B}\frac{d\mathbf{h}}{dt} = \mathbf{G} + \mathbf{S} + \mathbf{F} \tag{50}$$

where $\mathbf{A}$ and $\mathbf{B}$ are $n \times n$ matrices; $\mathbf{h}$ and $\mathbf{G}$, $\mathbf{S}$, $\mathbf{F}$ are vectors. $\mathbf{G}$, $\mathbf{S}$ and $\mathbf{F}$ represent the gravity term, the source and sink term and boundary flux term respectively. A fully implicit scheme is used for the time derivative. The iterative method put forward by Berg (1999), was extended to solve this nonlinear system for the 2D FEM. This scheme uses a gradually increasing under relaxation technique to obtain fast convergence and uses a standard chord slope approximation for the storage term C (Rathfelder and Abriola, 1994). Mass lumping was used to avoid unphysical numerical oscillation for both flow and transport models following Neuman (1973).

$$\frac{dh}{dt} = \frac{\sum_e \int_\Omega \left(C + \frac{\theta}{n} S_s\right) \frac{\partial h}{\partial t} N_i d\Omega}{\sum_e \int_\Omega \left(C + \frac{\theta}{n} S_s\right) N_i d\Omega} \tag{51}$$

$$\frac{\partial}{\partial t}\left(\theta c_R + \rho s_R\right) = \frac{\sum_e \int_\Omega \frac{\partial}{\partial t}\left(\theta c_R + \rho s_R\right) N_i d\Omega}{\sum_e \int_\Omega N_i d\Omega} \tag{52}$$

The final linear system is:

$$\left\{\mathbf{A} + \frac{\mathbf{1}}{\mathbf{\Delta t}}\mathbf{B}'\right\} \mathbf{h}_{t+\Delta t}^{k+1} = \frac{1}{\Delta t}\mathbf{B}'^{k}\mathbf{h}_t + \mathbf{G}^k + \mathbf{F}_t + \mathbf{S}_t \tag{53}$$

where, the superscript k indicates the iteration step during time t and $t + \Delta t$. $\mathbf{B}$ is the matrix in time derivative terms after mass lumping. To avoid excessive iteration, we use the source/sink term ($\mathbf{S_t}$) at the old timestep instead of putting it into the iteration. The reactive transport model is linear, thus no iteration method is needed.

5.3.2 Water and solute flux calculation

The method put forward by Yeh (1981) is used to calculate the nodal Darcy velocity.

$$\sum_{e} \int_{\Omega} q_i N_l d\Omega = -\sum_{e} \int_{\Omega} K_{i,j} \frac{\partial H}{\partial x_j} N_l d\Omega \tag{54}$$

where, Nl is the lth shape function on the corner of a specified element; q_i is the ith component of the unknown nodal Darcy velocity. Assuming that q_i varies linearly in the elements.

$$q_i = q_{i,l} N_l \tag{55}$$

the two (x,y directions) linear equations with unknown q_i, were solved to obtain each of the velocity components.

The hillslope discharge and its contribution of DOC concentration to the stream are calculated using

$$Q = \sum_{e_s} q_i l_i, C_{strm} = \frac{\sum\limits_{e_s} q_i l_i C_i}{\sum\limits_{e_s} q_i l_i} \tag{56}$$

where e_s is the number of boundary elements contained in the seepage face segment; q_i is the flow rate normal to the boundary element i; l_i is the length of the boundary element i. The above formulations hold when the seepage face coincides exactly on one of the node on the boundary. When the limit of the seepage face is not at one of the nodes, the following formulations are used.

$$Q = \sum_{e_s} q_i l_i + q_1 \left(x - \frac{x^2}{2L} \right) + \frac{q_2}{2L} x^2, C_{stm} = \frac{\sum\limits_{e_s} q_i l_i C_i + q_1 C_1 \left(x - \frac{x^2}{2L} \right) + \frac{q_2 C_2}{2L} x^2}{\sum\limits_{e_s} q_i l_i + q_1 \left(x - \frac{x^2}{2L} \right) + \frac{q_2}{2L} x^2} \tag{57}$$

where x is the length of seepage face above the top node of seepage face (i.e., the length of seepage face between two element nodes), and is determined by modifying the method of Beven (1977). L is the length of the element side that contains the

length x; q_1 and $C_1$are the nodal flux and concentration of the lower node of the element containing x; q_2 and C_2 are the nodal flux and concentration of the higher node this element. When x equals zero, equations (57) reduce to equations (56).

CHAPTER 4

A MODEL TO SIMULATE THE IN STREAM DISSOLVED ORGANIC CARBON DYNAMICS IN A HEADWATER WATERSHED

1 Introduction

Dissolved organic carbon (DOC) plays an important role in both aquatic and terrestrial ecosystem functioning and drinking water quality (McDowell, 2003). DOC supplies nutrients and energy for heterotrophic bacteria in surface waters and soils, affects the stream pH (Hruska et al., 2003), influences metal export and speciation in streams and rivers (Shafer et al., 1997), and affects attenuation of light in lakes (Morris et al., 1995). In forested upland watersheds, soil biota and terrestrial plants are the primary DOC sources to a stream (Thurman, 1985; Palmer et al., 2001). Hydrology function as the first order control on the temporal variability of stream water DOC (Laudon et al., 2011).

In small forested upland watersheds, stream DOC concentration variation reflects different hydrological conditions. Under baseflow conditions, the DOC concentration is relatively low and stable (Buffam et al., 2001); this stable concentration is generally attributed to the contribution of DOC from relatively deep groundwater (Hope et al., 1994), with relatively long residence time of water in the subsurface. The low DOC concentration is attributed to removal of DOC by adsorption and by bacterial consumption during the course of its transport through soils and rocks to the stream (Dawson et al., 1981). A diel concentration pattern presents in streams seasonally during base flow due to the activities of stream algae (Kaplan and Bott, 1982).

During storm events, the groundwater table rises and intersects shallow soil layers

with a high soil organic matter content (Hornberger et al., 1994); this increase in the elevation of the groundwater table will increase the groundwater DOC concentration. The high DOC concentration water, especially in the riparian zone, will be released to the stream when the groundwater is discharged to the stream (Y. Mei et al, The delivery of dissolved organic carbon from a forested riparian hillslope to a headwater stream, submitted to Water Resources Research, 2013). When overland flow occurs, either by Hortonian or by saturation-excess mechanisms, activate highly dynamic water and solution mass exchange at the soil surface where high soil organic carbon content is present (Wallach and Shabtai, 1992; Wallach et al., 2001). Both surface flow and groundwater flow DOC transport mechanisms can cause DOC to increase in the stream during storm events. A comprehensive modeling tool is needed to synthesize, to describe these coupled processes, and to evaluate the relative importance of different processes at the watershed scale.

Development of watershed hydrologic simulation incorporating multiple processes in the context of physically based theory has been ongoing for many years. For example: Abbott et al. (1986 (a) and Abbott et al. (1986 (b) introduced a physically-based distributed hydrological model MIKE-SHE. This model "weakly" coupled each processes by having independent governing equation and solution techniques [Singh, 1995]. It includes modules for water quality and sediment transport, which potentially could be used for DOC simulation. Other integrated hydrological models were also developed to simulate multiple mechanisms of rainfall-runoff mechanisms (VanderKwaak, 2000; Panday and Huyakorn, 2004; Yeh et al., 1998). The Penn State Integrated Hydrological Model (PIHM) is also one of this kind of model (Qu and Duffy, 2007).

Physically-based, watershed-scale DOC models are not currently available. Previous work has focused on the use of lumped models (Grieve, 1991; Hornberger et al., 1994; Boyer et al., 2000; Neff and Asner, 2001; Michalzik et al., 2003; Futter et al.,

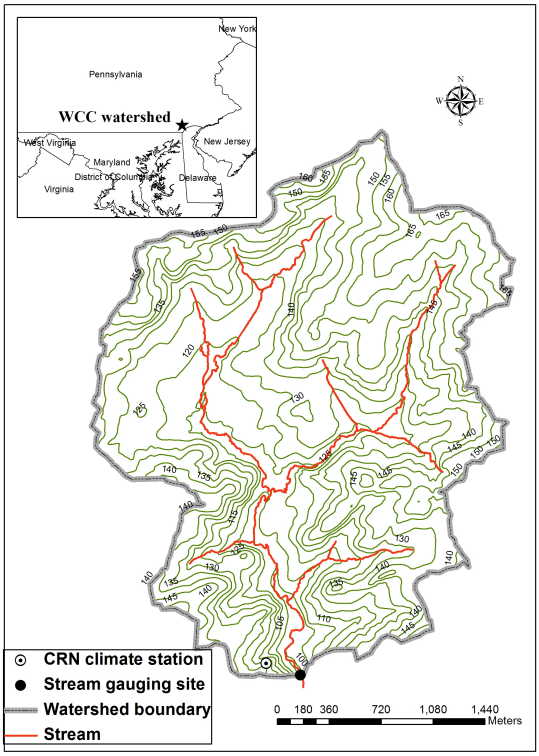

Figure 29: The White Clay Creek watershed location and contour map with its stream gauging and climate station locations

2007; Jutras et al., 2011; Xu et al., 2012) with varying degrees of disaggregation of model compartments. Physically-based models for DOC have focused on one-dimensional or two-dimensional treatments. Mei et al.[2012] developed an integrated dual-permeability model for a one-dimensional sopil column and pointed out that the DOC concentration in groundwater is inversely correlated to the groundwater table depth. Mei et al. [2013] present a two-dimensional hillslope finite element model to simulate the delivery process of DOC to the stream (Y. Mei et al, The delivery of dissolved organic carbon from a forested riparian hillslope to a headwater stream, submitted to Water Resources Research, 2013). A full catchment-scale modeling scheme using physically-based approaches to understand DOC fate and transport in catchments is lacking.

The main goal of this research is to develop a new hydrological simulation model for watershed DOC biogeochemistry. We adopted the PIHM framework as the basic hydrological simulation platform and coupled this model with a reactive transport DOC model across the watershed. The model was developed and calibrated against hydrological and stream DOC data from a headwater watershed, the White Clay Creek (WCC) watershed in southeastern Pennsylvania, USA. Our simulation results show that the model is able to capture stream discharge as well as DOC concentration dynamics at WCC during the simulation period, calendar year 2010, reasonably well. Our findings show that subsurface flow contributes more than 80% of the annual DOC export to WCC. This finding is consistent with previous research showing that subsurface DOC export contributes about 72% of the annual DOC export in WCC (Mei et al., 2012).

2 Study site and data collection

2.1 Site Description

This study was conducted within WCC watershed, a 3rd order watershed with an area of 7.25 km^2 (Figure 29). The stream drains the watershed with 12,878 m of total stream length and an average gradient of 0.008 m/m. Land use includes the following categories: a largely intact temperate deciduous riparian forest (27 %); pastures or hay fields (33 %); and row crop agriculture (27 %) (Newbold et al., 1997). WCC is the catchment has moderate relief, with land surface altitude ranging from 98 m at the watershed outlet to 174 m near the watershed divide. A 5 to 15 m deep saprolite lies beneath 1 to 2 m deep unglaciated soils that are primarily hapludults, except in the riparian zone, where aquic fragiudults predominate on top of largely crystalline and carbonate bedrock. The bedrock geology belongs to the Wissahickon formation and includes oligoclase-mica schist, mafic gneiss, felsic gneiss, setters quartizite, and metadolamite, with occasional pegmatite dikes (Tsang et al., 2013). Snow occurs

across the watershed intermittently from late December to early April.

2.2 Meteorological, hydrological and spatial GIS data

Most of the meteorology data used in our model were obtained from the US Climate Reference Network (CRN) "PA Avondale 2 N Stroud Water Research Center" station, 250 m northwest of the 3rd-order WCC stream gauge. The CRN station records real time meteorology data including precipitation, air temperature, solar radiation, and soil moisture. The averaged annual precipitation was 1243 mm/yr from 1996 to 2010.

The 3rd order stream is gauged with continuously recording instruments. Prior to June 2011 the 3rd-order gauge was a Leopold and Stevens model A-71 float gauge with strip-chart recorder, which was replaced by automated Telog and MiniTroll pressure transducers that recorded stage height at 15-min intervals. Stream stages were converted to stream discharges using rating curves developed from discharge measurements made with the velocity-cross-sectional area method and a handheld Marsh-McBirney flow meter. The mean annual discharge for the 3rd-order WCC averaged 127 L/s from 1996 to 2009, with a range of flows from 15 L/s to 47900 L/s. (Tsang et al., 2013).

U.S. Geological Survey (USGS) 10-m digital elevation model (DEM) data were used in this research for watershed delineation and preprocessing. The (leaf area index) LAI data were obtained from the Land Data Assimilation System (LDAS): (`http://ldas.gsfc.nasa.gov/nldas/web/web.veg.monthly.table.html`). Land use-land cover data (Figure 30) were obtained from the National Land Cover Data base (NLCD) (`http://www.epa.gov/mrlc/nlcd-2001.html`). Soil data (Figure 30) were obtained from the Natural Resources Conservation Service (NRCS) (`http://soils.usda.gov/survey/geography/ssurgo/description.html`)

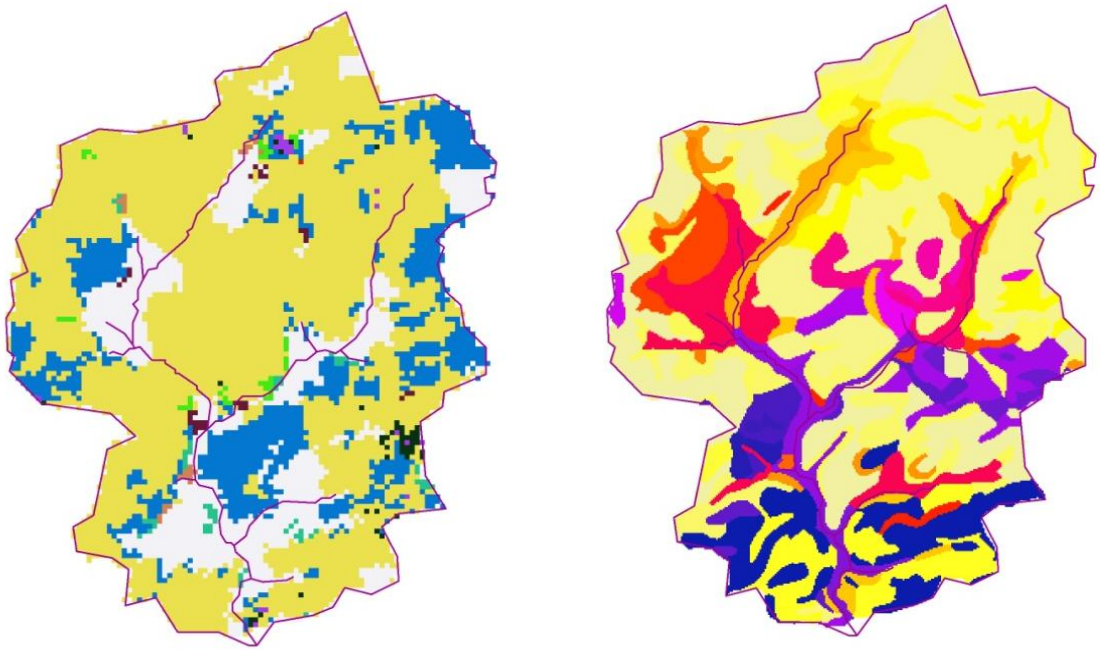

Figure 30: WCC land use and soil type GIS layers

2.3 Dissolved organic carbon biogeochemistry data

DOC storm samples were taken in the summer of 2010 every one or two hours using an ISCO (Teledyne Isco, Inc, Lincoln, Nebraska) sampler. Baseflow DOC samples were taken daily for 2010 at the WCC outlet.

Stream DOC concentrations at baseflow range from 0.8 to 2.0 ppm, and increase up to 15 ppm during stormflow (Mei et al., 2012). Water collected as overland flow during storms had the highest DOC concentrations with a mean of 11.01 ± 0.97 mg C/L (range from 4.96 to 17.85 mg C/L) [McLaughlin, 2012].

Wells in the WCC catchment have been sampled periodically for over ten years. DOC concentrations in 20 wells in the riparian zone average 1.5 ppm, ranging from 0.4 ppm to 9.7 ppm. Three deep wells located in the upland area have a mean DOC concentration of 0.51 ppm, ranging from 0.2 ppm to 0.9 ppm.

3 Mathematical model

3.1 Model development

3.1.1 Overview

Our model represents one of the first attempts to use a spatially distributed approach for watershed dissolved organic carbon simulation. The model uses the framework of PIHM (Penn State Integrated Hydrological model) (Qu and Duffy, 2007; Kumar et al., 2010) (Figure 31). PIHM is a physically based model handling catchment hydrological processes in a fully coupled manner. It considers the essential hydrological components in the watershed hydrological cycle, using physically-based partial and ordinary differential equations to describe all the processes. The key equations including the diffusive wave approximation of the Saint Venant equations for two-dimensional overland flow and one-dimensional open channel flow (Gottardi and Venutelli, 1993), the Penman-Monteith equation for evapotranspiration (Monteith, 1965), and the Richards equation for subsurface flow. Other processes such as snow melt and interception are also included in the model (Qu and Duffy, 2007). A solute fate and transport model based on the PIHM framework (Bhatt, 2012) is a part of the PIHM framework. A DOC model with a kinetic mass transfer connection with soil organic carbon pools was developed in this research and coupled with PIHM.

Soil organic matter (SOM) content was considered as the carbon source pool in our model. SOM was assumed to decline exponentially from the ground surface. The SOM source is modeled to account for leaching from the organic carbon rich layer of soil by soil water. Part of the DOC is available to be consumed by microbial activity, once converted from SOM to DOC.

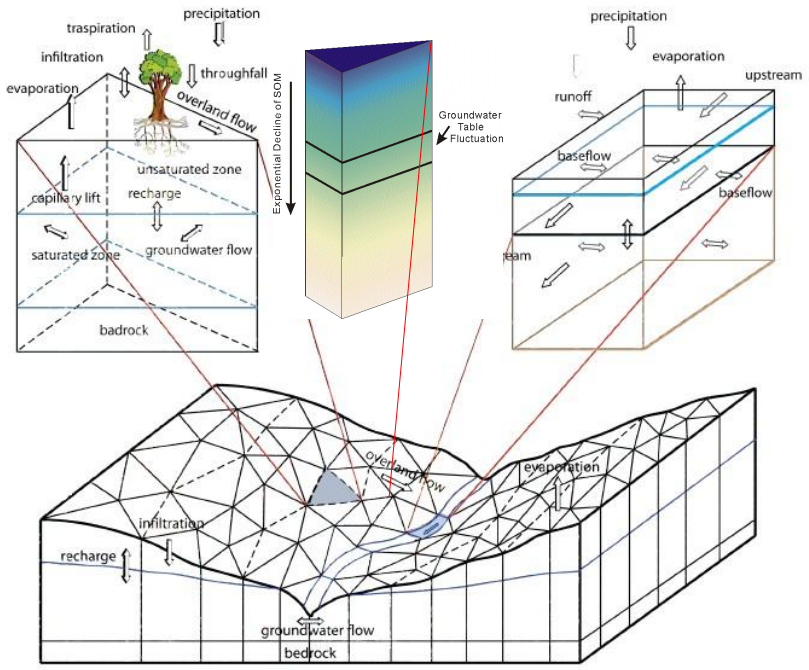

Figure 31: The spatial domain decomposition and numerical representation of PIHM. SOM was introduced as a new variable. (figure modified from Bhatt [2012])

3.1.2 Mathematical formulations

Soil organic carbon typically decreases rapidly with distance beneath the soil surface (Dawson et al., 1981; Mertens et al., 2007). Exponential functions have been used to describe the DOC concentration decline from the soil surface (Weiler and McDonnell, 2006; Seibert et al., 2009) which relates to the decline in SOM with depth (Jobbagy and Jackson, 2000). In our research, we use SOM as a simplified DOC source pool and impose an exponential decline model for SOM with depth below the soil surface.

$$s = s_0 e^{-\alpha(H-z)} \tag{58}$$

where s_0 is the soil organic carbon content [MM^{-1}] at the soil surface; s represents the soil organic carbon content as a function of soil depth; H is the aquifer depth [L]; α is the exponential decline rate of the soil organic carbon content with depth [-].

The exponential function is convenient within the PIHM framework and provides a simple parameterization.

Continuity equations describing mass balance of soil organic mass were adopted to describe both the dissolved and sorbed phase of DOC in our model. Adsorption is likely responsible for maintaining low DOC substrate concentrations in the mineral soil and preventing its loss into stream water. We used a one-site non-equilibrum, first-order kinetic model for DOC adsorption. Sorption was treated as a reversible process. A first order rate coefficient (τ) and a constant sorption equilibrium distribution coefficient (K_d) were applied to model DOC transfer between sorbed and dissolved phases: overland DOC

$$\frac{\partial C}{\partial t} = \nabla \cdot \left(D \frac{\partial C}{\partial x_i} - v_i C \right) + e_{ov} \tag{59}$$

subsurface DOC

$$\frac{\partial \left(\theta C + \rho s \right)}{\partial t} = \nabla \cdot \left(\theta D \frac{\partial C}{\partial x_i} - q_i C \right) - e_{ov} \tag{60}$$

$$\frac{\partial s}{\partial t} = -\tau \left(s - K_d C \right) \tag{61}$$

where, C is the resident concentration of DOC [ML^{-3}]; D is the dispersion coefficient [L^2T^{-1}]; q is the depth averaged specific discharge of subsurface flow [LT^{-1}]; v_i is the depth averaged water velocity of overland flow; $e_{ov}$is the DOC mass exchange term between overland flow and subsurface flow [$ML^{-3}T^{-1}$]; Kd is the sorption equilibrium distribution constant [L^3M^{-1}]; τ is the first order mass transfer coefficient [T^{-1}]; ρ is the bulk density of the soil [ML^{-3}]; s is the soil organic carbon content [MM^{-1}]; θ is the soil moisture [L^3L^{-3}];

3.1.3 Derivation of the general form of equation (Taking subsurface DOC transport equation as an example)

Following the semi-discrete finite volume approach presented by Qu and Duffy (2007), the global governing partial differential equations (PDE) can be reduced to a local ordinary differential equation (ODE) system by doing integration of the PDE over a local control volume, Ω.

$$\int_{\Omega} \frac{\partial \left(\theta C + \rho s\right)}{\partial t} dV = \int_{\Omega} \nabla \cdot \left(\theta D \frac{\partial C}{\partial x_i} - q_i C\right) dV - \int_{\Omega} e_{ov} dV \tag{62}$$

$$\int_{\Omega} \frac{\partial s}{\partial t} dV = \int_{\Omega} -\tau \left(s - K_d C\right) dV \tag{63}$$

The first term on the right hand side can be rewritten as integrals over the entire bounding surface of the control volume using Gausss divergence theorem. Vector n is the outward unit vector normal to the control volume surface. The time derivative of the first term on left-hand side was brought out of the volume integral by using assuming the control volume does not change at a given time instance.

$$\frac{\partial}{\partial t}\left(\int_{\Omega} \theta C dV + \rho \int_{\Omega} s dV\right) = \oiint_{s} \mathbf{n} \cdot \left(\theta D \frac{\partial C}{\partial x_i} - q_i C\right) dA - \int_{\Omega} e_{ov} dV \tag{64}$$

$$\frac{\partial}{\partial t} \int_{\Omega} s dV = -\tau \int_{\Omega} \left(s - K_d C\right) dV \tag{65}$$

Combine equation (64) with equation (65) and rearranging the terms yields:

$$\frac{\partial}{\partial t}\left(\int_{\Omega} \theta C dV\right) = \oiint_{s} \mathbf{n} \cdot \left(\theta D \frac{\partial C}{\partial x_i} - q_i C\right) dA - \int_{\Omega} e_{ov} dV + \tau \rho \int_{\Omega} \left(s - K_d C\right) dV \tag{66}$$

Using an average concentration in the control volume:

$$\int_{\Omega} \theta C dV = n \overline{C} V \tag{67}$$

$$\int_{\Omega} s dV = \overline{s} V \tag{68}$$

Thus:

$$nV\frac{\partial \overline{C}}{\partial t} + n\overline{C}\frac{\partial V}{\partial t} = \oiint_{s} \mathbf{n} \cdot \left(\theta D \frac{\partial C}{\partial x_i} - q_i C\right) dA - \int_{\Omega} e_{ov} dV + \tau\rho \int_{\Omega} (s - K_d C)\, dV \tag{69}$$

$$\overline{s}\frac{dV}{dt} + V\frac{d\overline{s}}{dt} = -\tau \int_{\Omega} (s - K_d C)\, dV \tag{70}$$

Rearranging the terms and integrating equation over an arbitrary time step Δt from t to $t + \Delta t$:

$$\begin{aligned}\int_{t}^{t+\Delta t} \frac{\partial \overline{C}}{\partial t} dt = \frac{1}{nV} \int_{t}^{t+\Delta t} \left[\oiint_{s} \mathbf{n} \cdot \left(\theta D \frac{\partial C}{\partial x_i} - q_i C\right) dA\right] dt \\ + \frac{1}{nV} \int_{t}^{t+\Delta t} \left[-\int_{\Omega} e_{ov} dV + \tau\rho \int_{\Omega} (s - K_d C)\, dV - n\overline{C}\frac{\partial V}{\partial t}\right] dt\end{aligned} \tag{71}$$

$$\int_{t}^{t+\Delta t} \frac{d\overline{s}}{dt} dt = \frac{1}{V} \int_{t}^{t+\Delta t} \left[-\tau \int_{\Omega} (s - K_d C)\, dV - \overline{s}\frac{dV}{dt}\right] dt \tag{72}$$

Using a simple Euler stepping, we can obtain the equation calculating the $\bar{C}$ and $\bar{s}$ at a given time step:

$$\begin{aligned}&\overline{C}^{t+\Delta t} = \overline{C}^{t} + \\ &\frac{\Delta t}{nV}\left[\oiint_{s} \mathbf{n} \cdot \left(\theta D \frac{\partial C}{\partial x_i} - q_i C\right) dA - \int_{\Omega} e_{ov} dV + \tau\rho \int_{\Omega} (s - K_d C)\, dV - n\overline{C}\frac{\partial V}{\partial t}\right]^{t}\end{aligned} \tag{73}$$

$$\overline{s}^{t+\Delta t} = \overline{s}^{t} + \frac{\Delta t}{V}\left[-\tau \int_{\Omega} (s - K_d C)\, dV - \overline{s}\frac{dV}{dt}\right]^{t} \tag{74}$$

The above derivation is a general strategy for PIHM to obtain ODEs from PDEs. The mass flux terms on the right hand side of the equation (73) was evaluated in PIHM depends on the location (overland flow, unsaturated zone, saturated zone).

3.1.4 The integrated form of DOC governing equations under PIHM frame work

PIHM uses the groundwater table to separate the triangular column into two parts (Duffy, 1996; Qu and Duffy, 2007). Thus the subsurface DOC transport was separated into unsaturated zone and saturated zone parts, allowing organic carbon mass exchange between these two zones. Under the PIHM framework, soil moisture is represented as integrated over the depth of the unsaturated zone and concentrations are averaged across the zone. We use the following formula to describe the depth distributed soil moisture, DOC concentration and soil organic carbon content in the unsaturated zone.

$$h^u = \int_{z_1}^{z_2} \frac{\theta}{\theta_s} dz = \frac{1}{n} \int_{z_1}^{z_2} \theta dz, h^g = H^g \tag{75}$$

$$\int_{z_1}^{z_2} \theta C dz = \overline{C^u} \int_{z_1}^{z_2} \theta dz, \overline{C^g} = \frac{\int_{z_0}^{z_1} h^g C dz}{h^g} \tag{76}$$

$$\overline{s^u} = \frac{1}{H^u} \int_{z_1}^{z_2} s_0 e^{-\alpha(H-z)} dz, \overline{s^g} = \frac{1}{H^g} \int_{z_0}^{z_1} s_0 e^{-\alpha(H-z)} dz \tag{77}$$

$$H^u = z_2 - z_1, H^g = z_1 - z_0 \tag{78}$$

where, z_2 z_1 z_0 is the elevation of the ground surface, water table and bed rock elevation respectively [L]; A_b is the area of each element [L^2]; (h^u, h^g) are the depth of water storage in the unsaturated zone and saturated zones respectively [L] (volume of stored water per unit projected horizontal element area); (H^u, H^g) are the lengths of the unsaturated zone and saturated zones; ($\bar{C}^u$, $\bar{C}^g$) are the average concentrations in unsaturated zone and saturated zone respectively; θ is the soil moisture [-];($\bar{s^u}$, $\bar{s^g}$) are the average SOM contents in unsaturated zone and saturated zone respectively. The total mass of DOC in the unsaturated zone, saturated zone, dissolved phase and

sorbed phase can be described as follows.

$$M_{sol}^{u} = A_b \int_{z_1}^{z_2} \theta C dz = A_b h^u n \overline{C^u}, M_{sob}^{u} = \rho A_b \int_{z_1}^{z_2} s_0 e^{-\alpha(H-z)} dz = \rho A_b \overline{s^u} H^u \tag{79}$$

$$M_{sol}^{g} = A_b \int_{z_1}^{z_2} \theta C dz = A_b h^g n \overline{C^g}, M_{sob}^{g} = \rho A_b \int_{z_0}^{z_1} s_0 e^{-\alpha(H-z)} dz = \rho A_b \overline{s^g} H^g \tag{80}$$

where, superscript u and g represent the unsaturated zone and groundwater zone respectively; subscript *sol* and *sob* represent the dissolved phase and sorbed phase respectively; $\bar{s^u}$ and $\bar{s^g}$ are the averaged soil organic matter content for both unsaturated zone and saturated zone in the sorbed phase; M_{sol} and M_{sob} represent the mass of organic carbon for the dissolved phase and sorbed phase respectively; The total sorbed soil organic carbon mass can then be calculated using the following formula.

$$M_{sol} = \left(H^u \overline{s^u} + H^g \overline{s^g}\right) A_b \rho = \rho A_b \int_{z_0}^{z_2} s_0 e^{-\alpha(H-z)} dz \tag{81}$$

The integrated form of the DOC convection dispersion equations are as follows.
overland DOC:

$$\frac{dM_{sol}^{s}}{dt} = \sum_{j=1}^{3} q_j + q_{ov} \tag{82}$$

unsaturated zone assuming no lateral flow:

$$\frac{d\left(M_{sol}^{u} + M_{sob}^{u}\right)}{dt} = q^0 - q_{ov} - q_s \tag{83}$$

$$\frac{dM_{sob}^{u}}{dt} = -\rho\tau\left(\overline{s} - K_d \overline{C}\right) H^u A_b - q_s \tag{84}$$

saturated zone:

$$\frac{d\left(M_{sol}^{g} + M_{sob}^{g}\right)}{dt} = -q^0 + \sum_{j=1}^{3} q_j + q_s \tag{85}$$

$$\frac{dM_{sob}^{g}}{dt} = -\rho\tau\left(\overline{s} - K_d\overline{C}\right)H^g A_b + q_s \tag{86}$$

where superscripts s, u, and g represent surface, unsaturated and groundwater zones respectively; M_{sol} and M_{sob} represent the mass of organic carbon for dissolved phase and sorbed phase respectively; q_i is the DOC mass flux from each side of the element boundary; q_{ov} is the mass transfer between overland flow and unsaturated flow, q_s is the sorbed SOM mass taken out or brought into the unsaturated zone by groundwater fluctuations. q^0 is the DOC mass flux exchange between saturated zone and unsaturated zone.

$$q^0 = C_R R A_b \tag{87}$$

where, R is the water flux across saturated-unsaturated interface (Duffy, 2004; Kumar et al., 2010) and C_R is the concentration of DOC in unsaturated zone or in saturated zone depending on the direction of the water flux across the saturated-unsaturated interface.

Significant quantities of agrochemicals that have been transferred from soil to surface runoff have been detected in watersheds. In this research, we apply first order, rate limited transfer kinetics to describe DOC mass transfer from organic soil to overland flow following (Wallach and Shabtai, 1992).

$$q_{ov} = k_{ov}\left(\overline{C^u} - \overline{C^s}\right)A_b \tag{88}$$

where, k_{ov} is the mass transfer coefficient [LT^{-1}]; $\bar{C}^u$, $\bar{C}^s$ are the average concentration in the unsaturated zone and overland runoff respectively. The rising and falling of the water table will add and remove SOM mass to the saturated zone and, concurrently remove and add SOM mass to the unsaturated zone. This amount of SOM mass can be calculated using:

$$q_s = \rho A_b \int_{z_{t1}}^{z_{t2}} s_0 e^{-\alpha(H-z)} dz \tag{89}$$

where, qs is the mass of SOM in the element that shifts from or to the unsaturated zone during time period (t_1, t_2) when the water table changes elevation from z_{t1} to z_{t2} ; $\sum_{j=1}^{3} q_j$ is the lateral mass flux across 3 element boundaries;

$$q_j = As_j \left(u_j C_j - D_j \frac{\partial C}{\partial n} \right) \tag{90}$$

where A_{sj} is the area of the jth side of the element.

3.2 Model implementation

Unstructured grids are generated for the WCC by the well-known triangle generating algorithm by (Shewchuk, 2002) which is implemented in PIHMgis (Bhatt et al., 2008), a prepocess and postprocess GIS tool designed for PIHM to visualize the inputs and the results. In our model, we created 774 triangle elements, with refined meshes along the stream channel. The stream channel generated in the model matched the perennial streams observed within the study watershed. In total 109 segments were generated to represent this 3rd order watershed (Figure 32).

The model was built by assuming a 5 meter thick aquifer (from the ground surface to 5 meters below the ground surface). Precipitation and other climate parameters were assumed to be uniformly distributed across the watershed. The model was initialized by running for one year prior to 2010, the year in which detailed measurements were made as part of this research.

Initial values of SOM in the watershed were assumed to be spatially distributed. The average values of SOM were obtained from NRCS associated with each soil type. These averaged values were then used to calculate the exponential decline along each triangular column. The spatially distributed s_0 values were multiplied by a numerical factor during model calibration.

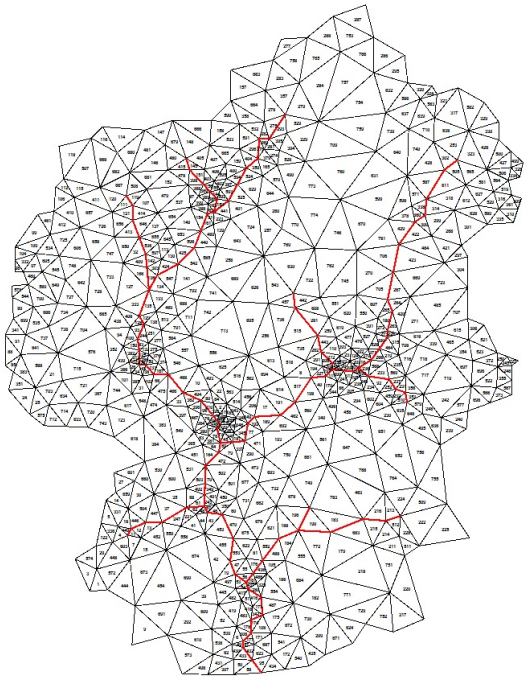

Figure 32: Spatial domain decomposition of White Clay Creek watershed. including in total 109 stream elements and 774 triangle elements

3.3 Model calibration

In the flow model, the parameters calibrated are: horizontal and vertical hydraulic conductivity of the saturated zone, macropore horizontal conductivity, macropore depth, vertical macropore hydraulic conductivity; vertical hydraulic conductivity; river depth, porosity; van Genuchten model parameter α; and van Genuchten model parameter n (Kumar et al., 2010). The calibration was done by trial and adjustment. In the DOC model, the parameters calibrated are distribution constant (K_d); first order rate coefficient (τ); exponential decay rate of the SOM along soil profiles (α) and the mass transfer coefficient (K_{ov}); the calibration was done by trial and adjustment.

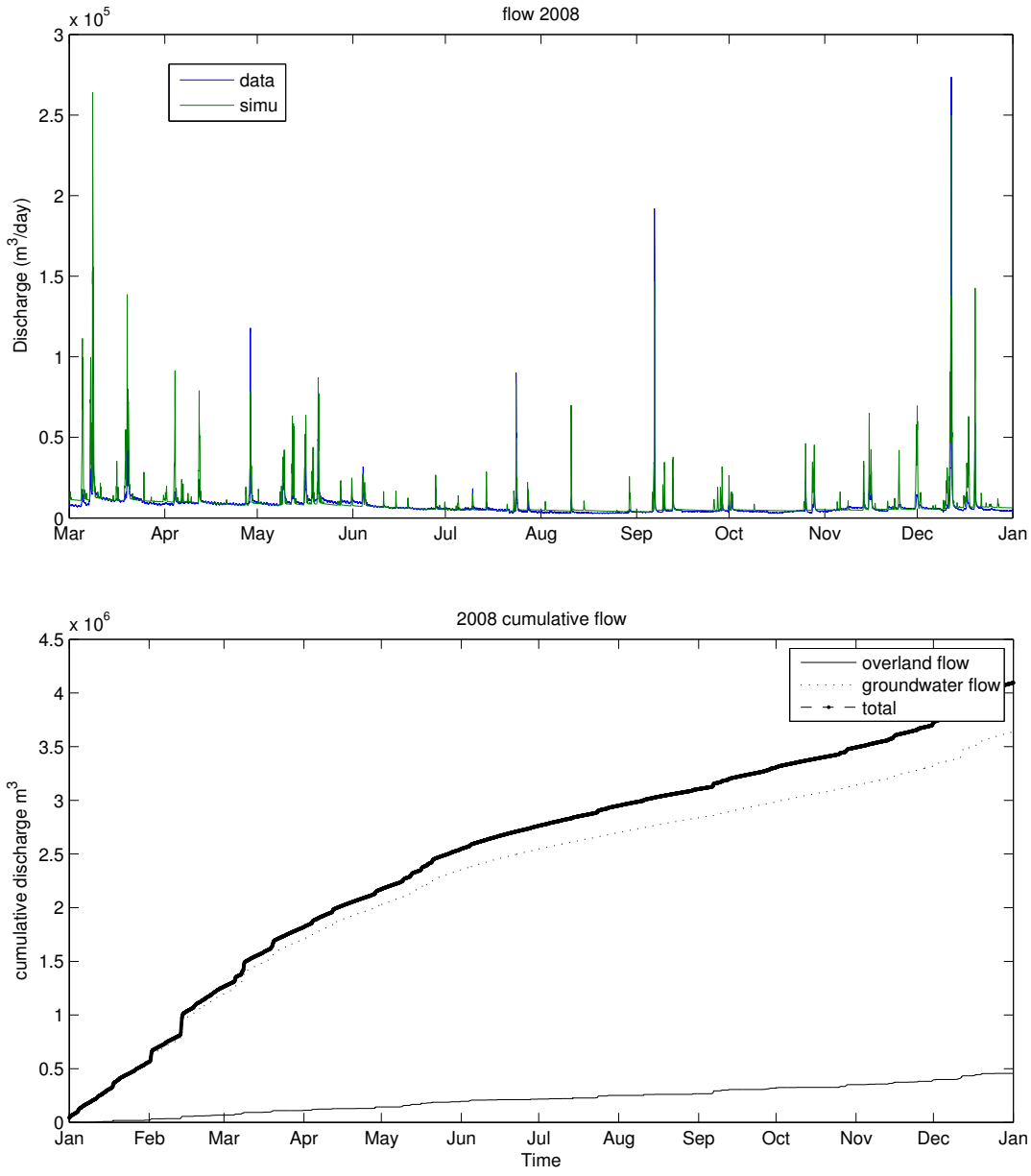

Figure 33: Flow calibration flow results for the year 2008

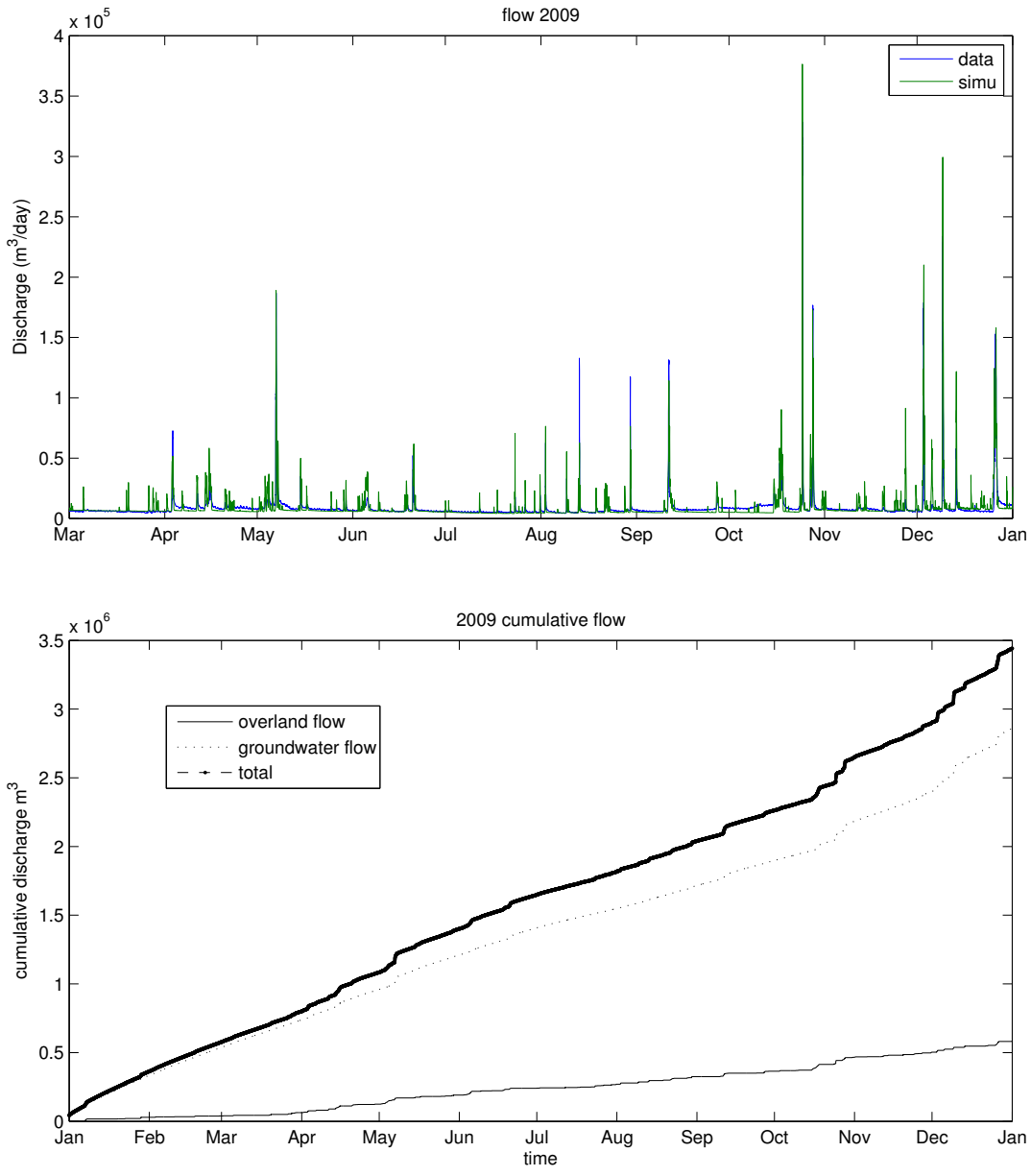

Figure 34: Flow calibration flow results for the year 2009

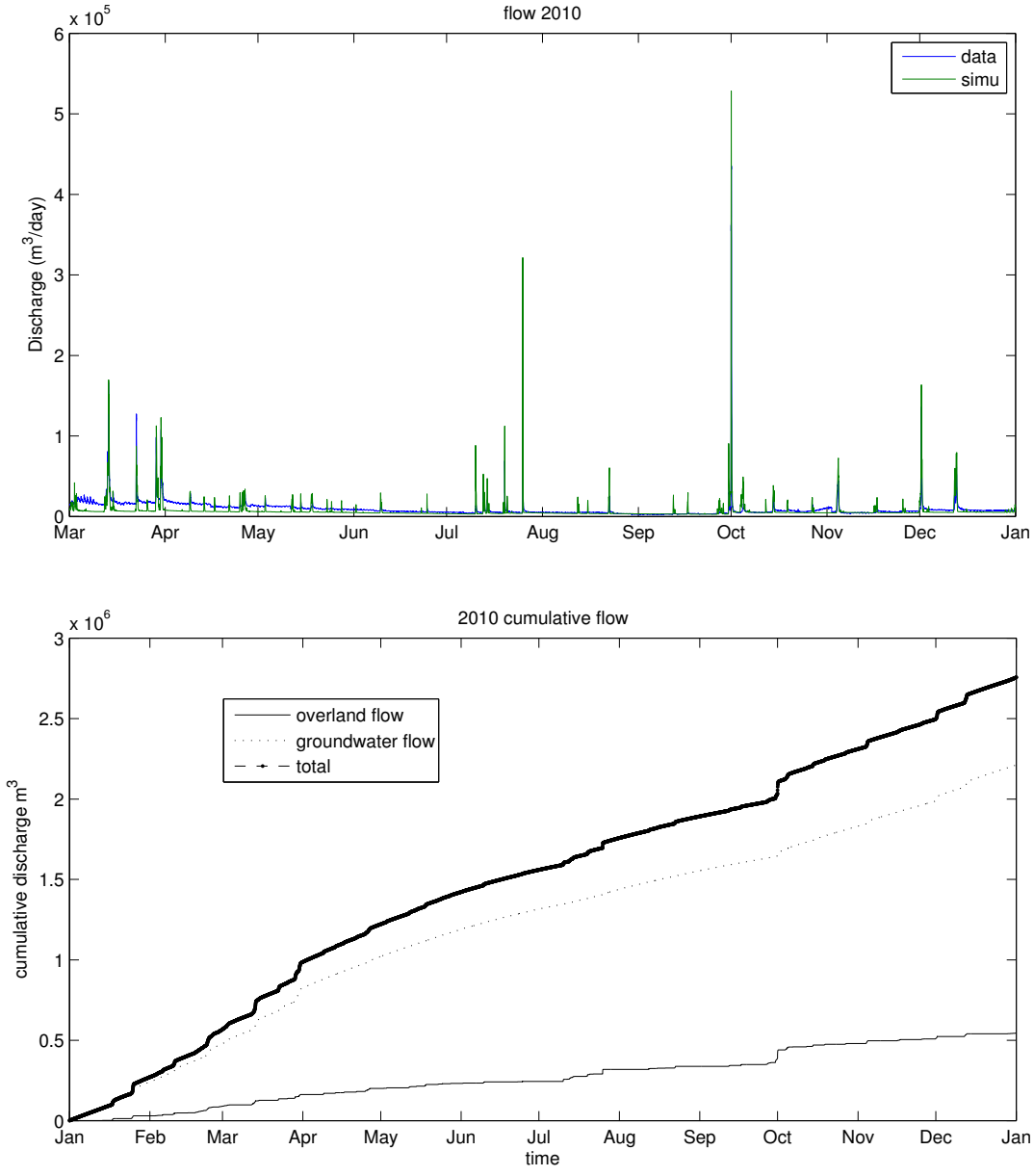

Figure 35: Flow calibration flow results for the year 2010

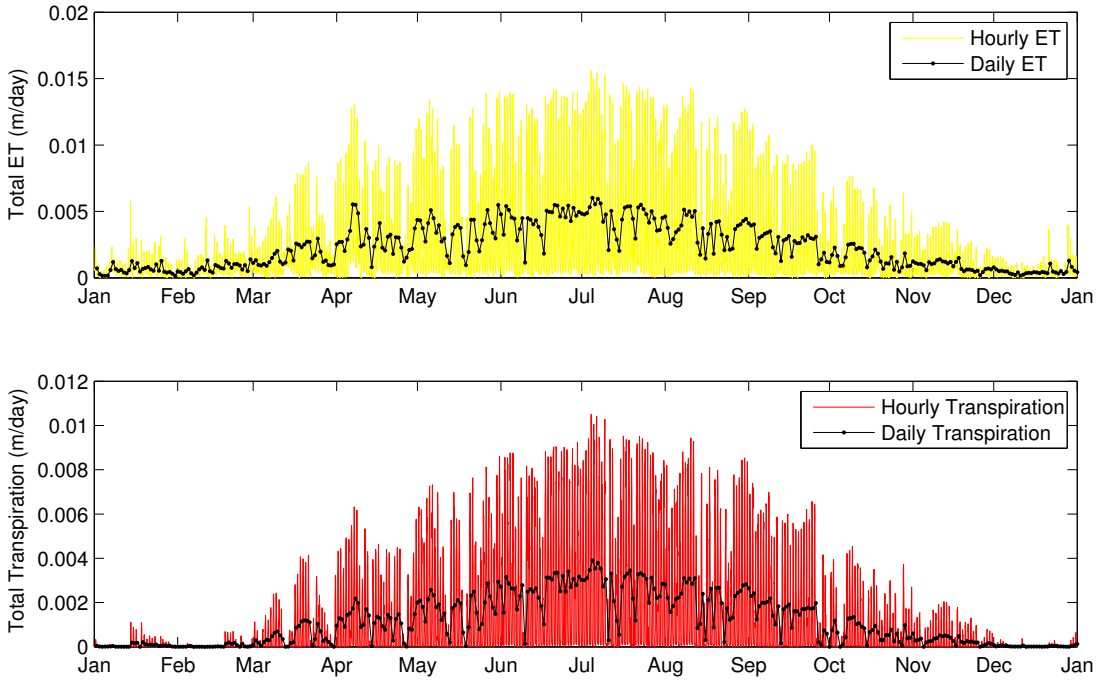

Figure 36: ET and transpiration of the year 2010

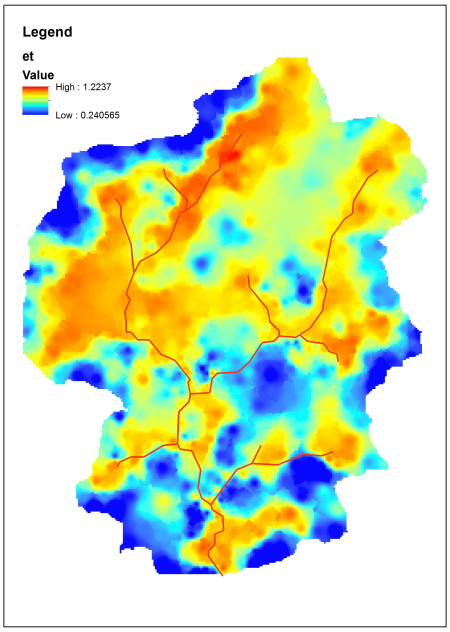

Figure 37: Spatial distribution of simulated ET of the year 2010

4 Results

4.1 Watershed simulation results

We calibrated the PIHM against discharge data collected during a three-year period, 2008, 2009, and 2010. The simulation results replicate the discharge at the watershed outlet reasonably well (Figure 33, 34, and 35), except January and February when some precipitation is in the form of snow. The baseflow recession curve at WCC watershed is very steep compared to some other watersheds, e.g. Shale Hill watershed (Qu and Duffy, 2007). The discharge curve responds quickly to precipitation and declines rapidly to baseflow conditions within several hours after the rainfall stops.

Subsurface flow contributes the bulk of the total discharge over the three years, 88%, 83% and 80% respectively. Overland flow contributes a relatively small amount, 12%, 17% and 20% for the three years respectively.

The evaportranspiration (ET) simulation results show a sinusoidal pattern over the course of one year (2010) (Figure 36). ET gradually increases from January to July and slowly declines to the end of the year. The simulated spatial distribution of ET shows that relatively higher ET is found in the riparian zone while a relatively lower ET is found in the upland area (Figure 37).

The simulated overland flow mostly occurs in the riparian zone (Figure 40). The groundwater depth in the watershed responds to precipitation relatively slowly (Figure 41), although the water table in the vicinity of the first- and second-order streams in the west branch of WCC experienced a rapid increase during the major event in 2010, with the water table in part of the area above the ground surface during the high flow period.

4.2 DOC simulation results

The simulated DOC at the outlet of the watershed captured the main pattern shown in the data. At baseflow, the DOC concentration is about 1.5 ppm and increases up to 15 ppm during major storms (Figure 38).

The simulated annual DOC export is about 8.8 tonnes (million grams) (Figure 38), with annual DOC export from the subsurface is of 7.4 tonnes (84.7% of the total) and annual DOC export from overland flow of 1.3 tonnes (15.3% of the total).

Groundwater DOC concentration increased during the rain and declined slowly after the rain (Figure 42). DOC concentrations in the riparian zone increased more than in the upland area. DOC in the riparian zone increased from about 1.5 ppm during baseflow to about 14 ppm during storm flow. The area around west branch of the first-order stream is where the highest DOC concentrations in groundwater were found (This is also where the Cockeysville marble is concentrated). The DOC concentrations in the upland area between the west branch and east branch of WCC are generally low with little change during storms.

5 Discussion

5.1 Watershed hydrology

5.2 Dissolved organic carbon dynamics in the WCC watershed

The model simulated total DOC mass export is about 8.8 tonne for 2010. A simple export mass calculation using all the DOC samples with all the discharge measurement from 2010 show that export DOC mass is about 9.9 ton, and the DOC export from year 2000 to year 2009 ranging from 5 ton to more than 20 ton (Figure 39). Hence our model simulated amount of DOC export is within the observed range.

The DOC export from subsurface flow is about 7.4 tonne, about 84.7 % of the total export. This export amount is broadly consistent with Mei et al. (2012) showing

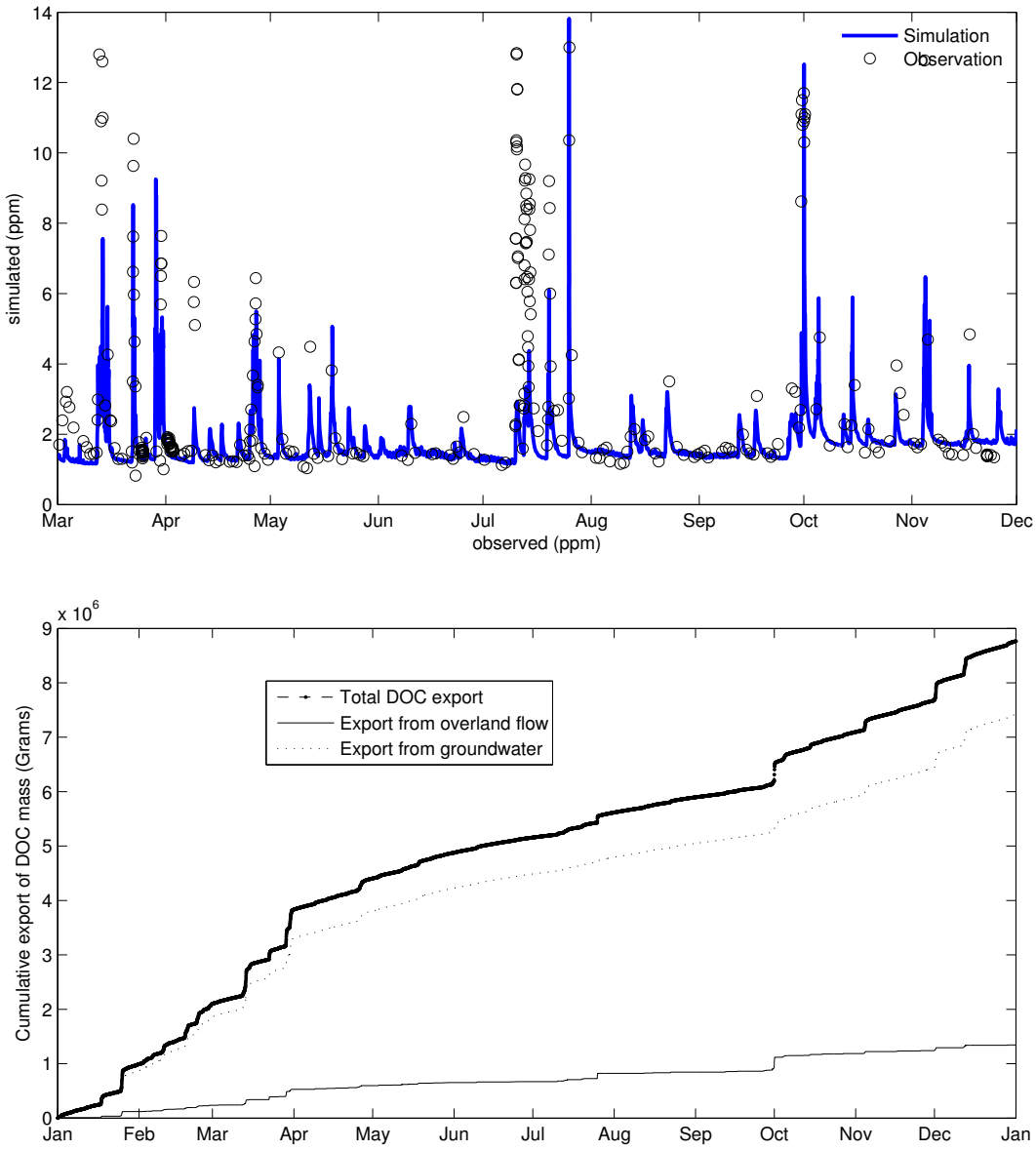

Figure 38: Stream DOC concentration simulation for 2010

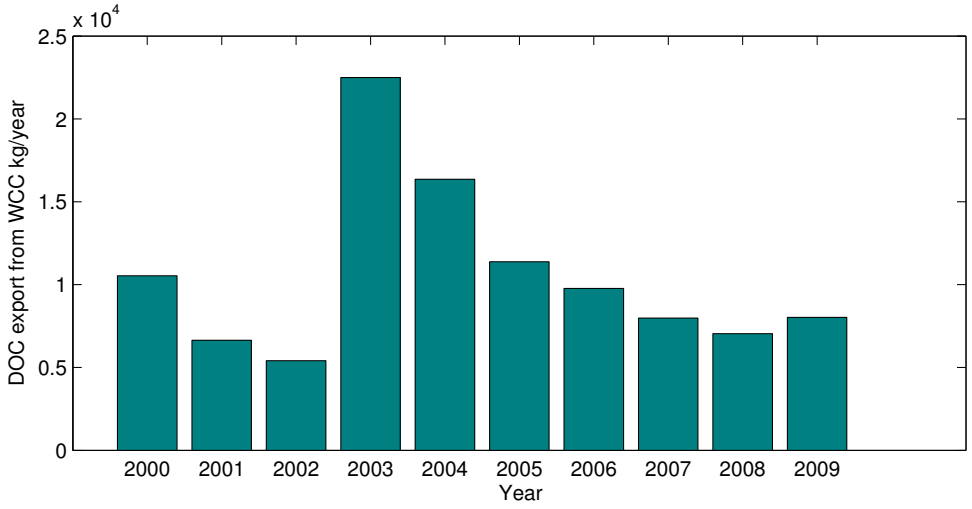

Figure 39: DOC export from WCC from the year 2000 to year 2009, calculated by simple interpolation between sampled values

that about 72% of DOC is exported from subsurface flow in WCC watershed during 1997. Raymond and Saiers (2010) reported as much as 86% of the annual DOC flux from 48 small eastern United States forested watersheds exported during storms, but they did not distinguish the amount from subsurface flow.

The calculated DOC export from overland flow is about 1.3 tonne, about 15.3 % of the total export. Our result is higher than what is reported from some watershed in the US. Boyer et al. (2000) reported that 2% of total DOC is delivered from overland flow annually from a seasonally snow covered headwater watershed in the Rocky Mountains in Colorado. Hornberger et al. (1994) reported about 10% of the DOC exported is from overland flow in the Snake River above Montezuma, Colorado. These lower overland export values might arise in snow dominant systems with less overland flow than in the WCC watershed.

The simulated results showed that the DOC concentration was higher in the riparian zone as opposed to the upland area (Figure 42). This result indicates that the majority of the DOC from subsurface flow to the stream during storms is derived from the riparian zone. This finding is consistent with previous research at this watershed showing that 91% of subsurface DOC export is from 12 % of the watershed

area in the riparian zone (Mei et al., 2012). It also is consistent with observations from other watersheds. Dosskey and Bertsch (1994) reported that the riparian wetland contributed 70% of the total export in the catchment that they studied. Hinton et al. (1998) point out that the importance of riparian area depends on the level of the water table relative to the organic rich soil horizons.

Topography has a primary control on the elevation of the water table. Hence, topography also controls groundwater DOC concentration by affecting the elevation of the water table relative to organic rich soil horizons. Our model demonstrated how this control mechanism works. The significant amount of DOC increase in groundwater simulated for the riparian zone of the west branch of WCC occurred where the water table easily rose to near the ground surface due to the relatively flat topography close to stream (Figure 41). As is pointed out by Vidon (2012) determining how the riparian zone hydrological conditions may change in response to precipitation in various geomorphic settings is critical to determine the occurrence of "hot moments" of biogeochemical transformations such as DOC export. Previous research has looked at watershed attributes as predictors of DOC export in numerous watersheds. Frost et al. (2006) use multiple regression to look at the effects of multiple landscape characteristics on DOM concentration and physicochemistry in a relatively large and heterogeneous watershed. They found that DOC decreases with catchment area, but they didnt explore the mechanisms. Ogawa et al. (2006) found a relationship between DOC and topographic index, but they didnt explore mechanisms involved in DOC delivery processes.

Responses of groundwater and stream water DOC concentrations to rainfall has been a topic of study in may catchments to understand mechanisms of export of organic carbon. Our model represents a workable computational tool to explore DOC dynamics at watershed scales. Future work could improve the model's ability to consider other processes, such as SOM production and CO_2 emission.

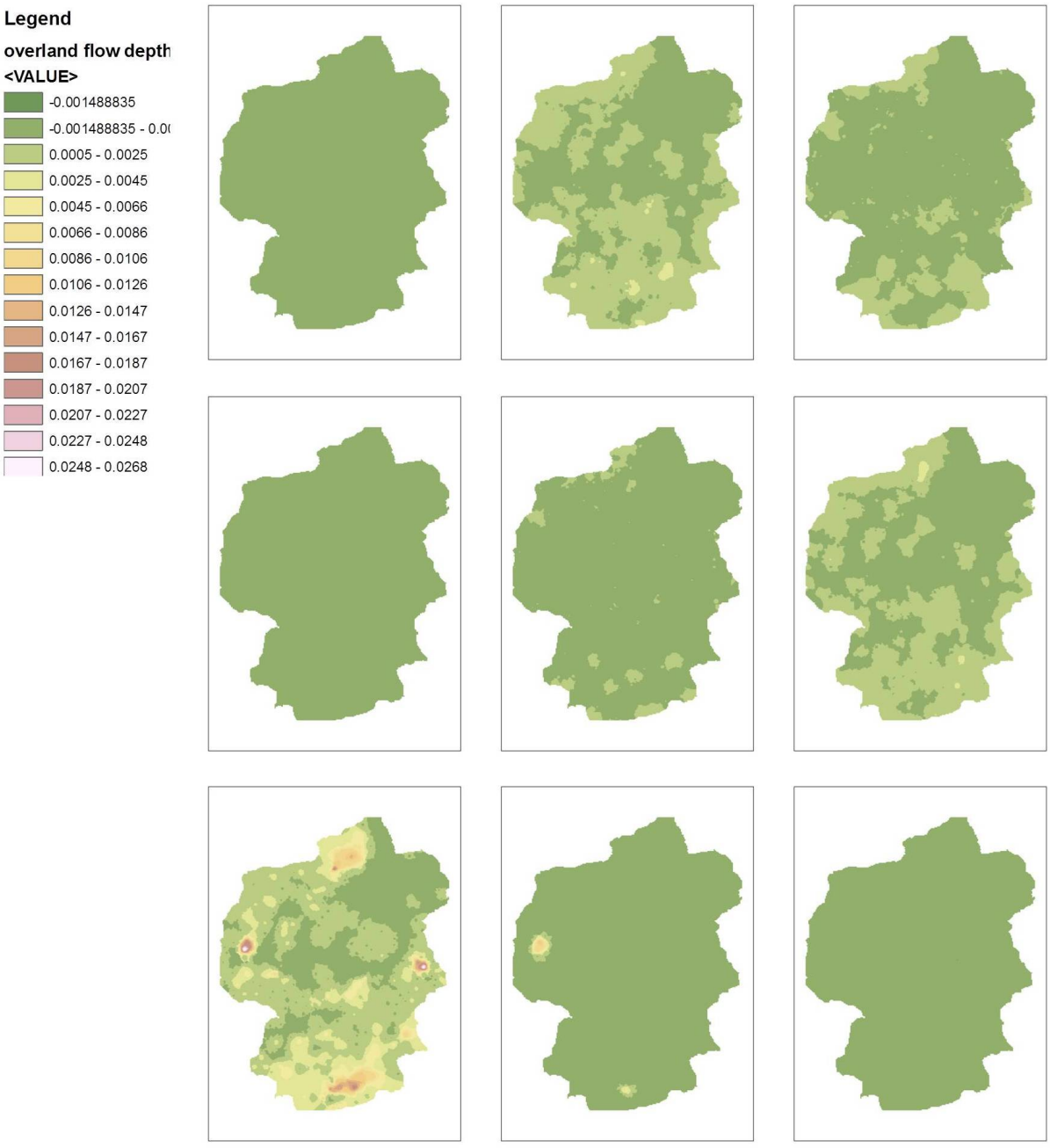

Figure 40: Simulation results of overland flow depth distribution over the major storm in 2010 (30-Sep-2010 02:00:00 to 01-Oct-2010 07:00:00). Values range from 0 to 0.027 m

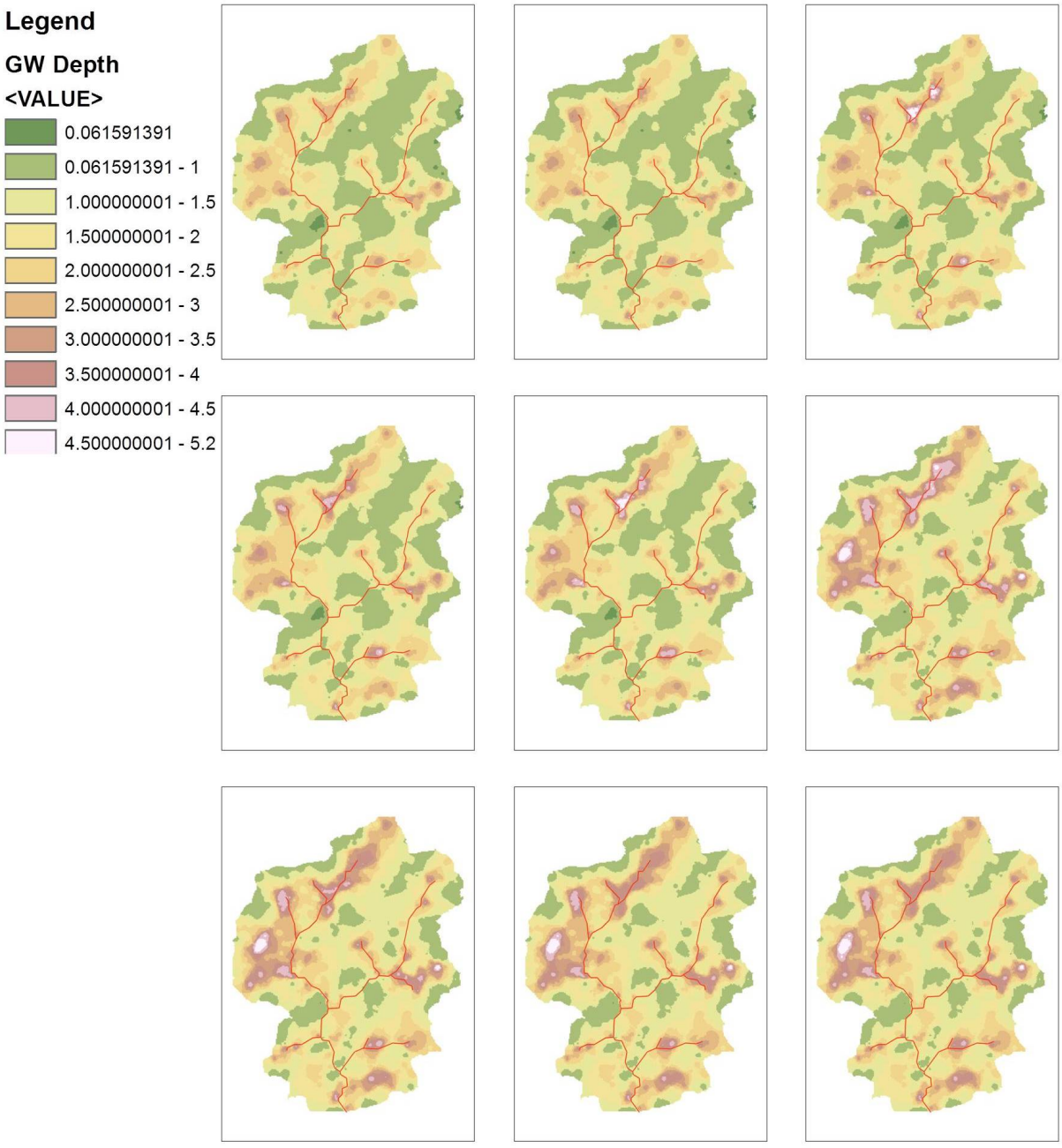

Figure 41: Simulation results of groundwater depth over the major storm in 2010 (30-Sep-2010 02:00:00 to 01-Oct-2010 07:00:00). Values range from 0 to 5.2 m

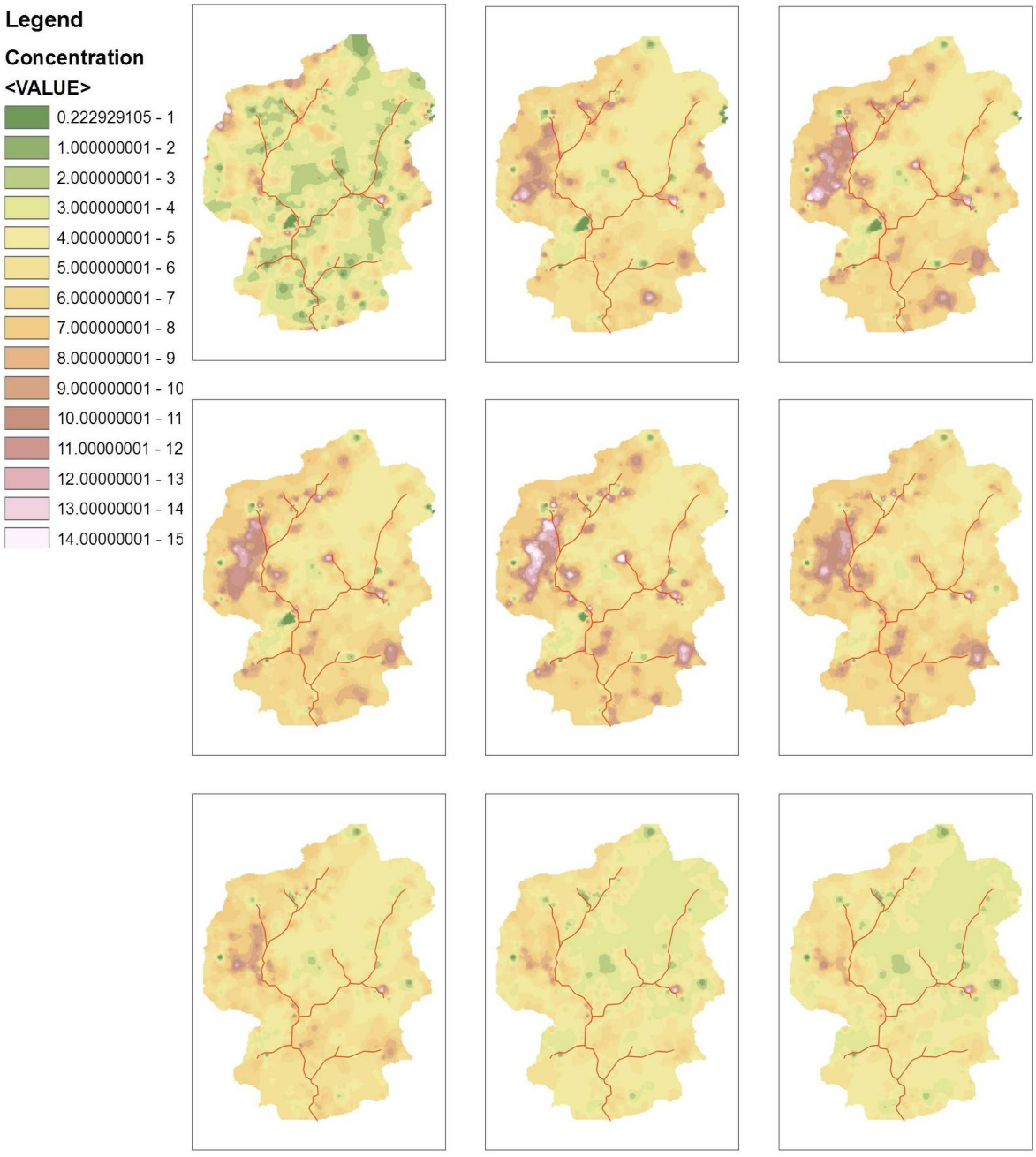

Figure 42: Groundwater DOC concentration over one of the major storms in 2010 (30-Sep-2010 02:00:00 to 01-Oct-2010 07:00:00) values range from 0 to 14 ppm

6 The derivation of the ordinary differential equations of DOC concentration and SOM content at each triangle element

Convection dispersion equation with source terms and a non-equilibrium sorption model:

$$\frac{\partial(\theta C+\rho s)}{\partial t}+\nabla(qC-D\nabla C)=\omega \tag{91}$$

$$\frac{\partial s}{\partial t}=-\tau(s-K_dC)+\chi \tag{92}$$

the global governing partial differential equations can be reduced to a local ODE system by doing integration of the PDE over a local control volume, Ω.

$$\int_\Omega \frac{\partial(\theta C+\rho s)}{\partial t}dV=\int_\Omega \nabla\cdot\left(\theta D\frac{\partial C}{\partial x_i}-q_iC\right)dV-\int_\Omega \omega dV \tag{93}$$

$$\int_\Omega \frac{\partial s}{\partial t}dV=\int_\Omega -\tau(s-K_dC)\,dV+\int_\Omega \chi dV \tag{94}$$

Apply the divergence theorem to the first term of the right hand side of the equation (93) yield:

$$\frac{\partial}{\partial t}\left(\int_\Omega \theta C dV+\rho\int_\Omega s dV\right)=\oiint_s \mathbf{n}\cdot\left(\theta D\frac{\partial C}{\partial x_i}-q_iC\right)dA-\int_\Omega \omega dV \tag{95}$$

In PIHM, the state variables are assumed to be uniform horizontally within a control column, thus the above equation could be written in the following form:

$$A_b\left(\frac{\partial}{\partial t}\int_{z_a}^{z_b}\theta C dz+\frac{\partial}{\partial t}\int_{z_a}^{z_b}\rho s dz\right)=\oiint_s \mathbf{n}\cdot\left(\theta D\frac{\partial C}{\partial x_i}-q_iC\right)dA-A_b\int_{z_a}^{z_b}\omega dz \tag{96}$$

$$A_b\frac{\partial}{\partial t}\int_{z_a}^{z_b}s dz=A_b\int_{z_a}^{z_b}-\tau(s-K_dC)dz+A_b\int_{z_a}^{z_b}\chi dz \tag{97}$$

Even though the state variable C and s are varying across soil horizons in the physical world, we use averaging values $\bar{C}$ and $\bar{s}$ to represent the values in a given vertical

volume.

$$\frac{\int_{z_a}^{z_b}\theta C dz}{\int_{z_a}^{z_b}\theta dz} = \overline{C}, Y = \int_{z_a}^{z_b}\frac{\theta}{\theta_s}dz = \frac{1}{n}\int_{z_a}^{z_b}\theta dz, \int_{z_a}^{z_b}\theta C dz = Yn\overline{C} \tag{98}$$

$$\int_{z_a}^{z_b} s_0 e^{-\alpha(H-z)}dz = \int_{z_a}^{z_b} s dz = H\bar{s} \tag{99}$$

Replace the left hand side of the equation (96) and (97) with the equation (98) and (99), yield:

$$A_b\frac{\partial}{\partial t}\left(Y\overline{\theta C}\right) + A_b\frac{\partial}{\partial t}\left(\rho H\bar{s}\right) = \oiint_s \mathbf{n}\cdot\left(\theta D\frac{\partial C}{\partial x_i} - q_i C\right)dA - A_b\int_{z_a}^{z_b}\omega dz \tag{100}$$

$$A_b\frac{\partial}{\partial t}\left(H\bar{s}\right) = -\tau A_b\left(H\bar{s} - YK_d\bar{C}\right) + A_b\int_{z_a}^{z_b}\chi dz \tag{101}$$

where $\bar{C}$ is the concentration in the unsaturated zone in an averaged sense. n is the porosity; H is the depth of the zone interested; θ is the soil moisture; ρ is the soil bulk density; D is the hydraulic dispersion coefficient; A_b is the bottom triangle area of the prism; K_d is the distribution coefficient; ω is the source term for mass in dissolved phase; χ is source term of the the mass in sorbed phase; θ_s is the saturated soil moisture; s_0 is the soil organic content on the top of the soil surface; τ is the kinematic transfer rate of dissolved organic carbon between sorbed and solute phase; Y is the depth of the water.

By using the specific mass flux terms and source terms (first and second term on the right hand side of the equation (100) and second term on the right hand side of equation (101) with regard to the different part of the prism, we can obtain the equations used in the model as follows:

Overland flow part:

In the overland flow, we do not use non-equilibrium sorptions, instead we used a first-order kinetic rated limited transfer between the DOC mass in the overland flow

and in the soil. The equation (100) and equation (101) are reduced to the following equation:

$$A_b\left(nY\frac{d\overline{C}}{dt}+n\overline{C}\frac{dY}{dt}\right)=\sum_{i=1}^{3}\left(u_iAs_iC_i-As_iD_iGradC_i\right)+A_bK_{ov}\left(C_{soil}-\overline{C}\right) \quad (102)$$

which results in an ordinary differential equation for C:

$$A_bYn\frac{d\overline{C}}{dt}=\sum_{i=1}^{3}\left(u_iAs_iC_i-As_iD_iGradC_i\right)+A_bK_{ov}\left(C_{soil}-C\right)-A_bn\overline{C}\frac{dY}{dt} \quad (103)$$

$$\frac{d\overline{C}}{dt}=\frac{1}{A_bYn}\sum_{i=1}^{3}\left(u_iAs_iC_i-As_iD_iGradC_i\right)+\frac{1}{Yn}K_{ov}\left(C_{soil}-C\right)-\frac{1}{Y}\overline{C}\frac{dY}{dt} \quad (104)$$

where, i represent the id of the flux from each of the three side of the triangle; A_s is the areas (triangle length of each side $\times$ water depth); K_{ov} is the mass transfer rate between overland flow and soil water.

In the unsaturated zone, PIHM does not consider the horizontal flow and mass transfer. Only vertical mass exchanged between unsaturated zone and saturated zone, vertical mass exchanged between unsaturated zone and overland flow are considered. The water fluctuation which caused sorbed mass transfer between the saturated zone and unsaturated zone is also considered.

total mass balance

$$\left\{A_b\frac{d\left(nY\overline{C}\right)}{dt}+\frac{dM_{sob}^{u}}{dt}\right\}=-A_bRC_s-A_bK_{ov}\left(C_{soil}-C_{ov}\right)+q_s \quad (105)$$

Sorbed phase:

$$\frac{\partial M_{sob}^{u}}{\partial t}=-\rho\tau\left(\overline{s}-K_d\overline{C}\right)\left(z_2-z_1\right)A_b+q_s \quad (106)$$

where:

$$q_s = \rho A_b \int_{z_{t1}}^{z_{t2}} s_0 e^{-\alpha(H-z)} dz \tag{107}$$

representing the mass removed or added to or from the saturated zone by watertable fluctuation. Replace the second term on the left hand side of equation (105) with equation 106, yield:

$$A_b \left\{ nY \frac{d\overline{C}}{dt} + n\overline{C} \frac{dY}{dt} + [\rho \frac{d\bar{s}}{dt} (z_2 - z_1)] \right\} = -A_b R C_s - A_b K_{ov} (C_{soil} - C_{ov}) \tag{108}$$

$$A_b \left\{ nY \frac{d\overline{C}}{dt} + n\overline{C} \frac{dY}{dt} - [\rho\tau (s - K_d C) (z_2 - z_1)] \right\} = -A_b R C_s - A_b K_{ov} (C_{soil} - C_{ov}) \tag{109}$$

The final equations for unsaturated zone:

$$\frac{d\overline{C}}{dt} = \frac{R\left(C_s - \overline{C}\right)}{nY} - \frac{1}{nY} K_{ov} (C_{soil} - C_{ov}) + \frac{1}{nY} [B_d \tau (s - K_d C) (z_2 - z_1)] \tag{110}$$

$$\frac{d\bar{s}}{dt} = -\frac{\tau}{(z_2 - z_1)} \left((z_2 - z_1) \bar{s} - Y K_d \bar{C} \right) + \frac{q_s}{(z_2 - z_1) A_b \rho} \tag{111}$$

In the saturated zone, PIHM considers both lateral mass exchange and recharge from the unsaturated zone. total mass balance

$$A_b n \frac{d\left(Y\overline{C}\right)}{dt} + \frac{dM_{sob}^g}{dt} = \sum_{i=1}^{3} (u_i A s_i C_i - A s_i D_i Grad C_i) + A_b R C_s - q_s \tag{112}$$

Sorbed phase:

$$\frac{\partial M_{sob}^g}{\partial t} = -\rho\tau \left(\overline{s} - K_d \overline{C}\right) (z_2 - z_1) A_b - q_s \tag{113}$$

Replace the second term on the left hand side of equation (112) with equation 113, yield:

$$A_b\left(nY\frac{d\overline{C}}{dt}+n\overline{C}\frac{dY}{dt}-\rho\left(z_1-z_0\right)\tau\left(\overline{S}-K_d\overline{C}\right)\right) = \sum_{i=1}^{3}\left(u_iAs_iC_i-As_iD_iGradC_i\right)+A_bRC_s \quad (114)$$

The final equations for the saturated zone:

$$\frac{d\overline{C}}{dt}=-\frac{1}{nY}\left[-\rho\left(z_1-z_0\right)\tau\left(\overline{S}-K_d\overline{C}\right)\right]+ \frac{1}{nYA_b}\left\{\sum_{i=1}^{3}\left(u_iAs_iC_i-As_iD_iGradC_i\right)+A_bRC_s-n\overline{C}\frac{dY}{dt}A_b\right\} \quad (115)$$

$$\frac{d\bar{s}}{dt}=-\tau\left(\bar{s}-K_d\bar{C}\right)-\frac{q_s}{\left(z_1-z_0\right)A_b\rho} \quad (116)$$

where, z_2, z_1, z_0 represent the elevation of the ground surface, water table, and bed rock respectively; R is the amount of recharged water to the saturated zone.

The DOC concentration and soil SOM content were updated every time step using an explicit time marching scheme and s_0, the SOM content at the ground surface, was updated at every time step using:

$$s_0=\frac{\alpha\left(M_{sob}^{u}+M_{sob}^{g}\right)}{\rho A_b\left(1-e^{-\alpha H}\right)} \quad (117)$$

where, α is the decay rate of the SOM along soil profile; H is the depth of the aquifer [L]; A_b is the area of the local triangle [L^2];

CHAPTER 5

DISSERTATION SYNTHESIS AND FUTURE RESEARCH

1 Dissertation synthesis and future research

1.1 Synthesis

The difficulties that arise in understanding the interactions between hydrological processes and biogeochemical processes stem from the complexity of water flow and biogeochemistry reactions occurring over a wide range of spatial and temporal scales. At the micro scale, high spatial heterogeneity of soil and subsurface materials microbial populations makes it nearly impossible to understand the details of how all the hydrological and biogeochemical components interact with each other at a purely mechanistic level. Nevertheless, the overall system behavior at a watershed or hillslope scale can be captured using a largely mechanistic approach with reasonable assumptions and approximations. It is essential to devise theoretical frameworks at reasonable complexity levels to understand complex catchment biogeochemistry systems, with respect to specific interests or research questions. A field scale approach coupling laboratory and field experiments and observations with physically-based distributed models is an important first step to reach a mechanistic understanding of watershed scale chemical delivery from terrestrial soils to the streams during baseflow and stormflow conditions.

In this dissertation, the origin, fate and transport of natural dissolved organic carbon is examined. The delivery of DOC from shallow soil horizons to groundwater and streams through an agricultural and forested watershed located in southeastern

Pennsylvania is explored at multiple spatial and temporal scales using mathematical models with results from field experiments and observations in a combined approach. This study has made a significant contribution to our knowledge about catchment scale control mechanisms of dissolved organic carbon delivery to the streams from terrestrial sources. We identified the significance of the riparian zone on DOC export from the research watershed, including the effects of macropores, passage of flood waves, soil properties and topography. Moreover, the novel modeling approaches for watershed DOC proposed in this dissertation have improved the existing watershed DOC models at different complexity levels. From a dual-permeability approach describing vertical DOC leaching through soils to lateral groundwater and soil DOC delivery modeling by 2D FEM variably saturated modeling approach to a whole catchment approach to DOC simulation, our models represent a series of new DOC model types which enrich the tools for watershed DOC simulations.

Almost all watershed DOC processes require a better understanding of the subsurface transport as the majority of the export DOC is from the terrestrial sources (Hynes, 1975). Surface soil horizons are where most of the soil organic matter is stored. To appropriately quantify the subsurface processes in surface soil layers, small scale (in-situ soil cores) studies are needed to quantify biogeochemical leaching processes at a fine spatial scale. The observed amount of DOC leaching from soil cores can be replicated and extrapolated to the catchment scale by upscaling of the one-dimensional numerical model (Chapter 2). One of the limitations of the integrated one-dimensional reactive transport model is its inability to describe the lateral DOC fate and transport along groundwater flow paths. This process is important because the extensions of riparian areas as different parts of hillslopes become hydrologically connected over the course of a storm (McGlynn and McDonnell, 2003) can dominate DOC delivery. Also the dynamics of the groundwater table in the riparian zone interacting with the stream fluctuation can have control on various patterns of the

DOC concentration in the stream (Mei et al. 2013, in review). Our two-dimensional Finite-Element Model offers an ideal tool to describe and understand those processes (Chapter 3). The major limitations for the small scale models and reduced dimension models is that such models can not generate a comprehensive picture of the real world (three-dimensional). The PIHM-doc model developed in the chapter 4 enables a three-dimensional view of the watershed DOC spatial and temporal variation. The development of our models scaled from the small scale (soil core), to hillslope scale (2-d hillslope transect) and to the large scale (three-dimensional watershed) represents an effort to advance the numerical simulation techniques of the hydro-biogeochemical systems.

Integrating the manuscript chapters provides a holistic understanding of processes of dissolved organic carbon leaching from the surface soil horizons and its delivery to the stream. Results from the leaching experiments of in-situ soil columns showed that a dual-permeability approach to account for macropore flow and transport is needed to describe the DOC leaching process (Chapter 2). By simulating the lateral flow path of DOC using our two-dimensional Finite-Element multispecies reactive transport model, we were able to simulate the infiltration and lateral transport process of DOC to the stream on a hillslope slice and finally be able to examine the controls of the flood wave and hillslope hydrological properties on the concentration-discharge relationships in the stream (Chapter 3). The watershed DOC model was able to simulate the dynamic processes of DOC at the watershed scale, the simulation results showed a control of topography on the DOC concentration in groundwater and in the stream (Chapter 4).

Our major hypothesis that the riparian zone is the first order control on DOC export (Chapter 1) has been examined through all of the three models (Chapter 2, 3, 4). An estimation of total contribution from the riparian zone is given in chapter 2 showing that more than 90% of the DOC was derived from the riparian area, less

than 12% of the total watershed area. Further, the DOC flux calculation along the selected hillslope transect shows a deep DOC mass flux decline curve from the stream side to the upland area during a storm, which reexamined the hypothesis (Chapter 3). The groundwater DOC concentration in the riparian zone experienced a much larger fluctuation than was observed from the simulation results from chapter 4, which implies the importance of the riparian zone again. Our finding is consistent with previous research showing the importance of riparian processes on DOC export (Dosskey and Bertsch, 1994; Hinton et al., 1998; Kohler et al., 2009). Our novel approach provides a new insight on this major control by showing the riparian DOC dynamics using mechanistically modeling techniques.

The "flushing" hypothesis was also explored in this study. The field monitoring work combined with a two dimensional flow and transport simulation conducted on a selected hillslope transect at WCC suggests that a flushing hypothesis is reasonable in explaining the DOC delivery to the stream at WCC watershed (Chapter 3). The rising groundwater table during rain events has significant effects on the export of DOC to the stream, especially in the riparian zone. This concept was further explored in the PIHM-doc model. The model results show that a precipitation event may produce a rise in DOC in the saturated zone when groundwater rises into a shallow soil horizon (Chapter 4).

DOC includes a wide range of organic carbon with different molecular size and eco-biology functionalities. Almost all the previous modeling work has considered the dissolved organic component together as a single mixture. In this dissertation, in order to understand the dynamics of bio-labile DOC versus refractory DOC, we used an experimental instrument a plug flow bioreactor that is able to separate the biodegradable DOC from the total DOC. Like other physical sciences, the advances of observation or experimental techniques can often lead to significant strides in theory development or even scientific revolution. The use of the BDOC measurement

methodology led us to further develop the related hydro-biogeochemical modeling techniques. The leaching of labile BDOC is examined using the dual-permeability approach with first order decay of DOC to represent microbial consumption. The percentage of labile BDOC contribution from the riparian zone versus the total DOC export was calculated in chapter 2 showing that almost all the labile BDOC contributed to the stream is from the riparian zone. The BDOC delivery to the stream is compared with the refractory DOC delivery through the model and field observation. The comparison results show that for most of the time, BDOC concentration in the stream rises faster and drops faster than RDOC in WCC. This result indicates that the soil organic carbon in the shallow soil horizon has higher biolability than the SOM at lower soil horizons.

Our calculation results of the total dissolved organic carbon mass export from WCC is about 9 tonnes a year (Mei et al., 2012). These amounts are a small fraction of the 2.5×10^8 tonnes of total riverine export of terrigenous DOC to the sea each year (Hansell and Carlson, 2002). The watershed scale model PIHM-DOC can be applied at a larger spatial scale and possibly can be used to explore issues such as whether terrestrial processes may explain part of the "missing" carbon sink.

We addressed uncertainties in the models by using UCODE to calculate the composite scaled sensitivities of all the parameters and running Monte Carlo simulations assumed distributions of the selected parameters. The output distribution was calculated and used to provide a hint about how the results vary by considering the uncertainties of the parameter inputs.

In summary, the importance of the riparian zone on DOC export from catchments has been examined through field observation and model calculation. This study provides evidence that the riparian zone is the first order control on DOC export at watershed scales through various types of model calculations, by comparison between the delivery of DOC mass to groundwater from the riparian zone versus upland area,

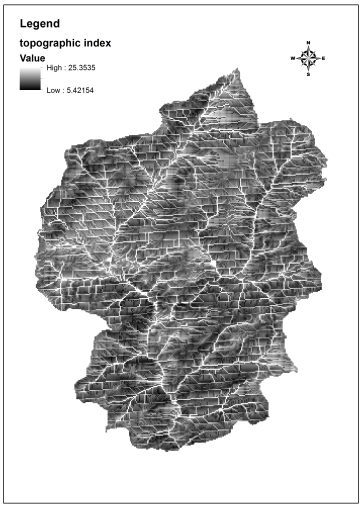

Figure 43: Topographic index of WCC

by integrating a single event DOC mass export along a hillslope groundwater flow path and by looking at the groundwater concentration variation in the riparian zone versus upland area. Macropores were found to have an important control on DOC delivery across soil horizons. The flood wave duration, hillslope soil hydrological properties were found to have important controls on the stream DOC concentration discharge relationship. Topographic control on the watershed DOC is also inferred from this study. The processes and mechanisms exposed in the WCC watershed are obviously site specific, controlled by local topography and hydrogeologic settings. Nevertheless, knowledge derived from this study could also be applied to other watersheds with similar landscape and geological characteristics.

1.2 Future research

1.2.1 Topographic control on DOC concentration

Topographic control on DOC export has been inferred from the chapter 4. Only a qualitative description was given in that chapter. A quantitative analysis of the relationship between the topographic attributes of the watersheds and watershed

DOC concentration will be needed in future research.

To establish relationship between the topographic factors and the groundwater and stream DOC concentrations, a first step is to find a way to quantify necessary topographic factors. The topographic index could be used as simple way to describe the topographic attributes (Figure 43).

$$TI = \ln(\alpha / \tan\beta) \tag{118}$$

where, TI is the topographic index; α is the upstream contribution area per unit contour length; $\tan\beta$ is the local slope. The simulation results of PIHM-doc could be used to explore this relationship between topographic index and watershed DOC concentration. This research will cast some light on how the landscape characteristics control catchment DOC and its export to the stream.

Previous research has looked at watershed attributes as predictors of DOC in numerous watersheds. Frost et al. (2006) use multiple regression to look at the effects of multiple landscape characteristics on DOM concentration and physicochemistry in a relatively large and heterogeneous river watershed. They found that DOC decreases with catchment area, but they did not explore the mechanisms. Laudon et al. (2011) put forward a conceptual model, but their explanation is more about land characteristics (although they acknowledge topography as well). Ogawa et al. (2006) found a relationship between DOC and topographic index, but they did not explore mechanisms involved in DOC delivery processes. Landscape forms were also found to be important in control DOC export (Dillon and Molot, 1997).

1.2.2 Whole basin approach for DOC export

A future objective is to integrate the water cycle and the carbon cycle across the entire Christina River Basin critical zone observatory . This requires a reliable model

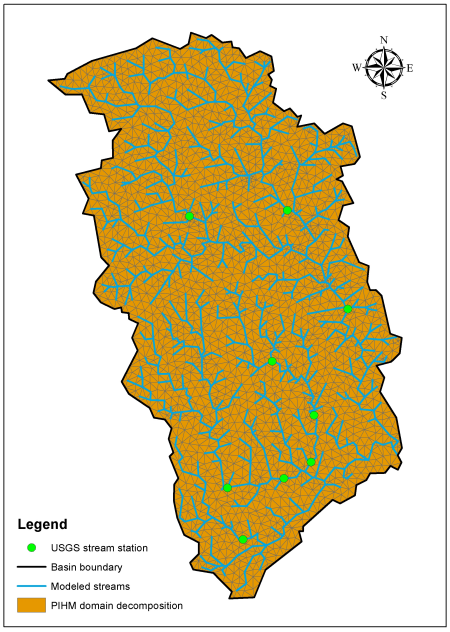

Figure 44: Spatial decomposition of the Christina River Basin

framework that can couple the major processes. The PIHM-doc developed in chapter 4 can be adopted as a modeling framework to achieve the goal. Ultimately we envision integrating a large number of high resolution GIS, satellite data, and meteorological data for the mesoscale watershed and using PIHM-doc to scale carbon fluxes across the basin. The physical mechanisms involved in all of the complex processes involved can only be investigated holistically by exploring results from such an integrated model.

To achieve this goal, the first step is to integrate all the GIS data (e.g., land use, soil type, DEM), into the model framework, and simulate the water flow and carbon flux across the watershed. To date, we have successfully set up the PIHM for the mesoscale watershed simulation. The 1440 km^2 watershed was divided into over 4000 mesh triangles (Figure 44). Stream discharge data from ten USGS stream stations within the Christina River Basin were used to guide the model development. In the next step, high resolution RADAR-derived, gauge-calibrated precipitation datasets

can be incorporated with PIHM to explore the hydrological response of the model at the basin scale. After the PIHM model calibration, the PIHM-doc model can be applied to estimate the basin scale carbon flux.

The finding of this future research could (i) advance our knowledge of mesoscale carbon cycling and budget, and cast light on the effects of climate change on regional carbon cycling and (ii) understand the fate and transport of carbon at the scale of the Christiana basin.

BIBLIOGRAPHY

Abbott, M. B.; Bathurst, J. C.; Cunge, J. A.; Oconnell, P. E., and Rasmussen, J. An introduction to the european hydrological system - systeme hydrologique europeen, she .1. history and philosophy of a physically-based, distributed modeling system. *Journal of Hydrology*, 87(1-2):45–59, 1986 (a).

Abbott, M. B.; Bathurst, J. C.; Cunge, J. A.; Oconnell, P. E., and Rasmussen, J. An introduction to the european hydrological system - systeme hydrologique europeen, she .2. structure of a physically-based, distributed modeling system. *Journal of Hydrology*, 87(1-2):61–77, 1986 (b).

Battin, T. J.; Kaplan, L. A.; Newbold, J. D., and Hendricks, S. P. A mixing model analysis of stream solute dynamics and the contribution of a hyporheic zone to ecosystem function. *Freshwater Biology*, 48(6):995–1014, 2003.

Bear, J. *Dynamics of fluids in porous media*. Dover Publications, 1988.

Berg, P. Long-term simulation of water movement in soils using mass-conserving procedures. *Advances in Water Resources*, 22(5):419–430, 1999.

Berg, T.M.; Miles, C.E.; Kuchinski, J.G.; Williams, , and Corporation, Heintz Map. *Geologic Map of Pennsylvania: Pennsylvania Geological Survey, 4th ser.,Map 1,2nd ed., 3sheets, Scale 1:250000*. Commonwealth of Pennsylvania, Department of Environmental Resources, Bureau of Topographic and Geologic Survey, 1980.

Beven, K. J.; Henderson, D. E., and Reeves, A. D. Dispersion parameters for undisturbed partially saturated soil. *Journal of Hydrology*, 143(1-2):19–43, 1993.

Beven, Keith. Hillslope hydrographs by the finite element method. *Earth Surface Processes*, 2(1):13–28, 1977.

Bhatt, G; Kumar, M, and Duffy, CJ. Bridging gap between geohydrologic data and integrated hydrologic model: Pihmgis. *International Environmental Modelling and Software Society (iEMSs), Barcelona, Catalonia*, pages 743–750, 2008.

Bhatt, Gopal. *A distributed hydrologic modeling system: framework for discovery and management of water resources*. PhD thesis, Pennsylvania State University, State College, 2012.

Boyer, E. W.; Hornberger, G. M.; Bencala, K. E., and McKnight, D. M. Response characteristics of doc flushing in an alpine catchment. *Hydrological Processes*, 11 (12):1635–1647, 1997.

Boyer, E. W.; Hornberger, G. M.; Bencala, K. E., and McKnight, D. M. Effects of asynchronous snowmelt on flushing of dissolved organic carbon: a mixing model approach. *Hydrological Processes*, 14(18):3291–3308, 2000.

Buffam, I.; Galloway, J. N.; Blum, L. K., and McGlathery, K. J. A stormflow/baseflow comparison of dissolved organic matter concentrations and bioavailability in an appalachian stream. *Biogeochemistry*, 53(3):269–306, 2001.

Butturini, A.; Gallart, F.; Latron, J.; Vazquez, E., and Sabater, F. Cross-site comparison of variability of doc and nitrate c-q hysteresis during the autumn-winter period in three mediterranean headwater streams: A synthetic approach. *Biogeochemistry*, 77(3):327–349, 2006.

Cahill, . Hydrologic analysis and evaluation of stormwater management criteria, london grove township, chester county, pa. Technical report, Cahill Associates, 1994.

Celia, M. A.; Bouloutas, E. T., and Zarba, R. L. A general mass-conservative numerical solution for the unsaturated flow equation. *Water Resources Research*, 26(7): 1483–1496, 1990.

Chanat, J. G. and Hornberger, G. M. Modeling catchment-scale mixing in the near-stream zone - implications for chemical and isotopic hydrograph separation. *Geophysical Research Letters*, 30(2), 2003.

Chanat, J. G.; Rice, K. C., and Hornberger, G. M. Consistency of patterns in concentration-discharge plots. *Water Resources Research*, 38(8), 2002.

Chung, S. O. and Horton, R. Soil heat and water flow with a partial surface mulch. *Water Resources Research*, 23(12):2175–2186, 1987.

Cooper, H.H. and Rorabaugh, M.I. *Ground-water Movements and Bank Storage Due to Flood Stages in Surface Streams*. U.S. Government Printing Office, 1963.

Creed, I. F.; Band, L. E.; Foster, N. W.; Morrison, I. K.; Nicolson, J. A.; Semkin, R. S., and Jeffries, D. S. Regulation of nitrate-n release from temperate forests: A test of the n flushing hypothesis. *Water Resources Research*, 32(11):3337–3354, 1996.

Davis, J.C. and Sampson, R.J. Statistics and data analysis in geology. 1986.

Dawson, H. J.; Hrutfiord, B. F.; Zasoski, R. J., and Ugolini, F. C. The molecular weight and origin of yellow organic acids. *Soil Science*, 132(3):191–199, 1981.

de Vries, D. A. Thermal properties of soils, 1963.

Dillon, P. J. and Molot, L. A. Effect of landscape form on export of dissolved organic carbon, iron, and phosphorus from forested stream catchments. *Water Resources Research*, 33(11):2591–2600, 1997.

Dixon, R. K.; Brown, S.; Houghton, R. A.; Solomon, A. M.; Trexler, M. C., and Wisniewski, J. Carbon pools and flux of global forest ecosystems. *Science*, 263 (5144):185–190, 1994.

Dosskey, M. G. and Bertsch, P. M. Forest sources and pathways of organic matter transport to a blackwater stream - a hydrologic approach. *Biogeochemistry*, 24(1): 1–19, 1994.

Duffy, C. J. A two-state integral-balance model for soil moisture and groundwater dynamics in complex terrain. *Water Resources Research*, 32(8):2421–2434, 1996.

Duffy, C.J. Semi-discrete dynamical model for mountain-front recharge and water balance estimation. American Geophysical Union, Washington, DC, 2004.

Evans, C. and Davies, T. D. Causes of concentration/discharge hysteresis and its potential as a tool for analysis of episode hydrochemistry. *Water Resources Research*, 34(1):129–137, 1998.

Falkengrengrerup, U. and Tyler, G. The importance of soil acidity, moisture, exchangeable cation pools and organic-matter solubility to the cationic composition of beech forest (fagus-sylvatica l) soil solution. *Zeitschrift Fur Pflanzenernahrung Und Bodenkunde*, 156(4):365–370, 1993.

Fan, Z. S.; Neff, J. C., and Wickland, K. P. Modeling the production, decomposition, and transport of dissolved organic carbon in boreal soils. *Soil Science*, 175(5): 223–232, 2010.

Fraser, C. J. D.; Roulet, N. T., and Moore, T. R. Hydrology and dissolved organic carbon biogeochemistry in an ombrotrophic bog. pages 3151–3166. John Wiley & Sons Ltd, 2001.

Frias, J.; Ribas, F., and Lucena, F. A method for the measurement of biodegradable organic carbon in waters. *Water Research*, 26(2):255–258, 1992.

Frost, P. C.; Larson, J. H.; Johnston, C. A.; Young, K. C.; Maurice, P. A.; Lamberti, G. A., and Bridgham, S. D. Landscape predictors of stream dissolved organic matter concentration and physicochemistry in a lake superior river watershed. *Aquatic Sciences*, 68(1):40–51, 2006.

Futter, M. N.; Butterfield, D.; Cosby, B. J.; Dillon, P. J.; Wade, A. J., and Whitehead, P. G. Modeling the mechanisms that control in-stream dissolved organic carbon dynamics in upland and forested catchments. *Water Resources Research*, 43(2):16, 2007.

Gardenas, A. I.; Simunek, J.; Jarvis, N., and van Genuchten, M. T. Two-dimensional modelling of preferential water flow and pesticide transport from a tile-drained field. *Journal of Hydrology*, 329(3-4):647–660, 2006.

Gerke, H. H. and van Genuchten, M. T. A dual-porosity model for simulating the preferential movement of water and solutes in structured porous media. *Water Resources Research*, 29(2):305–319, 1993a.

Gerke, H. H. and van Genuchten, M. T. Evaluation of a first-order water transfer term for variably saturated dual-porosity flow models. *Water Resources Research*, 29(4):1225–1238, 1993b.

Gottardi, G. and Venutelli, M. A control-volume finite-element model for 2-dimensional overland-flow. *Advances in Water Resources*, 16(5):277–284, 1993.

Grieve, I. C. A model of dissolved organic carbon concentrations in soil and stream waters. *Hydrological Processes*, 5(3):301–307, 1991.

Gu, C.; Hornberger, G. M.; Mills, A. L.; Herman, J. S., and Flewelling, S. A. Nitrate reduction in streambed sediments: Effects of flow and biogeochemical kinetics. *Water Resources Research*, 43(12), 2007.

Gu, C. H.; Hornberger, G. M.; Herman, J. S., and Mills, A. L. Influence of stream-groundwater interactions in the streambed sediments on no3- flux to a low-relief coastal stream. *Water Resources Research*, 44(11):13, 2008.

Gu, C. H.; Anderson, W., and Maggi, F. Riparian biogeochemical hot moments induced by stream fluctuations. *Water Resources Research*, 48, 2012.

Guber, A. K.; Pachepsky, Y. A.; van Genuchten, M. T.; Rawls, W. J.; Simunek, J.; Jacques, D.; Nicholson, T. J., and Cady, R. E. Field-scale water flow simulations using ensembles of pedotransfer functions for soil water retention. *Vadose Zone Journal*, 5(1):234–247, 2006.

Guo, Y. D.; Wan, Z. M., and Liu, D. Y. Dynamics of dissolved organic carbon in the mires in the sanjiang plain, northeast china. *Journal of Environmental Sciences-China*, 22(1):84–90, 2010.

Hagedorn, F.; Schleppi, P.; Waldner, P., and Fluhler, H. Export of dissolved organic carbon and nitrogen from gleysol dominated catchments - the significance of water flow paths. *Biogeochemistry*, 50(2):137–161, 2000.

Haitjema, H. M. and Mitchell-Bruker, S. Are water tables a subdued replica of the topography? *Ground Water*, 43(6):781–786, 2005.

Hamon, W. R. Computation of direct runoff amounts from storm rainfall. *International Association of Scientific Hydrology Publication*, 63:52–62, 1963.

Hansell, Dennis A and Carlson, Craig A. *Biogeochemistry of marine dissolved organic matter*. Academic Press, San Diego, CA, 2002.

Hill, M.C. Methods and guidelines for effective model calibration. Technical report, Denver,CO, 1998.

Hill, M.C. and Tiedeman, C.R. *Effective groundwater model calibration: With analysis of data, sensitivities, predictions, and uncertainty*. Wiley-Interscience, 2007.

Hinton, M. J.; Schiff, S. L., and English, M. C. The significance of storms for the concentration and export of dissolved organic carbon from two precambrian shield catchments. *Biogeochemistry*, 36(1):67–88, 1997.

Hinton, M. J.; Schiff, S. L., and English, M. C. Sources and flowpaths of dissolved organic carbon during storms in two forested watersheds of the precambrian shield. *Biogeochemistry*, 41(2):175–197, 1998.

Hope, D.; Billett, M. F., and Cresser, M. S. A review of the export of carbon in river water - fluxes and processes. *Environmental Pollution*, 84(3):301–324, 1994.

Hope, D.; Billett, M. F.; Milne, R., and Brown, T. A. W. Exports of organic carbon in british rivers. *Hydrological Processes*, 11(3):325–344, 1997.

Hopmans, J. W.; Simunek, J., and Bristow, K. L. Indirect estimation of soil thermal properties and water flux using heat pulse probe measurements: Geometry and dispersion effects. *Water Resources Research*, 38(1):14, 2002.

Hornberger, G. and Wiberg, P. *Numerical methods in the hydrological sciences*. American Geophysical Union, 2005.

Hornberger, G. M.; Bencala, K. E., and McKnight, D. M. Hydrological controls on dissolved organic carbon during snowmelt in the snake river near montezuma, colorado. *Biogeochemistry*, 25(3):147–165, 1994.

Hruska, J.; Kohler, S.; Laudon, H., and Bishop, K. Is a universal model of organic acidity possible: Comparison of the acid/base properties of dissolved organic carbon in the boreal and temperate zones. *Environmental Science & Technology*, 37(9): 1726–1730, 2003.

Hynes, H. B. N. The stream and its valley. *Verh. Internat. Verein. Limnol.*, 19:1–15, 1975.

Hynes, H. B. N. Groundwater and stream ecology. *Hydrobiologia*, 100:93–99, 1983.

Inamdar, S. P. and Mitchell, M. J. Hydrologic and topographic controls on storm-event exports of dissolved organic carbon (doc) and nitrate across catchment scales. *Water Resources Research*, 42(3), 2006.

Jardine, P. M.; Wilson, G. V.; McCarthy, J. F.; Luxmoore, R. J.; Taylor, D. L., and Zelazny, L. W. Hydrogeochemical processes controlling the transport of dissolved organic carbon through a forested hillslope. *Journal of Contaminant Hydrology*, 6 (1):3–19, 1990.

Jardine, P. M.; Dunnivant, F. M.; McCarthy, J. F., and Selim, H. M. Comparison of models for describing the transport of dissolved organic carbon in aquifer columns. *Soil Science Society of America Journal*, 56(2):393, 1992.

Jarvis, N. J. A review of non-equilibrium water flow and solute transport in soil macropores: principles, controlling factors and consequences for water quality. *European Journal of Soil Science*, 58(3):523–546, 2007.

Jencso, K. G.; McGlynn, B. L.; Gooseff, M. N.; Bencala, K. E., and Wondzell, S. M. Hillslope hydrologic connectivity controls riparian groundwater turnover: Implications of catchment structure for riparian buffering and stream water sources. *Water Resources Research*, 46, 2010.

Jobbagy, E. G. and Jackson, R. B. The vertical distribution of soil organic carbon and its relation to climate and vegetation. *Ecological Applications*, 10(2):423–436, 2000.

Jutras, M. F.; Nasr, M.; Castonguay, M.; Pit, C.; Pomeroy, J. H.; Smith, T. P.; Zhang, C. F.; Ritchie, C. D.; Meng, F. R.; Clair, T. A., and Arp, P. A. Dissolved organic carbon concentrations and fluxes in forest catchments and streams: Doc-3 model. *Ecological Modelling*, 222(14):2291–2313, 2011.

Kalbitz, K.; Solinger, S.; Park, J. H.; Michalzik, B., and Matzner, E. Controls on the dynamics of dissolved organic matter in soils: A review. *Soil Science*, 165(4): 277–304, 2000.

Kaplan, L. A. Comparison of high-temperature and persulfate oxidation methods for determination of dissolved organic carbon in freshwaters. *Limnology and Oceanography*, 37(5):1119–1125, 1992.

Kaplan, L. A. and Bott, T. L. Diel fluctuations of doc generated by algae in a piedmont stream. *Limnology and Oceanography*, 27(6):1091–1100, 1982.

Kaplan, L. A. and Bott, T. L. Microbial heterotrophic utilization of dissolved organic-matter in a piedmont stream. *Freshwater Biology*, 13(4):363–377, 1983.

Kaplan, L. A. and Newbold, J. D. Measurement of streamwater biodegradable dissolved organic carbon with a plug-flow bioreactor. *Water Research*, 29(12):2696–2706, 1995.

Kaplan, L. A. and Newbold, J. D. Evaluation of sources of pathogens and nom in watersheds, 2002.

Kaplan, L. A.; Wiegner, T. N.; Newbold, J. D.; Ostrom, P. H., and Gandhi, H. Untangling the complex issue of dissolved organic carbon uptake: a stable isotope approach. *Freshwater Biology*, 53(5):855–864, 2008.

Kasahara, T. and Wondzell, S. M. Geomorphic controls on hyporheic exchange flow in mountain streams. *Water Resources Research*, 39(1), 2003.

Kawasaki, M.; Ohte, N., and Katsuyama, M. Biogeochemical and hydrological controls on carbon export from a forested catchment in central japan. *Ecological Research*, 20(3):347–358, 2005.

Kawasaki, M.; Ohte, N.; Kabeya, N., and Katsuyama, M. Hydrological control of dissolved organic carbon dynamics in a forested headwater catchment, kiryu experimental watershed, japan. *Hydrological Processes*, 22(3):429–442, 2008.

Kim, S.; Kaplan, L. A., and Hatcher, P. G. Biodegradable dissolved organic matter in a temperate and a tropical stream determined from ultra-high resolution mass spectrometry. *Limnology and Oceanography*, 51(2):1054–1063, 2006.

Kodesova, R.; Vignozzi, N.; Rohoskova, M.; Hajkova, T.; Kocarek, M.; Pagliai, M.; Kozak, J., and Simunek, J. Impact of varying soil structure on transport processes in different diagnostic horizons of three soil types. *Journal of Contaminant Hydrology*, 104(1-4):107–125, 2009.

Kohler, S. J.; Buffam, I.; Seibert, J.; Bishop, K. H., and Laudon, H. Dynamics of stream water toc concentrations in a boreal headwater catchment: Controlling factors and implications for climate scenarios. *Journal of Hydrology*, 373(1-2):44–56, 2009.

Kumar, A.; Kanwar, R. S., and Ahuja, L. R. Evaluation of preferential flow component of rzwqm in simulating water and atrazine transport to subsurface drains. *Transactions of the Asae*, 41(3):627–638, 1998.

Kumar, M.; Bhatt, G., and Duffy, C.J. An object-oriented shared data model for gis and distributed hydrologic models. *International Journal of Geographical Information Science*, 24(7):1061–1079, 2010.

Laudon, H.; Berggren, M.; Agren, A.; Buffam, I.; Bishop, K.; Grabs, T.; Jansson, M., and Kohler, S. Patterns and dynamics of dissolved organic carbon (doc) in boreal streams: The role of processes, connectivity, and scaling. *Ecosystems*, 14(6): 880–893, 2011.

Leff, L. G. and Meyer, J. L. Biological availability of dissolved organic-carbon along the ogeechee river. *Limnology and Oceanography*, 36(2):315–323, 1991.

Levia, D. F.; Van Stan, J. T.; Inamdar, S. P.; Jarvis, M. T.; Mitchell, M. J.; Mage, S. M.; Scheick, C. E., and McHale, P. J. Stemflow and dissolved organic carbon cycling: temporal variability in concentration, flux, and uv-vis spectral metrics in a temperate broadleaved deciduous forest in the eastern united states. *Canadian Journal of Forest Research-Revue Canadienne De Recherche Forestiere*, 42(1):207–216, 2012.

Li, H. L.; Boufadel, M. C., and Weaver, J. W. Quantifying bank storage of variably saturated aquifers. *Ground Water*, 46(6):841–850, 2008.

Liu, S. Q.; Graham, W. D., and Jacobs, J. M. Daily potential evapotranspiration and diurnal climate forcings: influence on the numerical modelling of soil water dynamics and evapotranspiration. *Journal of Hydrology*, 309(1-4):39–52, 2005.

McClain, M. E.; Richey, J. E.; Brandes, J. A., and Pimentel, T. P. Dissolved organic matter and terrestrial-lotic linkages in the central amazon basin of brazil. *Global Biogeochemical Cycles*, 11(3):295–311, 1997.

McDowell, W. H. Dissolved organic matter in soils - future directions and unanswered questions. pages 179–186, 2003.

McDowell, W. H. and Likens, G. E. Origin, composition, and flux of dissolved organic carbon in the hubbard brook valley. *Ecological Monographs*, 58(3):177–195, 1988.

McDowell, W. H.; Zsolnay, A.; Aitkenhead-Peterson, J. A.; Gregorich, E. G.; Jones, D. L.; Jodemann, D.; Kalbitz, K.; Marschner, B., and Schwesig, D. A comparison of methods to determine the biodegradable dissolved organic carbon from different terrestrial sources. *Soil Biology & Biochemistry*, 38(7):1933–1942, 2006.

McGlynn, B. L. and McDonnell, J. J. Role of discrete landscape units in controlling catchment dissolved organic carbon dynamics. *Water Resources Research*, 39(4), 2003.

McKay, M. D.; Beckman, R. J., and Conover, W. J. A comparison of three methods for selecting values of input variables in the analysis of output from a computer code. *Technometrics*, 21(2):239–245, 1979.

Mei, Y.; Hornberger, G.M.; Kaplan, L.A.; Newbold, J.D., and Aufdenkampe, A.K. Estimation of dissolved organic carbon contribution from hillslope soils to a headwater stream. *Water Resources Research*, 48(9):W09514, 2012.

Mertens, J.; Vanderborght, J.; Kasteel, R.; Putz, T.; Merckx, R.; Feyen, J., and Smolders, E. Dissolved organic carbon fluxes under bare soil. *Journal of Environmental Quality*, 36(2):597–606, 2007.

Michalzik, B.; Tipping, E.; Mulder, J.; Lancho, J. F. G.; Matzner, E.; Bryant, C. L.; Clarke, N.; Lofts, S., and Esteban, M. A. V. Modelling the production and transport of dissolved organic carbon in forest soils. *Biogeochemistry*, 66(3):241–264, 2003.

Monteith, JL. Evaporation and environment. volume 19, page 4, 1965.

Moore, T. R. Dynamics of dissolved organic-carbon in forested and disturbed catchments, westland, new-zealand .1. maimai. *Water Resources Research*, 25(6):1321–1330, 1989.

Morris, Donald P.; Zagarese, Horacio; Williamson, Craig E.; Balseiro, Esteban G.; Hargreaves, Bruce R.; Modenutti, Beatriz; Moeller, Robert, and Queimalinos, Claudia. The attenuation of solar uv radiation in lakes and the role of dissolved organic carbon. *Limnology and Oceanography*, 40(8):1381–1391, 1995.

Mulholland, P. J. Organic carbon flow in a swamp-stream ecosystem. *Ecological Monographs*, 51(3):307–322, 1981.

Neff, J. C. and Asner, G. P. Dissolved organic carbon in terrestrial ecosystems: Synthesis and a model. *Ecosystems*, 4(1):29–48, 2001.

Nelson, P. N.; Baldock, J. A., and Oades, J. M. Concentration and composition of dissolved organic carbon in streams in relation to catchment soil properties. *Biogeochemistry*, 19(1):27–50, 1993.

Neuman, S. P. Saturated-unsaturated seepage by finite elements. *J. Hydraul. Div*, 99:2233?250, 1973.

Neuman, S. P. and Withersp, P.A. Analysis of nonsteady flow with a free surface using the finite element method. *Water Resources Research*, 7(3):611–&, 1971.

Newbold, J. D.; Bott, T. L.; Kaplan, L. A.; Sweeney, B. W., and Vannote, R. L. Organic matter dynamics in white clay creek, pennsylvania, usa. *Journal of the North American Benthological Society*, 16(1):46–50, 1997.

Ogawa, A.; Shibata, H.; Suzuki, K.; Mitchell, M. J., and Ikegami, Y. Relationship of topography to surface water chemistry with particular focus on nitrogen and organic carbon solutes within a forested watershed in hokkaido, japan. *Hydrological Processes*, 20(2):251–265, 2006.

Palmer, S. M.; Hope, D.; Billett, M. F.; Dawson, J. J. C., and Bryant, C. L. Sources of organic and inorganic carbon in a headwater stream: Evidence from carbon isotope studies. *Biogeochemistry*, 52(3):321–338, 2001.

Panday, Sorab and Huyakorn, Peter S. A fully coupled physically-based spatially-distributed model for evaluating surface/subsurface flow. *Advances in Water Resources*, 27(4):361–382, 2004.

Paustian, K.; Andren, O.; Janzen, H. H.; Lal, R.; Smith, P.; Tian, G.; Tiessen, H.; Van Noordwijk, M., and Woomer, P. L. Agricultural soils as a sink to mitigate co2 emissions. *Soil Use and Management*, 13(4):230–244, 1997.

Pinder, G. F. and Gray, W. G. Finite element simulation in surface and subsurface hydrology. *San Diego, California*, 295, 1977.

Poeter, Eileen P. and Hill, Mary C. Ucode, a computer code for universal inverse modeling. *Computers & Geosciences*, 25(4):457–462, 1999.

Qu, Y. and Duffy, C. J. A semidiscrete finite volume formulation for multiprocess watershed simulation. *Water Resources Research*, 43(8), 2007.

Qualls, R. G. Comparison of the behavior of soluble organic and inorganic nutrients in forest soils. *Forest Ecology and Management*, 138(1-3):29–50, 2000.

Qualls, R. G. and Haines, B. L. Biodegradability of dissolved organic matter in forest throughfall, soil solution, and stream water. *Soil Science Society of America Journal*, 56(2):578–586, 1992.

Raats, P. A. C. Steady flows of water and salt in uniform soil profiles with plant roots. *Soil Science Society of America Journal*, 38(5):717–722, 1974.

Rathfelder, K. and Abriola, L. M. Mass conservative numerical solutions of the head-based richards equation. *Water Resources Research*, 30(9):2579–2586, 1994.

Raymond, P. A. and Saiers, J. E. Event controlled doc export from forested watersheds. *Biogeochemistry*, 100(1-3):197–209, 2010.

Redfield, A.C. The biological control of chemical factors in the environment. *American Scientist*, 46(3), 1958.

Ribas, F.; Frias, J., and Lucena, F. A new dynamic method for the rapid determination of the biodegradable dissolved organic carbon in drinking water. *Journal of Applied Bacteriology*, 71(4):371–378, 1991.

Roulet, N. and Moore, T. R. Environmental chemistry - browning the waters. *Nature*, 444(7117):283–284, 2006.

Sanderman, J.; Lohse, K. A.; Baldock, J. A., and Amundson, R. Linking soils and streams: Sources and chemistry of dissolved organic matter in a small coastal watershed. *Water Resources Research*, 45:13, 2009.

Schaap, M. G.; Leij, F. J., and van Genuchten, M. T. Rosetta: a computer program for estimating soil hydraulic parameters with hierarchical pedotransfer functions. *Journal of Hydrology*, 251(3-4):163–176, 2001.

Schiff, S.; Aravena, R.; Mewhinney, E.; Elgood, R.; Warner, B.; Dillon, P., and Trumbore, S. Precambrian shield wetlands: Hydrologic control of the sources and export of dissolved organic matter. *Climatic Change*, 40(2):167–188, 1998.

Schiff, S. L.; Aravena, R.; Trumbore, S. E., and Dillon, P. J. Dissolved organic carbon cycling in forested watersheds: A carbon isotope approach. *Water Resources Research*, 26(12):2949–2957, 1990.

Seibert, J.; Grabs, T.; Kohler, S.; Laudon, H.; Winterdahl, M., and Bishop, K. Linking soil- and stream-water chemistry based on a riparian flow-concentration integration model. *Hydrology and Earth System Sciences*, 13(12):2287–2297, 2009.

Senior, L.A. and Koerkle, E.H. Simulation of streamflow and water quality in the white clay creek subbasin of the christina river basin, pennsylvania and delaware, 1994-98. Technical report, New Cumberland, Pennsylvania, 2003.

Servais, P.; Anzil, A., and Ventresque, C. Simple method for determination of biodegradable dissolved organic carbon in water. *Applied and Environmental Microbiology*, 55(10):2732–2734, 1989.

Shafer, M. M.; Overdier, J. T.; Hurley, J. P.; Armstrong, D., and Webb, D. The influence of dissolved organic carbon, suspended particulates, and hydrology on the concentration, partitioning and variability of trace metals in two contrasting wisconsin watersheds (usa). *Chemical Geology*, 136(1-2):71–97, 1997.

Shewchuk, Jonathan Richard. Delaunay refinement algorithms for triangular mesh generation. *Computational geometry*, 22(1):21–74, 2002.

Sieber, A. and Uhlenbrook, S. Sensitivity analyses of a distributed catchment model to verify the model structure. *Journal of Hydrology*, 310(1-4):216–235, 2005.

Simunek, J and Sejna, M. The hydrus-2d software package for simulating the two-dimensional movement of water, heat, and multiple solutes in variably-saturated media. Technical report, 1999.

Simunek, J.; Jarvis, N. J.; van Genuchten, M. T., and Gardenas, A. Review and comparison of models for describing non-equilibrium and preferential flow and transport in the vadose zone. *Journal of Hydrology*, 272(1-4):14–35, 2003.

Simunek, J.; Van Genuchten, M. T., and Sejna, M. The hydrus-1d software package for simulating the one-dimensional movement of water, heat, and multiple solutes in variably-saturated media. Technical report, 2005.

Sophocleous, M. Analysis of water and heat flow in unsaturated-saturated porous media. *Water Resources Research*, 15(5):1195–1206, 1979.

Sundquist, E. T. The global carbon-dioxide budget. *Science*, 259(5097):934–941, 1993.

Thurman, E. M. *Organic geochemistry of natural waters*. Springer, 1985.

Tsang, Yin-Phan; Hornberger, George; Kaplan, Louis A.; Newbold, J. Denis, and Aufdenkampe, Anthony K. A variable source area for groundwater evapotranspiration: impacts on modeling stream flow. *Hydrological Processes*, pages n/a–n/a, 2013.

Tyndall, John. On heat as a germicide when discontinuously applied.[abstract]. *Royal Society of London Proceedings Series I*, 25:569–570, 1876.

van Genuchten, M. T. A closed-form equation for predicting the hydraulic conductivity of unsaturated soils. *Soil Science Society of America Journal*, 44(5):892–898, 1980.

van Genuchten, M. T. A numerical model for water and solute movement in and below the root zone. Technical report, 1987.

van Genuchten, M. T. and Parker, J. C. Boundary conditions for displacement experiments through short laboratory soil columns. *Soil Science Society of America Journal*, 48(4):703–708, 1984.

van Verseveld, W. J.; McDonnell, J. J., and Lajtha, K. A mechanistic assessment of nutrient flushing at the catchment scale. *Journal of Hydrology*, 358(3-4):268–287, 2008.

VanderKwaak, Joel E. Numerical simulation of flow and chemical transport in integrated surface-subsurface hydrologic systems. *Dissertation Abstracts International Part B: Science and Engineering*, 60(7):3170, 2000.

Vidon, P. Towards a better understanding of riparian zone water table response to precipitation: surface water infiltration, hillslope contribution or pressure wave processes? *Hydrological Processes*, 26(21):3207–3215, 2012.

Vidon, P. and Cuadra, P. E. Impact of precipitation characteristics on soil hydrology in tile-drained landscapes. *Hydrological Processes*, 24(13):1821–1833, 2010.

Vidon, P.; Wagner, L. E., and Soyeux, E. Changes in the character of doc in streams during storms in two midwestern watersheds with contrasting land uses. *Biogeochemistry*, 88(3):257–270, 2008.

Volk, C.; Renner, C.; Robert, C., and Joret, J. C. Comparison of two techniques for measuring biodegradable dissolved organic carbon in water. *Environmental Technology*, 15(6):545–556, 1994.

Volk, C. J.; Volk, C. B., and Kaplan, L. A. Chemical composition of biodegradable dissolved organic matter in streamwater. *Limnology and Oceanography*, 42(1):39–44, 1997.

Vrugt, J. A.; Hopmans, J. W., and Simunek, J. Calibration of a two-dimensional root water uptake model. *Soil Science Society of America Journal*, 65(4):1027–1037, 2001.

Wallach, R. and Shabtai, R. Surface runoff contamination by soil chemicals - simulations for equilibrium and 1st-order kinetics. *Water Resources Research*, 28(1): 167–173, 1992.

Wallach, R.; Grigorin, G., and Rivlin, J. A comprehensive mathematical model for transport of soil-dissolved chemicals by overland flow. *Journal of Hydrology*, 247 (1-2):85–99, 2001.

Wallis, PM. Sources, transportation and utilization of dissolved organic matter in groundwater and streams. *Kananaskis Centre for Environmental Research, Calgary University, Alberta, Canada. Inland Waters Directorate, Water Quality Branch, Ottawa, Canada 1979. Scientific Series*, (100), 1979.

Weiler, M. and McDonnell, J. R. J. Testing nutrient flushing hypotheses at the hillslope scale: A virtual experiment approach. *Journal of Hydrology*, 319(1-4): 339–356, 2006.

Whiting, P. J. and Pomeranets, M. A numerical study of bank storage and its contribution to streamflow. *Journal of Hydrology*, 202(1-4):121–136, 1997.

Winterdahl, M.; Futter, M.; Kohler, S.; Laudon, H.; Seibert, J., and Bishop, K. Riparian soil temperature modification of the relationship between flow and dissolved organic carbon concentration in a boreal stream. *Water Resources Research*, 47, 2011.

Worrall, F. and Burt, T. Predicting the future doc flux from upland peat catchments. *Journal of Hydrology*, 300(1-4):126–139, 2005.

Xu, N. and Saiers, J. E. Temperature and hydrologic controls on dissolved organic matter mobilization and transport within a forest topsoil. *Environmental Science & Technology*, 44(14):5423–5429, 2010.

Xu, N.; Saiers, J. E.; Wilson, H. F., and Raymond, P. A. Simulating streamflow and dissolved organic matter export from a forested watershed. *Water Resources Research*, 48, 2012.

Yano, Y.; McDowell, W. H., and Aber, J. D. Biodegradable dissolved organic carbon in forest soil solution and effects of chronic nitrogen deposition. *Soil Biology & Biochemistry*, 32(11-12):1743–1751, 2000.

Yeh, G. T. On the computation of darcian velocity and mass balance in the finite element modeling of groundwater flow. *Water Resources Research*, 17(5):1529–1534, 1981.

Yeh, Gour-Tsyh; Cheng, Hwai-Ping; Cheng, Jing-Ru; Lin, Hsin-Chi J, and Martin, William D. A numerical model simulating water flow and contaminant and sediment transport in watershed systems of 1-d stream-river network, 2-d overland regime, and 3-d subsurface media (wash123d: Version 1.0). Technical report, 1998.

Yin, Y. J.; Impellitteri, C. A.; You, S. J., and Allen, H. E. The importance of organic matter distribution and extract soil : solution ratio on the desorption of heavy metals from soils. *Science of the Total Environment*, 287(1-2):107–119, 2002.

You, S. J.; Yin, Y. J., and Allen, H. E. Partitioning of organic matter in soils: effects of ph and water/soil ratio. *Science of the Total Environment*, 227(2-3):155–160, 1999.

Yurova, A.; Sirin, A.; Buffam, I.; Bishop, K., and Laudon, H. Modeling the dissolved organic carbon output from a boreal mire using the convection-dispersion equation: Importance of representing sorption. *Water Resour. Res*, 44, 2008.

Zheng, C and Wang, PP. Mt3dms: A modular three-dimensional multispecies transport model for simulation of advection, dispersion, and chemical reactions of contaminants in groundwater systems; documentation and user's guide. Technical report, Vicksburg, MS, 1999.